ACTIVATION OF ALUMINOSILICATE MATERIALS

By

KOSAR HASSANNEZHAD

Submitted to the Graduate School of Engineering and Natural Sciences in partial fulfillment of the requirements for the degree of Master of Science

Sabanci University

December 2020

ACTIVATION OF ALUMINOSILICATE MATERIALS

APPROVED BY:

DATE OF APPROVAL: 25/12/2020

ABSTRACT

ACTIVATION OF ALUMINOSILICATE MATERIALS

KOSAR HASSANNEZHAD

Materials Sciences and Nano Engineering, Master Thesis, December 2020

Supervisor: Prof. Dr. Mehmet Ali Gulgun

Keywords: Calcined Schist, Activated Feldspar, Calcined Carbonate, Cement Substitute, Compressive Strength, SCM

Supplementary Cementitious Materials (SCMs) are the proper partial substitute for Ordinary Portland Cement (OPC) to reduce the production of carbon dioxide and fossil fuel consumption. Sufficient clay containing schist type materials, therefore, are promising substitutes. The schist-type raw powders contain clays, feldspars, carbonates, and some minor chemical phases. Recent studies described the effectiveness of pure calcined clay materials (kaolinite) as a proper partial replacement for cement. This study explores and illustrates the possibility of activating and using schist type materials as a more accessible source for partial replacement of cement. Furthermore, the positive effect of calcined calcium carbonates in the pozzolanic reactions of SCM substituted

OPC was also illustrated in this study. Activated carbonates were effective in accelerating the pozzolanic reactions and forming additional Calcium Alumino Silicate Hydrate (CASH). Five schist minerals containing various types and amounts of clays were mineralogically augmented with additional calcite. The total carbonate amount was adjusted to 15, 22.5, and 30 wt% of the resource. Virgin and augmented resources were activated through a thermal or mechanical activation process. The proper activation method for schist type materials depends on their phase composition and the portion of clay and feldspar. The thermal activation includes a calcination process up to 80%, 100%, and 110% of the respective potentials by heat treatment and air quenching. This study claims that an efficient calcination process for specific schist can be designed by calculating the amount of energy that is needed for de-stabilizing the activatable aluminosilicate and carbonate phases. Phase content and decomposition behavior of the active components were investigated by Thermo Gravimetric Analysis (TGA), X-Ray Diffraction (XRD), and Scanning Electron Microscopy (SEM). Blended cement paste samples were prepared with 30 wt% replacement of OPC by activated schist SCMs. Cement paste samples from this blend were hydrated for 2, 7, 28, 50, and 90 days. The mechanical strength of the samples was measured at the end of the determined curing times by compression testing. Cement paste prepared with activated calcium augmented SCMs reached strength values that are better than 90% of the compressive strength of pure OPC.

ÖZET

ALÜMİNOSİLİCAT MALZEMELERİN ACTİVASYONU

KOSAR HASSANNEZHAD

Malzeme Bilimi ve Nano-mühendislik, Yüksek Lisans Tezi, Aralık 2020

Danışman: Prof. Dr. Mehmet Ali Gülgün

Anahtar Kelimeler: Kalsine Şist, Aktif Edilmiş Feldispat, Kalsine Karbonat, Çimento İkamesi, Basınç Dayanımı, SCM

Tamamlayıcı Çimentolu Malzemeler (SCM'ler), karbondioksit üretimini ve fosil yakıt tüketimini azaltmak için Sıradan Portland Çimentosunun (OPC) uygun kısmi ikamesidir. Bu nedenle, yeterli miktarda kil içeren şist tipi malzemeler ümit verici ikamelerdir. Şist tipi işlenmemiş tozlar kil, feldispat, karbonat ve bazı küçük kimyasal fazlar içerir. Son çalışmalar, saf kalsine kil materyallerinin (kaolinit) etkinliğini çimento için uygun bir kısmi ikame olarak tanımladı. Bu çalışma, şist tipi malzemelerin, çimentonun kısmi ikamesi için daha erişilebilir bir kaynak olarak aktive edilip kullanılmasını araştırmakta ve göstermektedir. Ayrıca SCM ikameli OPC'nin puzolanik reaksiyonlarında kalsine kalsiyum karbonatların olumlu etkisi de bu çalışmada

gösterilmiştir. Aktif karbonatlar, puzolanik reaksiyonların hızlandırılmasında ve daha fazla Kalsiyum Alümino Silikat Hidrat (CASH) oluşumunda etkili olmuştur. Çeşitli tip ve miktarlarda kil içeren beş şist minerali ilave kalsit ile mineralojik olarak zenginleştirilmiştir. Toplam karbonat miktarı, kaynağın ağırlıkça %15, %22.5 ve %30'una ayarlandı. İşlenmemiş ve miktarı arttırılmış kaynaklar, termal veya mekanik bir aktivasyon süreciyle etkinleştirildi. Şist tipi malzemeler için uygun aktivasyon yöntemi, faz bileşenlerine ve kil ve feldispat kısmına bağlıdır. Termal aktivasyon, ısıl işlem ve hava ile hızlı soğutma potansiyellerinin % 80, % 100 ve% 110'una kadar bir kalsinasyon işlemi içerir. Bu çalışma, aktifleştirilebilir alüminosilikat ve karbonat fazlarını de-stabilize etmek için gerekli olan enerji miktarını hesaplayarak spesifik şist için verimli bir kalsinasyon işleminin tasarlanabileceğini öne sürmektedir. Aktif bileşenlerin faz içeriği ve dekompozisyon davranışı Termo Gravimetrik Analiz (TGA), X Işını Kırınımı (XRD) ve Taramalı Elektron Mikroskobu (SEM) ile incelendi. Harmanlanmış çimento macunu numuneleri, ağırlıkça OPC'nin %30'unu aktifleştirilmiş şist SCM'leri ile değiştirerek hazırlanmıştır. Bu karışımdan elde edilen çimento macunu numuneleri 2, 7, 28, 50 ve 90 gün süreyle su ile reaksiyona bırakıldı. Numunelerin mekanik dayanımı, belirlenen kürleme süreleri sonunda bastırma testi ile ölçülmüştür. Aktifleştirilmiş kalsiyum takviyeli SCM'lerle hazırlanan çimento macunu, saf OPC'lerin basınç dayanımlarının %90'ından daha iyi olan mukavemet değerlerine ulaştı.

ACKNOWLEDGMENTS

Writing a scientific thesis would not be possible without the guidance and support of various people.

First and foremost, I would like to express my sincere gratitude and appreciation to my supervisor Prof. Dr. Mehmet Ali Gülgün for giving me the opportunity to do this research. His continuous support, unbelievable energy, sincerity, immense knowledge, and motivation have deeply inspired me and helped me in all the time of this research.

Besides my supervisor, I would like to thank the rest of my thesis committee: Prof. Dr. Cleva Ow-Yang and Dr. Zeynep Başaran Bundur for reading my thesis and making useful comments.

My special appreciation to my labmates and friends' support for providing sincere assistance to complete this research. My special thanks goes to Pozhhan Mokhtari, who supported me like an older brother. Thanks to Sirous Khabbaz (Hamid) for his kind gesture in helping me especially in SEM training. Thanks to Yasemin Akyol and Sezen Dönmez.

I am very grateful to my true friends at Sabanci University for their kindness and mental support; Milad, Maryam, and Madineh. I am very lucky for having you by my side guys ☺

Last but not the least, I am extremely grateful to my family for their love and sacrifices for preparing me for my future.

To MY FAMILY

Table of Contents

List of Figures

List of Tables

List of Abbreviations

Abbreviations	Definition
Cement Notation	
C	Calcium Oxide, CaO
S	Silicon Oxide, SiO_2
A	Aluminum Oxide, Al_2O_3
F	Iron Oxide, Fe_2O_3
H	Water, H_2O
$\bar{C}$	Carbonate, CO_2
Cement Phase	
C_3S	TriCalcium Silicate
C_2S	DiCalcium Silicate
C_3A	TriCalcium Aluminate
C_4AF	TetraCalcium Aluminoferrite
CH	Portlandite or Calcium Hydroxide
C-S-H	Calcium Silicate Hydrate (Tobermorite)
C-A-S-H	Al- Calcium Silicate Hydrate (Al- Tobermorite)
AFt	Ettringite
AFm	Monosulfo/Carboaluminate
OPC or PC	Ordinary Portland Cement
SCM	Supplementary Cementitious Materials
w/s	Water-to-Solid Ratio
Methods	
SEM	Scanning Electron Microscope
EDS	Energy Dispersive X-ray Spectroscopy
TGA	Thermogravimetric Analysis
DTG	Differential Thermogravimetry
DSC	Differential Scanning Calorimetry
XRD	X-Ray Diffraction
UCS	Uniaxial Compressive Strength

CHAPTER 1

1. Introduction

1.1. Cement Industry and Environment

Cement industry has been always one of the main sources of CO_2 generation among industrial activities which generates 5-7% of global anthropogenic CO_2 emission [1, 2]. From the beginning of cement industrial production in the middle of the 19th century, it has gone through a huge development process. One of the most common types of cement is Portland cement which contains 95% cement clinker. The conventional clinker production process comprises several chemical and physical reactions occurring at high temperatures (~1400°C). These processes include combustion of fossil fuels and de-carbonization of limestone ($CaCO_3$) to Calcia (CaO) which are the major sources of CO_2 emission in the cement manufacturing process [3-5]. Recently, many types of research all over the world aimed to curb the negative effects of the cement industry on the environment and also to provide more economical methods in cement production. There are many studies focused on launching applicable mechanisms to mitigate the CO_2 emission coming from cement manufacture [3, 5-10]. To this end, some approaches such as replacement of fossil fuels with alternative and biomass fuels [5, 11], using solar thermal calciner technology [6], reusing waste building materials [8], and using industrial wastes as both fuel and raw materials [3] have been proposed. Nevertheless, one of the most practical approaches is clinker substitution. The

addition of several additives such as Supplementary cementitious materials (SCMs) to cement leads to a considerable reduction in production and usage of clinker.

1.2. Supplementary Cementitious Materials (SCMs)

SCMs are now increasingly being added to the composite cement (blended cement) or concrete. These materials including natural pozzolans, industrial by-products, and wastes are predominantly aluminosilicate materials with lower calcium contents than Portland cement and silica to alumina ratio (Si/Al) of about 2 [12]. Figure 1 [13] shows the position of different types of SCMs in the ternary phase diagram of CaO, SiO_2, and Al_2O_3.

Portland cement hydration reaction (Eq. 1) mainly results in the formation of C–S–H, Portlandite (CH) [14]. C–S–H is the main hydration product with binding properties and strengthening of cement is mostly attributed to this product [12-20]. It is the most voluminous hydration phase and the stability and strength of the C-S-H mostly depend on its Ca/Si ratio which ranges from 1.3 to 2.1 [21] with a mean of 1.75 [22] in neat Portland cement. Initially, it starts to form as an amorphous binding phase. However, it will crystallize to tobermorite over time. Tobermorite is the most common hydrated OPC phase with $Ca_5Si_6O_{16}\ (OH)_2.4H_2O$ formula. The Ca/Si ratio in tobermorite is ~0.83. Nevertheless, tobermorite is not the only crystalline phase that crystallizes out of the amorphous C-S-H gel. There is also a Ca-rich phase which is called jennite ($Ca_9Si_6O_{18}(OH)_6{\cdot}8H_2O$) with the Ca/Si ratio of ~1.5 [23-25]. Kunther et al. [25] investigated the effect of the Ca/Si ratio on the strength of hydrated cement (C-S-H) and indicated that the compressive strengths and also durability of the C–S–H increase by decreasing the Ca/Si ratio. As a comparison between the two Si-rich (tobermorite) and Ca-rich (jennite) C-S-H crystalline phases, tobermorite with a lower Ca/Si ratio has higher strength as well as more durability. Therefore, the addition of pozzolans to cement will increase the strength of hardened OPC especially at late ages of hydration i. e. enhanced durability.

The presence of significant amounts of active constituents in SCMs is the main factor controlling their activity in the cement hydration process. These active constituents (mainly silica and aluminosilicates – known as Pozzolans) react with the calcium hydroxide (CH) obtained from Portland cement hydration (Eq. 1). Together, they form more calcium silicate hydrates (CSH) (Eq.

2) which has a tobermorite-like structure and is the major strength provider of hydrated cement [13].

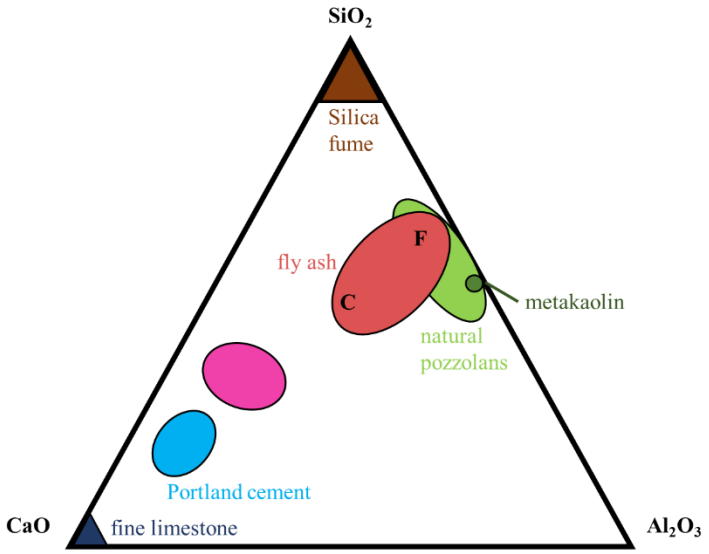

Figure 1. CaO-Al2O3 -SiO2 ternary diagram of cementitious materials [13]

Equation 1. Cement Hydration Reaction

$$Portland\ Cement\ +\ water\ \rightarrow\ C\ -\ S\ -H\ +\ CH \qquad \text{(Eq. 1)}$$

Equation 2. Pozzolanic Reaction

$$Pozzolans\ +\ CH\ +\ water\ \rightarrow\ C\ -\ S\ -\ H\ and\ C-A-S-H \qquad \text{(Eq. 2)}$$

1.2.1. Common Types of SCMs

Today utilization of various types of SCMs was developed due to technical, economical, and environmental reasons. Several types of pozzolanic materials such as natural pozzolans, blast furnace slag, fly ash, and silica fume are widely used as SCMs in cement or concrete [26-32].

Natural pozzolanic materials are all derived from the eruption of volcanic rocks which leads to the creation of a large amount of lava flows. This molten aluminosilicate material then turns into an amorphous or glass-like structure due to rapid cooling [33]. Volcanic ash is a traditional pozzolan which first has been used by Romans [34] to enhance the chemical and mechanical properties of concrete, especially durability. Shi et al. [35] used a chemical activation method for a natural pozzolan by mixing it with 20 wt% lime and some chemical activators. This activation method causes to enhance strength development. Celik et al. [36] reported an improvement in strength development and durability by replacement of Portland cement using 45 wt% of basaltic ash (natural pozzolan) and limestone. Colak [37] used a natural pozzolan together with a small amount of superplasticizer as SCMs in blended cement. This study indicated an increase in freeze and thaw resistance and a decrease in durability against sulfate attack when high content of natural pozzolan was used as a substituent.

Slag is a co-product obtained in the process of metal production into a blast furnace. It consists mostly of silicates, aluminosilicates, and calcium-alumina-silicates. Slag produced by blast furnaces is between 260 kg and 300 kg for every one tonne of iron [38]. There are many studies focused on the use of blast furnace slag in blended cement [19, 27, 31, 32, 39-43]. Besides, copper slag is also possible to be used as a substituent in cement partial replacement. Shi et al. [26] reviewed the properties of copper slag and its effects on the strength of cement and concrete. They proved that the copper slag acts as both an iron adjusting and mineralizing component and also improves the grind-ability of the clinker.

Fly ash is another type of SCMs which is a product of coal combustion power plants. It has hollow spherical particles and consists mainly of SiO_2, Al_2O_3, and also possibly small quantities of Fe_2O_3, CaO, MgO, K_2O, Na_2O and SO_3 [13, 44]. Fly ash was classified into two main types, related to their CaO ratio; C-type and F-type. C-type fly ash is a calcium-rich glass that contains more $CaSO_4$, free lime, Alite and MgO, and therefore, it is a cementitious (hydraulic) material. Whereas, F-type fly ash is a pozzolanic material containing mostly quartz and aluminosilicate glass [45]. Hanif et al. [46] reviewed the use of fly ash in cement-based composites and summarized the influences of different types of fly ash on the mechanical, functional, structural properties and the durability of composite cement.

Silica fume is an amorphous silica and a by-product of the silicon and ferrosilicon alloy production with a relatively high pozzolanic activity. Besides participating in pozzolanic reactions, there are some studies claiming that silica fume can also be used as an accelerator in cement hydration reactions. According to Cheng-Yi et al. [28], there is an acceleration in both C_3S and C_3A hydration in the first few hours by utilizing silica fume as cement substituent. Besides, Langan et al. [47] investigated the hydration of silica fume-fly ash-Portland cement mixture and showed that although fly ash acts as a retarder in cement hydration, silica fume accelerates hydration reaction at high water/cementitious ratios and retards it at low water/cementitious ratios.

1.2.2. Calcined Clays

There are some obstacles that limit the use of the mentioned types of SCMs. Substitution of more than a certain percentage of SCMs leads to a reduction in the mechanical properties of concrete, particularly at early age [48]. Furthermore, the availability of commonly used SCMs such as fly ash and blast furnace slags is limited or locally imbalanced around the world [12]. Nonetheless, clays being uniformly distributed all over the earth's crust offer a logistical advantage over the other resources of SCMs. Clay minerals are hydrous aluminosilicates and layered sandwich-like structures composed of octahedral aluminum hydroxide sheets and tetrahedral silica layers. Table 1 lists the main classes of clays that are most frequently found in the earth's crust and their compositions [49-53].

Table 1. Chemical Formulas of main Clay Minerals [49]

Ideal Chemical Formulas of the Clay Minerals	
Kaolinite	$Al_2(Si_2O_5)(OH)_4$
Halloysite	$Al_2(Si_2O_5)(OH)_4.2H_2O$
Pyrophyllite	$Al_2(Si_2O_5)_2(OH)_2$
Montmorillonite	$(Al_{1.67}Na_{0.33})(Si_2O_5)_2(OH)_2$ or $(Al_{1.67}Mg_{0.33})(Si_2O_5)_2(OH)_2$
Mica	$Al_2K(Si_{1.6}Al_{0.5}O_5)_2(OH)_2$
Illite	$Al_{2-x}Mg_xK_{1-x}(Si_{1.5}Al_{0.5}O_5)_2(OH)_2$

Based on the degree of ordering, clay minerals are classified into three categories; kaolinitic, smectitic, illitic [54]. Kaolinitic clays consist of tetrahedral silicate sheets and octahedral aluminum hydroxide (gibbsite), creating 1:1 layered structures. Whereas, the other two main classes of clay minerals, illites, and smectites have 2:1 structures made up of an octahedral layer between two layers of tetrahedral silica, making 2:1 structures [49]. Figure 2 shows the layered structure of three types of clays which are examples of the three different categories (kaolinitic, smectitic, illitic).

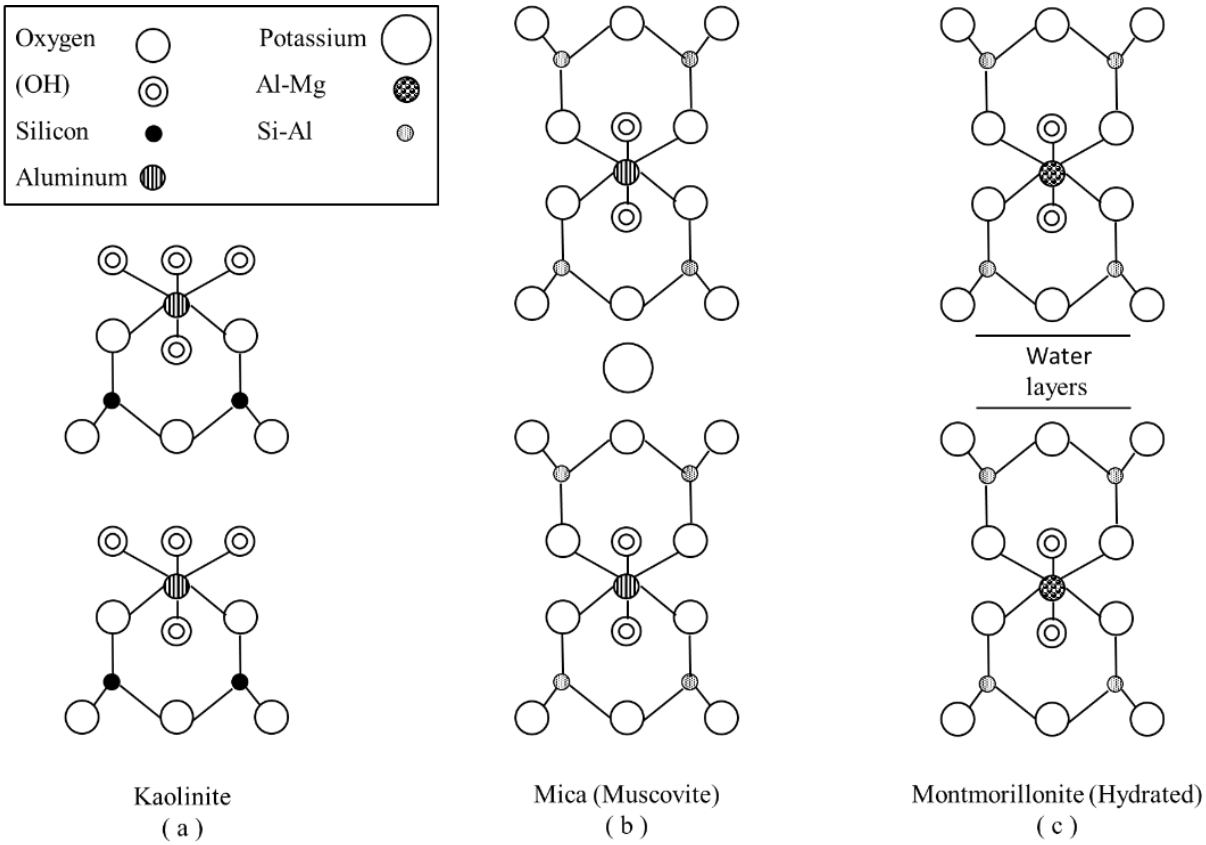

Figure 2. The layered structure of three types of clays, (a) Kaolinitic – kaolinite, (b) Illitic – Muscovite, (c) Smectitic – Montmorillonite [49]

Using alternative sources of SCMs such as calcined clays (aluminosilicate hydrates) could provide an alternative and efficient source. The activation of clay materials happens through the de-stabilization of aluminum hydroxide layers. De-hydroxylation of kaolinite (Eq. 3) as the simplest clay structure takes place in the temperature range of 400-700ºC. In this temperature range, water

vapor leaves the kaolinite structure. This water evaporation leads to the conversion of kaolinite to a more disordered and unstable structure called metakaolin which is highly reactive in cement hydration reactions i. e. high pH values [53, 55-57]. De-hydroxylation of Kaolinite is associated with weight loss due to water evaporation. As it can be seen in equation 4 and calculations, kaolinite loses almost 14% of its initial weight during calcination. Briefly, every 100g of kaolinite turns into 86 g of metakaolin at the end of the decomposition process. Figure 3 illustrates the schematic of the kaolinite de-hydroxylation process [58].

Equation 3. Kaolinite Calcination Reaction

$$Al_4Si_4O_{10}(OH)_8 \rightarrow 2Al_2Si_2O_7 + 4H_2O\ (\uparrow) \qquad \text{(Eq. 3)}$$

Equation 4. Weight Loss Process of Kaolinite during Calcination

$$4(27) + 4(28) + 10(16) + 8(16 + 8(1) \rightarrow 2[2(27) + 2(28) + 7(16)] + 4[2(1) + 16] \qquad \text{(Eq. 4)}$$

$$516 \rightarrow 444 + 72\ (\uparrow) \qquad \Longrightarrow \qquad \left(\frac{72}{516}\right) \times 100 \simeq 14\%$$

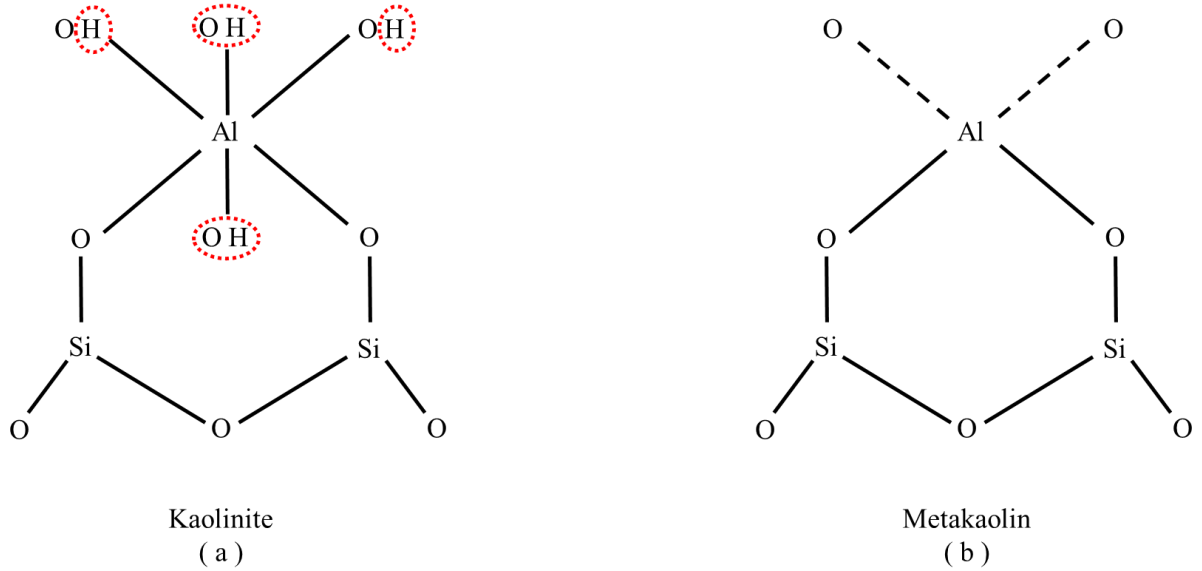

Figure 3. Structure of (a) Kaolinite and (b) Metakaolin

He et al. [59] evaluated the pozzolanic reactivity of heat-treated kaolin with four different calcination temperatures in the range of 550-950°C and reported that the optimum calcination temperature for kaolinite is 550°C. However, there are some other types of clays with more complex structures than kaolinite that could be used as SCMs after being calcined. Therefore, the efficiency and pozzolanic reactivity of the calcined clays depends on some other factors than calcination temperature such as the type of the clay, the duration of heat treatment, and the design of heating and cooling processes [60]. Changling et al. [61] studied the pozzolanic reactivity and technological effects of six principal clay minerals. They obtained the optimum calcination temperature for each type of clay and also confirmed that the most effective method for activating the pozzolanic reactivity of clays is damaging and destroying the crystal structure of clays through a calcination process. Hence, by performing a simple heat treatment process that is unique for every type of clay, the clays can be activated and show excellent pozzolanic properties (Eq. 5 and 6) [55, 60, 61]. Figure 4 illustrates the hydration products of blended cement in the CaO, SiO_2 and Al_2O_3 system. So far, the clay calcination methods used in literature are only based on decomposition temperature range and. However, there are other factors besides temperature influencing the success of calcination such as the extent of heat treatment and the amount (volume) of material. In order to determine the most efficient procedure for calcination of any clayey material, it would be better to define a more reliable parameter than temperature. This parameter should cover calcination temperature and time, and also should be independent of the amount of the material. The best parameter that could be measured to control all effective factors would be the amount of ENERGY induced to the materials during calcination.

Equation 5. Dissolution of Quartz in Water

$$SiO_2 + 2H_2O \rightarrow H_4SiO_4 \qquad (Quartz + Water \rightarrow Silicic\ Acid) \qquad \text{(Eq. 5)}$$

Equation 6. Pozzolanic Reaction of Kaolinite and CH

$$Ca\,(OH)_2 + H_2O \rightarrow Ca^{2+} + 2OH^-$$
$$Al_2Si_2O_7 + H_4SiO_4 \rightarrow 2\,(SiO_4)^{4-} + 4\,H^+ + Al_2O_3 \quad \text{(Eq. 6)}$$

$TOBERMORITE$

$(CSH - Ca_5Si_6O_{16}\,(OH)_2.4H_2O)$

$Al - TOBERMORITE$

$(CASH - Ca_5Al_2Si_6O_{16}\,(OH)_2.4H_2O)$

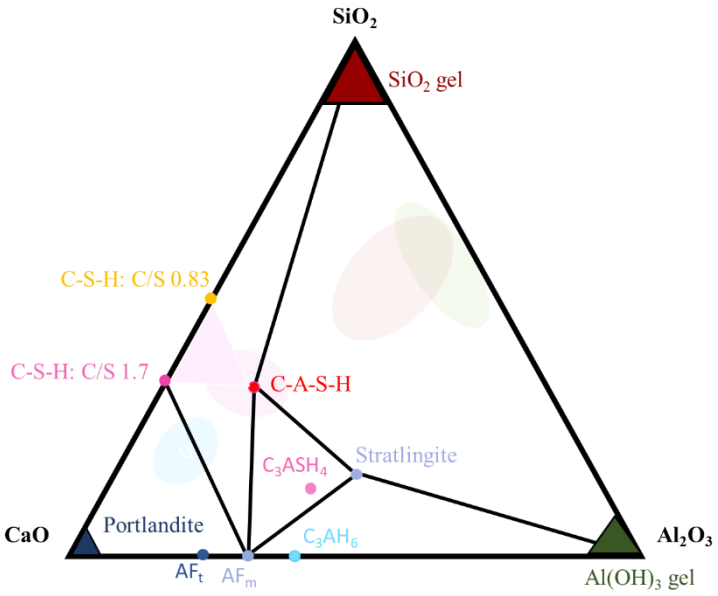

Figure 4. Hydrate phases in the CaO–Al_2O_3–SiO_2 system. Note that in the absence of carbonate or sulfate, C_3AH_6 will be more stable than the AFm phases [13].

1.2.3. Schist Type Materials

Since there are very rare sources of pure clay minerals such as kaolinite in the world, utilizing them as a pozzolanic material source is not cost-effective and environmentally-friendly [48].

According to the equations of pozzolanic reactions (eq. 4 and 5), using any other substances that contain silica-alumina bonding as a pozzolanic material, can be an efficient alternative way for substitution of cement. Schist minerals which could be found almost everywhere in the world, generally consist of quartz, carbonates, various types of clay components, and feldspars. Therefore, schists contain the two main ingredients for pozzolanic reactions in cement, siliceous minerals, and an abundant calcium source, carbonates. However, these materials also have to be activated before they can be used as SCMs. Similar to kaolinite, clayey minerals in schists which have more complex structures, attain their maximum degree of disorder in the temperature range of 700 and 800ºC. Mokhtari et al. [48] determined that the optimum and safe activation ratio of clay containing schist-type materials is associated with 80 wt% of the total weight loss due to the de-hydroxylation reactions. Over-heating of clays was shown to lead to sintering and diminished reactivity due to the recrystallization [48, 62]. The reactivity and therefore the success of schist-type materials as SCMs are directly associated with the proper activation of clay [48, 60, 62, 63] and calcium sources [48].

1.2.4. Feldspars

Besides various types of clay, schist minerals also usually contain feldspars [64] which are another type of aluminosilicates [65]. Feldspars are a group of anhydrous aluminosilicates containing K^+, $Na^{+,}$ or Ca^{2+}. The three major compositional sorts of feldspars are K-feldspar (microcline or orthoclase) [$K(AlSi_3)O_8$], Albite [$Na(AlSi_3)O_8$], and Anorthite [$Ca(Al_2Si_2)O_8$] [49]. Figure 5 shows the compositional phase diagram of feldspars and the classification based on their chemical composition. There are some solid solution series within this ternary system. Feldspars are also chemically divided into two groups; alkali feldspars and plagioclases. Alkali feldspars are between Orthoclase and Albite endmembers, whereas, plagioclase feldspars are between Albite and Anorthite. Since the ionic radii and charges of K and Ca ions are different, there are no stable solid solutions of feldspars between K (Orthoclase) and Ca (Anorthite) endmembers [65, 66]. Table 2 shows the physical properties (cleavage and crystal system) and the theoretical composition of principle feldspars [65].

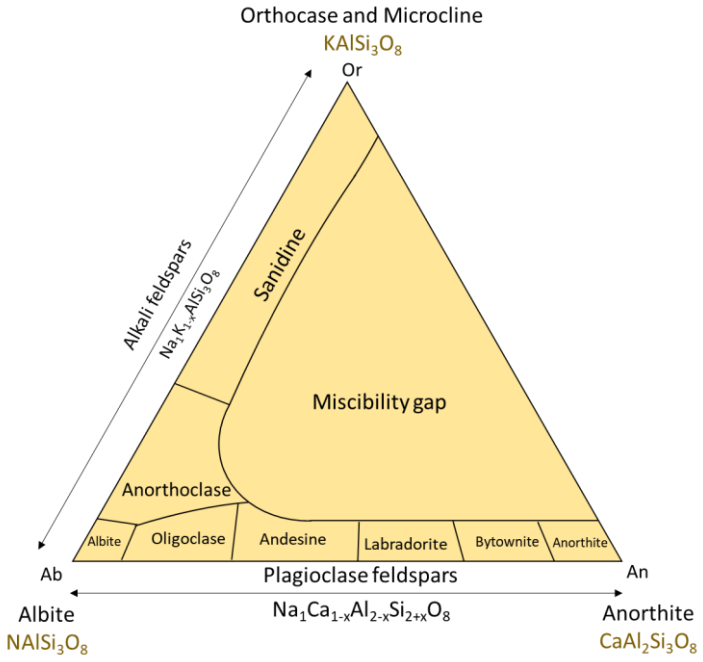

Figure 5. Compositional phase diagram of the different minerals that constitute the feldspar solid solution [65].

Table 2. Physical properties and theoretical composition of principle feldspars. Note that only (0 0 1) surfaces contain the aluminum sites [65, 66]

Physical Properties	**Albite**	**Orthoclase**	**Anorthite**
Cleavage	(001) Perfect, (010) Good	(001) Perfect, (010) Good	(001) Perfect, (010) Good
System	Triclinic	Monoclinic	Triclinic
Theoretical Composition			
K_2O (wt%)	---	16.9	---
Na_2O (wt%)	11.8	---	---
CaO (wt%)	---	---	20.1
Al_2O_3 (wt%)	19.4	18.4	36.6
SiO_2 (wt%)	68.8	64.7	43.3

Since it is very simple to convert crystalline clays to amorphous and highly reactive materials i.e. calcined clays, nowadays only the clay containing aluminosilicates are possible to be activated and used as SCMs. During de-hydroxylation reactions, the Al-Si bonds are getting destabilized which are further attacked by the high pH conditions in cement hydration reactions [55]. So far, there is no direct indication that the feldspars can also be attacked by the same high pH conditions which are provided by CH. Nature shows that feldspars are the precursors for the clays and it means that there is already a natural way to destabilize and breakdown the feldspars into clay under certain conditions [67]. Therefore, by generating similar conditions and destabilizing the Al-Si bonds of the feldspars, it would be possible to decompose them into pre-clays or anhydrous clays even faster than nature. It has been widely accepted that the dissolution of feldspars in nature occurs through a weathering process [68]. Geologists recognized two categories of weathering processes; physical weathering, including disintegration of minerals by a mechanical process, and chemical weathering which involves reactions of minerals with water, oxygen, and carbon dioxide and leads to the decomposition of minerals [69]. According to the literature [68-71], for converting feldspar to clay, the most appropriate method is chemical weathering. Because after weathering (decomposition), the products react with their new environment to produce new minerals that are more stable under earth surface conditions, and clay minerals are one of the most stable phases. Wollast [72] offered a low-temperature weathering method for K-feldspar in buffered solutions. In this method alteration of a K-feldspar occurs exposing to solutions with a pH value of 4-10, and it leads to release of Si and Al through exchange of H^+ for K^+. On the other hand, Correns and Engelhardt [71, 73] reported that converting a feldspar into kaolinite (clay) is possible only by reactions among dissolved substances. Tazaki et al. [74] studied the clay formation on a type of K-feldspar and investigated intermediate states between feldspar and crystalline clay products with the help of High-resolution transmission electron microscopy. They showed that the weathering process of feldspar leads to the formation of a clay precursor on its surface. Keller [75] illustrated the kaolinization of feldspar with the aid of scanning electron microscopy. This study proved that various types of clay minerals are possible to be formed from the same feldspar. Thus, by applying a proper activation method on feldspars, it would be possible to activate the feldspars inside schists and take advantage of them as pozzolanic materials beside calcined clays and carbonates.

1.2.5. Limestone and Calcined Limestone

The addition of limestone (as SCM) to the cement is an efficient way to enhance the mechanical properties. This additive not only leads to early hydration but also influences the hydrated structure of cement pastes. Pera et al. [76] observed physical and chemical changes during hydration by adding various amounts of calcium carbonate to cement. It has been proved that calcium carbonate causes an acceleration in cement hydration and also the formation of some calcium carbosilicate hydrates.

Besides, a mixture of a pozzolanic material and limestone also would be an efficient cement substituent. Romans were the first to extensively use natural volcanic ash together with limestone to make blended cement [77]. Recently, metakaolin was used together with virgin calcium carbonate (calcite) in blended cement [57, 78-80]. Calcite reactions with the cement during hydration were claimed to give additional benefits to the hardened paste [41, 76, 81-88]. It is also claimed that in the presence of limestone ($CaCO_3$), hemi-carboaluminate instead of mono-sulfoaluminate will be the stable phase in the blended cement paste at an early age and room temperature. This phase will be later converted to mono-carboaluminate after 90 days (Eq. 7) [57, 89]. In such a way, the amount of sulfate in the system increases and it leads to the formation and stabilization of ettringite which is an expansive phase and a necessary component of Portland cement systems [90]. As long as the system does not have an excessive amount of limestone, an increased volume of ettringite will not be a danger to the strength of hardened cement. Antoni et al. [57] reported that the amount of limestone in the blended cement mixture should not exceed 5 wt%.

Equation 7. Creation of Monocarboaluminate in cement hydration reactions

$$A + C\bar{C} + 3\,CH + H \;\rightarrow\; C_3\,A.\,C\bar{C}.\,H_{12} \quad Monocarboaluminate \qquad \text{(Eq. 7)}$$

Besides, Limestone imparts a filler effect [91] that causes hydration acceleration of Portland Clinker grains (esp. C_3A) at early ages [92] which:

- Improves the particle packing of the cementitious system.
- Provides new nucleation sites for calcium hydroxide.
- Produces the formation of calcium carboaluminate as the result of the reaction between C_3A and $CaCO_3$.

Figures 6 and 7 show a simulated model for illustrating the influence of limestone as fine filler, providing additional surfaces for the nucleation and growth of hydration products, the microstructural development substitution of limestone after hydration, and at a degree of hydration of 0.9 [92].

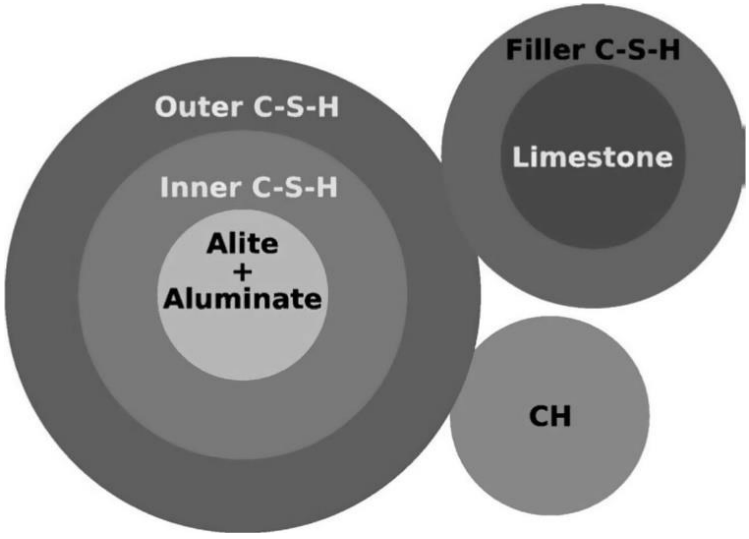

Figure 6. Example of different materials and particle types defined in a simulation [92]

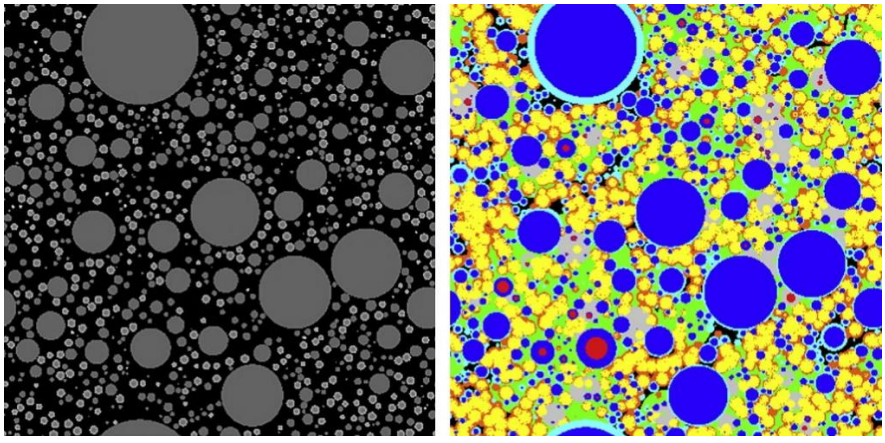

Figure 7. A slice from the simulation of 20% limestone substitution of cement paste. Fraction the pore are shown in black, alite in dark grey and limestone in white. (Left) slice before hydration, (right image) after 0.9 hydration, where all hydration compounds [92]

In LC^3 method [93] it was claimed that by the addition of both calcined clay and limestone to cement, much stronger pozzolanic reactivity than calcined clay can be obtained [57]. The pozzolanic reaction uses CH which is produced during the hydration reaction and produces more C-S-H or C-A-S-H by incorporation of aluminum. Since the pozzolanic reaction is dependent on the CH formation (Eq. 2), it takes time to begin. Furthermore, the silica reacts slowly in the pozzolanic reaction since it involves the dissolution of $(SiO_4)^{4-}$ and $(AlO_4)^{6-}$. Hence, the pozzolanic reaction mostly provides late strength. This is one of the reasons that SCM could only be a partial replacement for cement [89, 94]. Besides, calcined clay's highly reactive aluminate will react with more calcite. The affinity between monocarbonate obtained from limestone reactions and the aluminous content of the pozzolanic material makes it beneficial to use both limestone and calcined clays in the blended cement [57, 85, 87, 95, 96].

There are already some studies focused on utilizing pozzolanic materials such as calcined clays and finely ground virgin limestone particles as substituent materials in the cement structure [20, 39-42, 57]. On the other hand, calcite can also be decomposed in a temperature range of 700-900ºC [97]. The calcination of carbonate would result in free lime and carbon dioxide. Heat treatments at temperatures in excess of 900ºC cause reactions between clays and carbonate leading to metastable calcium aluminosilicates (e.g Wollastonite, Anorthite, and Gehlenite) [87, 98-100]. Traore et al. [99] mentioned the formation of calcium aluminosilicate between 820-905ºC. Gehlenite was observed to form in the temperature range of 850-1000ºC [61, 100]. Mokhtari et al [48] carried out a calcination process on a schist type material containing clays and calcium carbonate to use it as cement substituent. This study investigated the effect of calcined clay + calcined carbonate on cement strength and indicated that it is possible to achieve a reasonable strength by using calcined clay and calcined carbonate as a cement substituent.

In this study, the effect of limestone and calcined limestone on the blended cement properties has been evaluated for different activated calcium carbonate amounts. Activated aluminosilicates and calcium-containing carbonate phases were shown to take part in the hydration reactions of blended Portland cement. This composite cement can maintain its mechanical properties even if amounts as high as 30 wt% of pozzolanic materials and calcium carbonates were used to replace OPC.

1.3. Aims of this work

1. As it was mentioned, in the previous studies in literature kaolinite was activated as the simplest clay structure and it is very easy to be decomposed. Production of pure kaolinite is not that affordable and there is a rare mine of kaolinite in the world with feasible purity. In this work, we activated a schist-type material which is mainly mine overburden. Schist type material is widely accessible in the whole world and affordable to exploit. Schist consists of quartz, clay, feldspar, carbonates, and some other chemical phases. In most cases, the clayey portion of the schist consists of complex structure clays such as smectite, illite, montmorillonite, and muscovite. Furthermore, in this study activation of feldspars in order to be used in OPC replacement has been investigated for the first time. We have received almost waste materials, reactivated them, and used them as a pozzolan.

2. In LC^3 technology, the pure and not-treated limestone was added to the mixture of OPC and pozzolanic material in order to make carboaluminate which is another minor strength provider in composite cement. However, in this work, we decided to take the advantage of calcined carbonate (activated to Calcia). To this end, schist type materials augmented with additional calcite went through a calcination process together, instead of separate calcination. This will provide an excess source of calcium ion according to Eq. 1 and 2. By adding several amounts of calcined limestone to OPC, the Ca/Si ratio of C-S-H will also be controlled. Briefly, we show how the SCMs can be adjusted in their Ca/Si ratio with the aim of generating certain types of crystalline C-S-H (tobermorite or jennite) with certain properties.

3. In any other study related to this topic, all information about the calcination method was summarized as temperature and time. However, there are some errors arising from these two parameters due to the difference in the amount of material between laboratory scale and industrial scale. As it was mentioned earlier, it is better to define a parameter that does not change with the sample's mass. This parameter is the ENERGY that we induce to the material during calcination. In this way, we will be able to reactivate any type of clayey material on any scale. None of the existent studies have talked about this constrain to achieve the maximum activation of clayey materials without dead-burning them.

CHAPTER 2

2. Materials and Experimental Procedures

2.1. Materials

Five different schist-type samples taken from two different mines were used in this study that the main experimental procedures were performed on them; Muratbey and Ladik samples. These two samples were taken from two different mines belonging to AkcanSA cement manufacture in Istanbul/Turkey and Samsun/Turkey. In Muratbey mine, there were four different sections with different colors. This color variety could be an indication of variation in chemical composition as well. Therefore, four samples with different colors were taken from the different parts of this mine; Green (G), Brown-Chocolate (C), Pink (P), and Black (B). In addition, only one type of schist sample was also taken from the Ladik quarry designated as L. After performing a grinding process on the schist samples at AkcanSA cement manufacture, chemical compositions, phase structure, and also the potential of the all as-received (virgin) powders were evaluated with the help of the listed characterization methods. Figure 8 shows the ground schist-type samples.

Figure 8. Ground powder schist-type samples ready for activation as a) G, b) C, c) P, d) B, and e) L

Two different types of limestone powders ($C\bar{C}$) from the Muratbey and Ladik quarries with a particle size of ≤ 5 µm was provided by AkçanSA.

The feldspar (Albite) powder was provided by ESAN industrial mineral and metallic mineral producer company. The listed characterization methods were also carried out on the as-received albite sample.

The Ordinary Portland Cement (OPC) which is an ENS 197-1 CEM 42.5 R type cement was also provided by AkçanSA Cement Manufacturer.

Besides, some materials were used in experiments as additives or benchmark samples such as pure kaolin (from SIGMA-ALDRICH), $Ca(OH)_2$ (from EMSURE), and NaOH (from EMBOY).

2.2. Experimental Procedures

All schist samples (G, C, P, B, and L) and also the feldspar sample (albite) went through a specific (thermal or mechanical) activation process. The process was performed either on as-received or calcium carbonate augmented schists. All activated samples were then analyzed with the help of several characterization methods. Afterward, the activated samples were added to OPC paste as SCMs to check the effects of the schists on the strength development.

2.2.1. Thermal Activation Process

The decomposition behavior of schist-type materials with and without carbonate additions was investigated with the help of TGA. In addition, total weight losses due to de-hydroxylation were calculated. According to the thermal decomposition behavior observed in the thermal analysis, a safe and optimum activation degree for the virgin schists and also the schists augmented with calcium carbonate was determined. Proper activation requires calcination at temperatures that assure de-stabilization of clayey minerals without overheating which may cause dead burning. To check the effect of calcination temperature accurately, the samples were calcined up to the calcination temperature associated with 80%, 100%, and “110%” of their total weight losses. Therefore, the proper calcination temperature for each sample was calculated.

All virgin Powders were then heat-treated up to the calculated proper temperature with a heating rate of 10°C/min. The calcination method steps are as follows: 150 g of each powder was put into a crucible, first heated up to the starting point of the decomposition which is generally 300℃ for most of the samples. To homogenize the heat distribution within the powder, a dwell time of 1 hour was performed at this temperature. Subsequently, they were heated up to the temperature associated with 80%, 100%, or 110% of total weight losses and kept there for 2 hours. Afterward, air quenching was performed on the heat-treated powders to cool them down to room temperature.

To investigate the effect of activated calcium carbonate on the strength development of SCM added OPC, a certain amount of limestone powder was added to the virgin schist samples. The carbonate amount in schist powders was varied from 15 to 30 wt%. The $C\bar{C}$ augmented samples were denoted as G_{Lx}, B_{Lx}, P_{Lx}, $K_{Lx,}$ and L_{Lx} that x indicates the total $C\bar{C}$ wt% inside the schist sample and $0<x\leq30$. The upper limit of calcium carbonate content was chosen as 30 wt% in order not to produce extra Portlandite (CH) during the hydration of composite cement. Calcium carbonate added schists were subjected to the same heat treatment as the virgin powders, such that the decomposition was driven to 80%, 100%, or 110% of the total weight loss of the sample. These calcination temperatures were usually higher than the temperatures for samples without calcium carbonate additions.

Moreover, in order to be more precise about the calcination method, we decided to calculate the energy given to each sample during calcination with the help of DSC test method. To this end, some schist samples which contain different portions of clay and calcium carbonate were analyzed by DSC. These clayey samples were L, $L_{L15,}$ and L_{L30}. Additionally, to confirm the accuracy of the characterization method and calculations, one more DSC test was also performed on a pure kaolinite sample as a benchmark. The DSC test can be used to measure some thermal behavior of the materials such as the heat capacity or the change of enthalpy (ΔH) for dramatic phase transformation processes, chemical reactions, decomposition, ionizations, dissolutions in solvents, and vacancy formation. The DSC measurement setup consists of a furnace and an integrated sensor connected to thermocouples with designated positions for the sample and the reference pans. The temperature of the sample and the reference are controlled independently using separate but identical ovens. The DSC measurement is carried out in three steps: baseline measurement using empty pan and reference, standard reference measurement to test accuracy, and the sample measurement. In order to calculate the enthalpy change of any thermal event with the help of the Heat Flow - Temperature curve extracted from DSC, the following steps need to be taken into account: 1) Integrate the area under the peak for the thermal event. 2) Find the total weight loss associated with the same thermal event. 3) With respect to the total weight loss value, calculate the real weight of the decomposed phase (or phases) according to the chemical formula. 4) Divide the integrated number by the real weight associated with the same thermal event.

2.2.2. Mechanical Activation Process

As it was mentioned earlier, most of the schist-type materials contain feldspar minerals (besides clays) which are not activatable by heat-treatment. For this reason, a mechanical activation process was carried out on the L sample with and without $C\bar{C}$ additions. The mechanical activation method was a common ball-milling process in which 350 g of virgin L, heat-treated L, and heat-treated L_{L30} were ball-milled with alumina balls (d = 10 mm) for 24 hours, with a rotation speed of 150 rpm, and the ball to powder volume ratio of 1:2. To control the effect of ball-milling, all of the mechanically activated samples were also analyzed by XRD and SEM before and after activation.

In order to de-stabilize (activate) the pure albite, several ball-milling processes were also carried out with the procedures as follow:

- 100 g of as-received albite was ball-milled for 6 and 24 hours – balls: alumina (d = 10 mm) – ball to powder volume ratio: 1:2 – common ball milling – rotating speed: 200 rpm
- 100 g of as-received albite was ball-milled for 6 and 24 hours – balls: steel (d = 9 mm) – ball to powder volume ratio: 1:2 – common ball milling
- 30 g of as-received albite was ball-milled for 15 and 30 minutes – balls: steel (d = 9, 5, 3 mm) – ball to powder volume ratio: 1:2 – planetary ball milling – rotating speed: 35 hertz or 2100 rpm
- 100 g of albite-$Ca(OH)_2$-NaOH mixture (70 wt%-15 wt%-15 wt%) was ball-milled for 24 hours – balls: steel (d = 9 mm) – ball to powder volume ratio: 1:2 – common ball milling
- 100 g of albite-$Ca(OH)_2$-NaOH mixture (70 wt%-15 wt%-15 wt%) was ball-milled with water for 24 hours, dried in the oven and ground – balls: steel (d = 9 mm) – ball to powder to water volume ratio: 1:2:1 – common ball milling

These samples were also analyzed by XRD and SEM to check the effects of ball-milling and also the additives.

2.2.3. Composite Cement Paste Samples

Schist type materials with and without carbonate additions were activated by a proper activation method. These SCMs were added to the ordinary Portland cement on the order of about 30 wt% to generate blended cement composites. Subsequently, these cement composites were tested for their strength development. Several composite cement paste samples were prepared for strength measurement. These composite cement paste samples were obtained by mixing 700 g of cement, 300 g of one of the activated schist or schist+limestone materials, and 500 g (500 mL) of water (water/solid ratio of 0.5). Composite cement cubic samples were then prepared for compression test in the molds with the dimensions of 40×40×40 mm. The strength of the composite cement samples was benchmarked with pure OPC paste, prepared with the same procedure. After 24 h, the molded samples were separated from the molds and put into circulating water kept at 23°C. Samples were tested after 2, 7, 28, 50, and 90 days of hydration. In addition, the phase distribution of the composite cement samples was investigated with the aid of XRD analysis after the mentioned days of hydration.

2.3. Characterization Methods

2.3.1. Thermal Analysis

Thermo-gravimetric analysis of the samples was done in a temperature range between 30ºC and 1000ºC under Nitrogen gas using simultaneous thermal analysis equipment [TGA/DTA] (NETZSCH STA 449 JUPITER, Selb, Germany). To eliminate the oxygen in the air which could react with some components of samples (e.g. Sulfur and graphite) the TGA was done under a Nitrogen atmosphere. The heating rate was 10 K/min. Only 50 mg of powder sample was used in every run. According to the thermogravimetric analysis of each schist sample, some beneficial data about the decomposition behavior of the sample would be extracted. Briefly, a TGA graph related to each virgin schist sample indicates the temperature ranges of the clay and $C\bar{C}$ decomposition (weight loss), and the amount of weight loss relates to the potential reactivity of it. Based on this information, the proper temperatures for activating the schists were determined. Additionally, in order to control the effectiveness of the calcination process to reach the desired activation, heat-treated powders were evaluated again by TGA.

Moreover, in order to measure the energy consumption of the materials during decomposition, the second type of thermal analysis DSC measurement [Differential Scanning Calorimetry - DSC] (Mettler Toledo TGA/DSC) was performed on the materials. The temperature range, heating rate, and the atmosphere were the same as TGA analysis.

2.3.2. Phase Analysis

In order to determine the phase content of schist and albite samples, quantitative XRD analysis was employed. X-ray diffraction analysis was done using Bruker D2 phaser (Bruker AXS GmbH, Karlsruhe, Germany) diffractometer utilizing Cu-Kα (λ=1.54 Å) radiation. The divergence slit size is fixed and was 0.5°. Samples were scanned on a rotating stage between 5 to 90 [$°2\theta$] using a step size of 0.02 $°2\theta$ and time per step of 1s. Rietveld analysis was carried out to quantify the amount of clayey and inert phases. In addition, the so-called "amorphousness" to the crystallinity ratio of all samples was determined by using the same software. It is noteworthy to state that these ratios which were directly calculated by the software are not reliable. To get the true values, they should be corrected. The XRD diffractogram of thermally or mechanically activated powders was also analyzed and compared to the virgin powders to observe the outcome of the activation processes. It should be mentioned that in the case of $C\bar{C}$ added samples, powder, the comparison was performed between schist with calcium carbonate (before activation) and the same mixture after activation.

2.3.3. Microstructure Analysis

To identify the changes that occurred during thermal or mechanical activation in the microstructure, powders before and after activation were investigated using a scanning electron microscope (LEO Supra 35VP field emission, ZEISS, Oberkochen Germany) equipped with an Energy Dispersive X-ray microanalyzer (EDX – Roenteg, Xflash, Karlsruhe, Germany). Imaging of samples was done by using an ET-type Secondary Electron detector and an aperture size of 30 µm. Images of powder samples were taken at different magnifications to show the overall appearance of powder morphology as well as changes that occurred due to the activation process. EDX analysis and x-ray mapping of the samples were done at an accelerating voltage of 20 kV.

2.3.4. Compressive Strength Measurements

Evaluation of the effect of activated samples on the early and late strength of blended cement pastes was done by performing a compression test were on all composite cement samples. The compressive strength measurement is the best indication to evaluate the potential candidates for cement substitution. This test was carried out on the 40×40×40 (mm) composite cement paste cubic samples until failure using a compression test machine (MATEST E161N Servo-plus Evolution, Bergamo, Italy). For each composition and each hydration time, the given compressive strength values in the results section are the average of the strength of three samples. The compressive strength of the activated schist or activated schist+carbonate added blended cement samples were then compared to each other and to the 100% OPC samples to evaluate the effects of activated clay materials and also limestone on the early and late strength.

CHAPTER 3

3. Results

3.1. Characterization of Untreated (as-received) Materials

Before performing any activation process, the virgin (as-received) materials first should be assessed with the help of some common characterization methods. This evaluation step guides us to identify the elements and phases and also to anticipate the pozzolanic potential of each schist-type material. Therefore, it would be useful on designing an appropriate method for activating them to use as a pozzolan source.

3.1.1. Phase Distribution Analysis

In order to assess the phase distribution and the amounts of crystalline or amorphous content within the samples, XRD analysis was performed. Figures 9-14 illustrate the x-ray diffractograms of G, C, P, B, L, and Albite samples without any modification on carbonate amounts, respectively. In addition, tables 3-7 list the quantitative phase composition of the same samples and the atomic percentage of each phase. The physical and chemical information of the listed phases (i.e. crystal structure and chemical formula) is also included in the tables. The numbers at the peaks in the figures correspond to the phases listed in tables.

3.1.1.1. G Schist

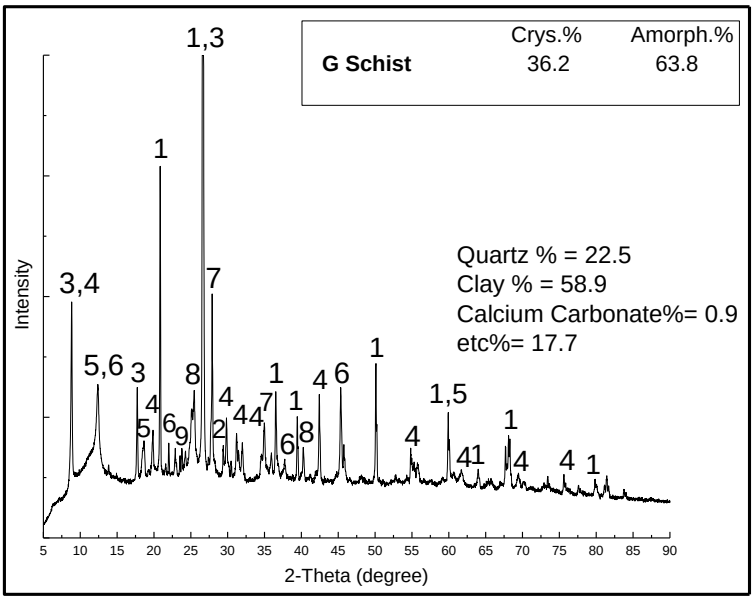

Figure 9. XRD spectra of G schist powder (as-received). The peaks are labeled with numbers are corresponding to the numbers and the phases given in table 3.

Phase analyses of G schist powder indicated that this sample contains 36.2% crystalline phases besides 63.8% amorphous content. The crystalline phases including quartz, calcite, and several types of clay minerals are listed in table 3.

Table 3. The phase distribution, the atomic percentage and chemical formula of each phase, and information about the crystal structure of G virgin powder

Peak Number	Chemical Phases	at%	Crystal Structure	Chemical Formula
1	Quartz	22.5	Hexagonal	SiO_2
2	Calcite	0.9	Rhombo	$CaCO_3$
3	illite	24.5	Monoclinic	$(K, H_3O)Al_2Si_3AlO_{10}(OH)_2$
4	Muscovite	23.1	Monoclinic	$KAl_2Si_3AlO_{10}(OH)_2$
5	Clinochlore	6.5	Monoclinic	$(Mg_{2.96}\,Fe_{1.55}\,Fe_{1.36}\,Al_{1.275})(Si_{2.622}\,Al_{1.376}O_{10})(OH)_8$
6	Dickite	4.8	Monoclinic	$Al_2Si_2O_5(OH)_4$
7	Anorthite	12.1	Triclinic	$Na_{0.25}Ca0_{.71}(Al_2Si_2O_8)$
8	Titanium Oxide	1.8	Monoclinic	Ti_3O_5
9	Albite	3.8	Triclinic	$(Na\ ,Ca)(Si,\ Al)_4O_8$

The amount of inert quartz phase was calculated by software as 22.5 at% and the total clayey content portion was around 58.9 at%, including illite, muscovite, clinochlore, and dickite. The dominant clayey phase is illite (24.5 at%). During the activation process, the degree of activation of these chemical phases could determine the reactivity of the schist type sample. Note that only dickite (4.8 at%) is a kaolinitic-type clay with a simple structure and easy to be activated. The other types of clay minerals have more complex structures and are estimated to be decomposed at slightly higher temperatures. The amount of calcium carbonate phase was calculated as 0.9 at%. Other phases including minor amounts of feldspars (albite and anorthite) and titanium oxide constituted 17.7 at%.

3.1.1.2. C Schist

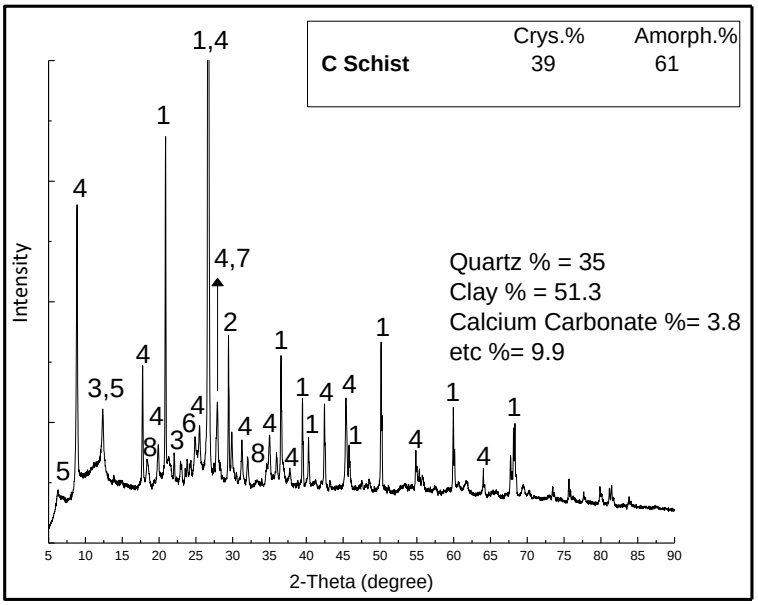

Figure 10. XRD spectra of B schist powder (as-received). The peaks are labeled with numbers are corresponding to the numbers and the phases given in table 4.

The G and C schist-type materials were taken from two neighboring mines, and they have similar chemical and phase compositions as expected. However, there were some differences in their clayey contents. In addition, the calcium carbonate amount in C sample is higher than G. The XRD software also estimated 39% crystalline versus 61% amorphous content in C sample. These values were similar to G schist.

Table 4. The phase distribution, the atomic percentage and chemical formula of each phase, and information about the crystal structure of C virgin powder

Peak Number	Chemical Phases	at%	Crystal Structure	Chemical Formula
1	Quartz	35	Hexagonal	SiO_2
2	Calcite	3.8	Rhombo	$CaCO_3$
4	Muscovite I	28.2	Monoclinic	$KAl_2(AlSi_3O_{10})(OH)_2$
4	Muscovite II	16.1	Hexagonal	$(K, Na)(Al, Mg, Fe)_2(Si_{3.1}Al_{0.9})O_{10}(OH)_2$
9	Albite	4	Triclinic	$(Na, Ca)(Si, Al)_4O_8$
5	Clinochlore	3.3	Monoclinic	$(Mg_5Al)(Si, Al)_4O_{10}(OH)_8$
3	Kaolinite	3.7	Triclinic	$Al_2(Si_2O_5)(OH)_4$
7	Anorthite	5	Triclinic	$Ca(Al_2Si_2O_8)$
8	Titanium Oxide	0.9	Orthorhombic	Ti_3O_5

As it can be seen in table 4, the clayey portion of this schist was 51.3 at% and the calcium carbonate content was 3.8 at%. The dominant crystalline clay phase is muscovite (44.3 at%) which an illitic type clay, known as a complex clay. Other crystalline phases including anorthite and albite feldspars that have glass-like chemical compositions and also titanium oxide were around 9.9 at%.

3.1.1.3. P Schist

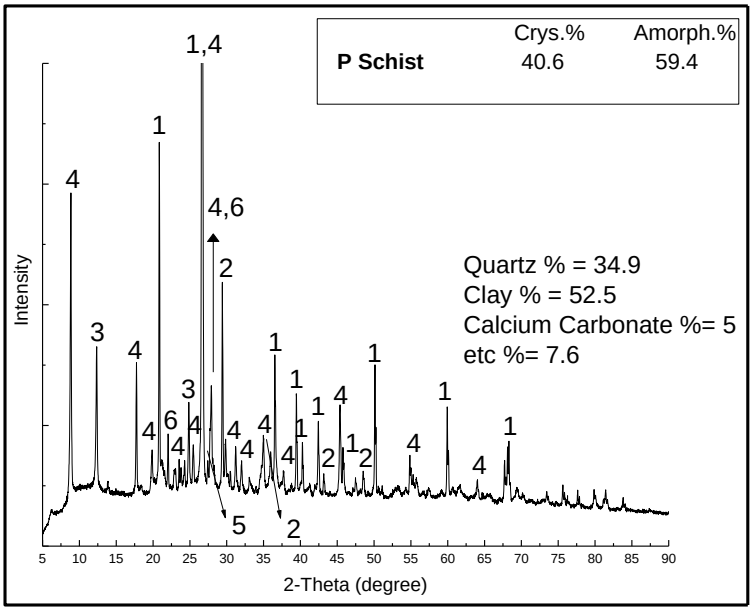

Figure 11. XRD spectra of P schist powder (as-received). The peaks are labeled with numbers are corresponding to the numbers and the phases given in table 5.

The XRD software determined 40.6% crystallinity and 59.4% amorphous content for the P schist sample. The inert quartz phase was estimated ~34.9 at% while it contained 52.5 at% of clayey phases. The calcium carbonate amount is ~5 at% which is still low for a strong influence on cement hydration reactions. Table 4 lists the phase composition of P sample and their crystal structure and weight percentages.

Table 5. The phase distribution, the atomic percentage and chemical formula of each phase, and information about the crystal structure of P virgin powder

Peak Number	Chemical Phases	at%	Crystal Structure	Chemical Formula
1	Quartz	34.9	Hexagonal	SiO_2
2	Calcite	5	Rhombo	$CaCO_3$
3	Kaolinite	5.85	Triclinic	$Al_2(Si_2O_5)(OH)_4$
4	Muscovite I	28.4	Monoclinic	$K(Al_{1.88}Fe_{0.12})(Si_3Al)O_{10}(OH)_2$
4	Muscovite II	18.2	Hexagonal	$(K, Na)(Al, Mg, Fe)_2(Si_{3.1}Al_{0.9})O_{10}(OH)_2$
8	Rutile	0.4	Tetragonal	Ti_3O_5
9	Albite	5.8	Triclinic	$NaAlSi_3O_8$

The clayey structures of P sample included kaolinite with a simple structure and muscovite with a more complex structure than kaolinite. According to the x-ray diffraction analysis results, this sample also contained 5.8 at% of albite and a very small amount of rutile (0.4 at%). In this schist, the feldspar portion is lower than G and C samples.

3.1.1.4. B Schist

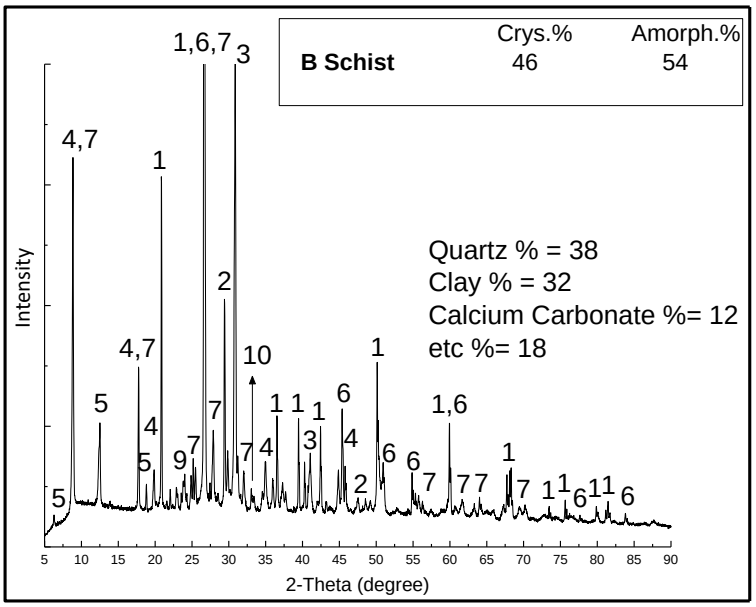

Figure 12. XRD spectra of B schist powder (as-received). The peaks are labeled with numbers are corresponding to the numbers and the phases given in table 6.

XRD analysis indicated that the virgin B schist powder contains 46% crystalline and 54% amorphous amounts. The amount of crystalline phases in the B sample is higher than in G, C, and P samples. Crystalline phases included quartz, calcite, ankerite, graphite, pyrite, a type of feldspar minerals (albite), and also various types of clayey minerals. The amount of inert quartz phase was estimated as 38 at% and the total clayey content portion was around 32 at%. The dominant clayey phase is muscovite (19.7 at%) which has a complex structure. The other types of clays which are listed in Table 6 have also complex structures. The lack of kaolinitic clay structures in this sample would affect the decomposition behavior of clays during the activation process. The amount of calcium carbonate was calculated as ~19 at% (calcite + ankerite) and the amount of feldspar (albite) was 3.7 at% which is counted as a small amount. Other phases constituted ~6.4 at%.

Table 6. The phase distribution, the atomic percentage and chemical formula of each phase, and information about the crystal structure of B virgin powder

Peak Number	Chemical Phases	at%	Crystal Structure	Chemical Formula
1	Quartz	38	Hexagonal	SiO_2
2	Calcite	4.7	Rhombo	$CaCO_3$
3	Ankerite	14.3	Rhombo	$Ca(Mg_{0.67}Fe^{+2}_{0.33})(CO_3)_2$
4	Muscovite I	19.7	Hexagonal	$(K, Na)(Al, Mg, Fe)_2(Si_{3.1}Al_{0.9})O_{10}(OH)_2$
5	Clinochlore	3.7	Monoclinic	$(Mg_{2.8}Fe_{1.7}Al_{1.2})(Si_{2.8}Al_{1.2})O_{10}(OH)_8$
6	Graphite	5	Hexagonal	C
7	Mg-Annite	8.77	Monoclinic	$K(Mg, Al)_{2.04}(Si_{3.34}A_{l0.66})O_{10}(OH)_2$
8	Rutile	1.32	Tetragonal	TiO_2
9	Albite	3.7	Triclinic	$NaAlSi_3O_8$
10	Pyrite	0.9	Cubic	FeS_2

3.1.1.5. L Schist

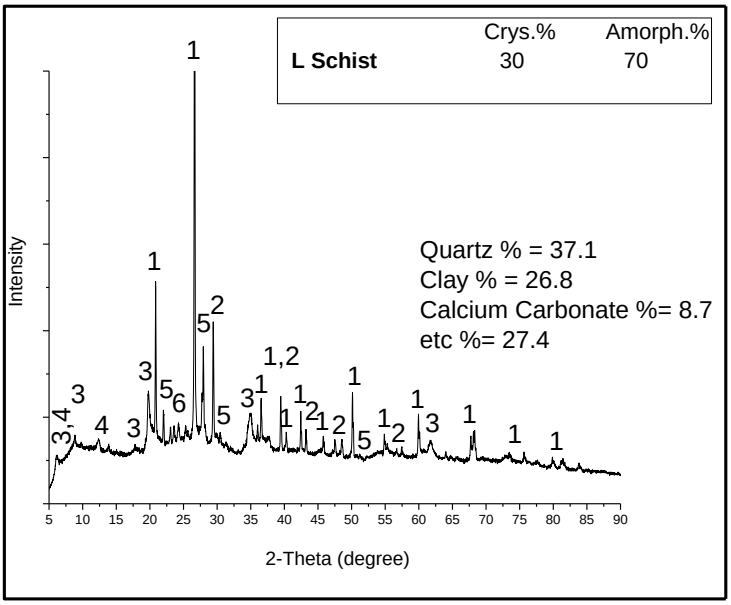

Figure 13. XRD spectra of L schist powder (as-received). The peaks are labeled with numbers are corresponding to the numbers and the phases given in table 7.

The crystalline phase portion of the L schist which was taken from a different mine is ~30% and its amorphousness was ~70%. The quartz phase amount was nearly the same as the other samples. The main difference between this schist and the other four samples was its lower clay content.

Two different clayey phases were detected in this sample with a total portion of ~27 at%. Both clayey phases (montmorillonite and Clinochlore) are smectite type clay with a complex structure. Besides, a considerable amount (25.4 at %) of feldspar (albite) was also detected in L sample. As it was mentioned, the feldspar aluminosilicate minerals are rarely activatable by thermal treatments.

Table 7. The phase distribution, the atomic percentage and chemical formula of each phase, and information about the crystal structure of L virgin powder

Peak Number	Chemical Phases	at%	Crystal Structure	Chemical Formula
1	Quartz	37.1	Hexagonal	SiO_2
2	Calcite	8.7	Rhombo	$CaCO_3$
3	Montmorillonite	8.9	Monoclinic	$(Na, Ca)_{0.3}(Al, Mg)_2Si_4O_{10}(OH)_2.xH_2O$
3	Montmorillonite-22A	9.4	Monoclinic	$Na_{0.3}(Al, Mg)_2Si_4O_{10}(OH)_2.8H_2O$
4	Clinchlore	8.5	Monoclinic	$(Mg_{2.96}Fe_{1.55}\ Fe_{0.136}Al_{1.275})(\ Si_{2.622}Al_{1.376}O_{10})(OH)_8$
5	Albite	25.4	Triclinic	$(Na, Ca)\ (Si, Al)_4\ O_8$
6	Titanium Oxide	2	Orthorhombic	Ti_3O_5

3.1.1.6. Albite

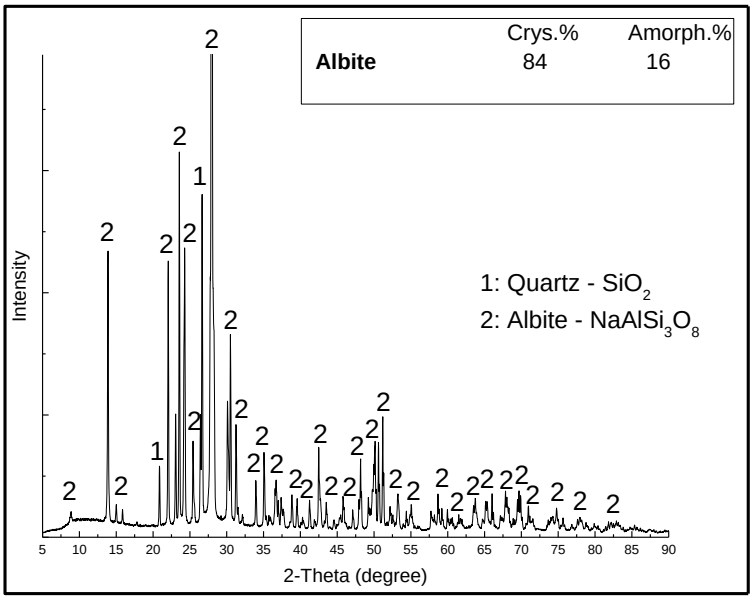

Figure 14. XRD spectra of Albite feldspar powder (as-received).

As it is visible in figure 14, XRD analysis of albite indicated that this sample contains 84% crystalline phases including albite and a small portion of quartz as impurity.

3.1.2. Thermal Decomposition Behavior

The main purpose of this study is to determine the most appropriate method for activation of any type of aluminosilicate materials together with limestone ($C\bar{C}$) in order to use for cement partial substitution. In this regard, it is very important to find a proper calcination temperature for a schist-limestone mixture. The calcination temperature should be enough for the decomposition and activation of the clayey minerals and also limestone. In addition, it should not be so high such that causes overheating and dead-burning of clay. To determine the best calcination temperature that should be applied to each sample, the TGA analysis was performed. The results threw light into the thermal decomposition behavior of the samples. In the subsequent section, first, we will go through the TGA-DTG diagram of each virgin (as-received) powder including G, C, P, B, and L schist samples. These TGA-DTG diagrams illustrate the decomposition temperature ranges associated with the activatable phases i. e. clays, and $C\bar{C}$. Afterward, the TGA diagrams and total weight losses of the schist and limestone augmented schist with different amounts of $C\bar{C}$ will be presented. The proper calcination temperatures were calculated based on the TG analyses of the schist and schist+carbonate samples. The calcination temperature of each schist or limestone augmented schist will correspond to 80%, 100%, or "110%" of the total weight loss due to de-hydroxylation reactions of the same sample. The proper calcination temperatures extracted from the TGA diagrams are listed in Tables 8-12. For the albite sample, only the TGA-DTG diagram is presented.

3.1.2.1. G Schist

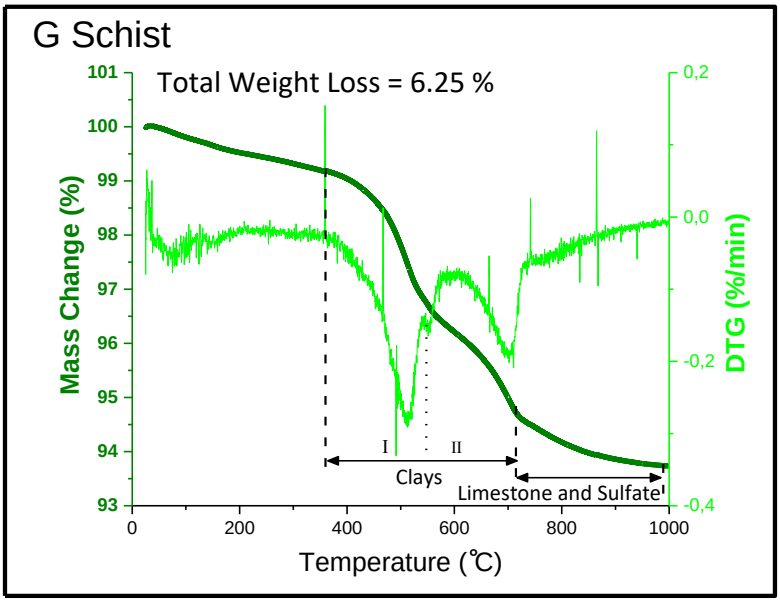

Figure 15. TGA/DTG analysis of G schist powder (as-received) – Left axis: TGA (mass change), Right axis: DTG

Figure 15 illustrates the TGA/DTG diagram of the G sample. The TGA diagram shows that the total weight loss due to the clay and carbonate decomposition of this sample between 0-1000℃ was 6.25 wt%. According to the DTG diagram, there were three decomposition ranges associated with different existing phases. The low-temperature weight loss up to 300ºC was related to the non-structural water existing as moisture inside the powder. The main decomposition started around 350°C, and this decomposition reaction went up to ~650°C. This weight loss was probably related to the decomposition of clayey materials. Since there are several types of clayey components in the schist samples, DTG showed a series of weight losses in the temperature range associated with the de-hydroxylation of clayey materials (350-650℃). The total weight loss associated with clayey phases was around 5 wt%. The last decomposition range that started around 650℃ was most likely related to calcium carbonate decomposition which generally takes place between 650°C to 850°C.

Figure 16 shows the TGA diagram of untreated virgin and limestone augmented G schist sample.

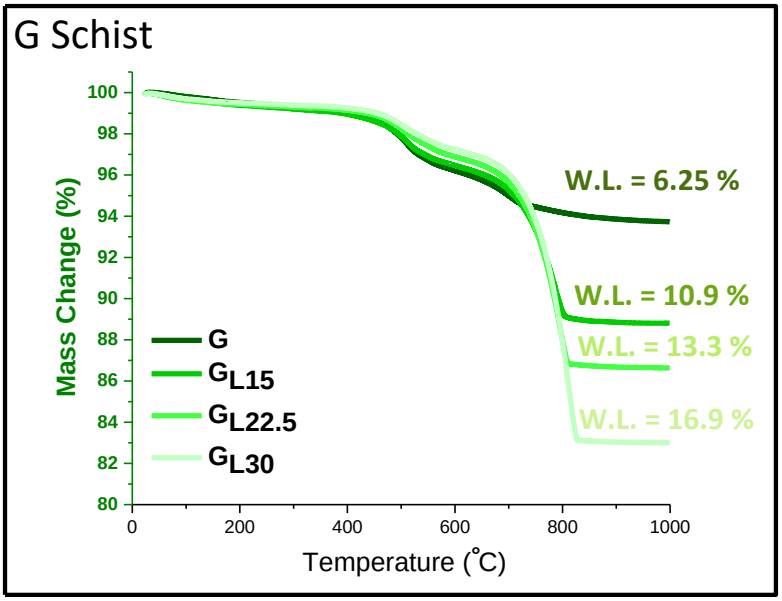

Figure 16. TGA diagram of G: G schist (as-received), G_{L15}: G schist with 15 wt% $C\bar{C}$ addition, $G_{L22.5}$: G schist with 22.5 wt% $C\bar{C}$ addition, and G_{L30}: G schist with 30 wt% $C\bar{C}$ addition

Based on TG analysis of each schist or schist+carbonate mixture, the calcination temperatures that would correspond to 80%, 100%, and "110%" of the total weight losses due to de-hydroxylation or decomposition reactions were calculated. These temperature ranges are listed in Table 8.

Table 8. Calcination temperatures and total weight loss for virgin or limestone augmented G schist

Sample	Total weight Loss (wt%)	Calcination Temperature 80% of total weight loss (°C)	Calcination Temperature 100% of total weight loss (°C)	Calcination Temperature 110% of total weight loss (°C)
G	6.25	640	900	1000
G_{L15}	10.9	770	950	1050
$G_{L22.5}$	13.3	790	-	-
G_{L30}	16.9	810	-	-

3.1.2.2. C Schist

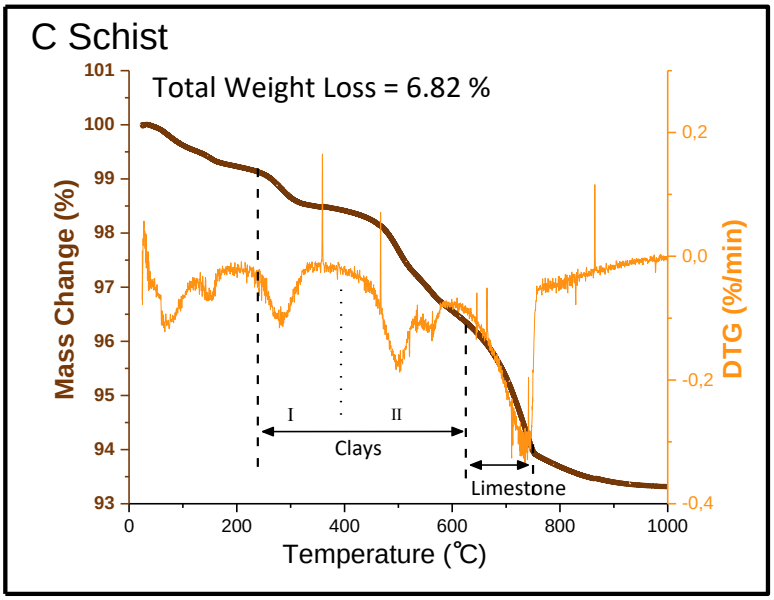

Figure 17. TGA/DTG analysis of C schist powder (as-received) – Left axis: TGA (mass change), Right axis: DTG

The total weight loss due to the clay and carbonate decomposition in the C sample was 6.82 wt% which was not very different than G. The low-temperature weight loss up to 250ºC again was related to the moisture inside the powder. The thermo-gravimetric analysis of this sample represented the early decomposition of some clayey components. The first DTG peak after 250°C must be related to kaolinite decomposition (part I in figure 17) and the other weight losses (part II) until 650°C was associated with decomposition of the more stable clayey materials i. e. muscovite and clinochlore. The carbonate decomposition took place between 650°C to ~800°C.

Figure 18 shows the TGA diagram of untreated virgin and limestone augmented C schist sample.

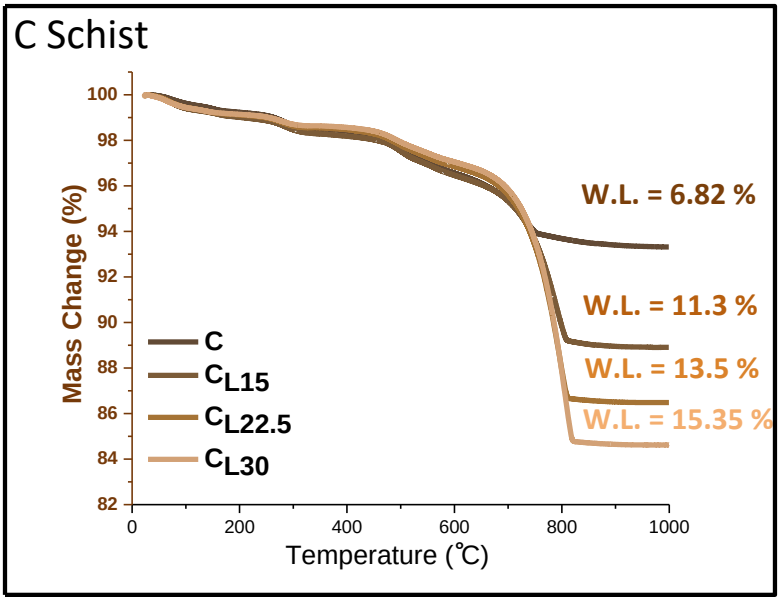

Figure 18. TGA diagram of C: C schist (as-received), C_{L15}: C schist with 15 wt% $C\bar{C}$ addition, $C_{L22.5}$: C schist with 22.5 wt% $C\bar{C}$ addition, and C_{L30}: C schist with 30 wt% $C\bar{C}$ addition

According to TGA diagrams of C schist and limestone augmented C schist, the calcination temperatures that would correspond to 80% and of the total weight loss due to de-hydroxylation or decomposition reactions were calculated and listed in Table 9.

Table 9. Calcination temperatures and total weight loss for virgin or limestone augmented C schist

Sample	Total weight Loss (wt%)	Calcination Temperature 80% of total weight loss (℃)
C	6.82	680
C_{L15}	11.3	770
$C_{L22.5}$	13.5	790
C_{L30}	15.35	810

3.1.2.3. P Schist

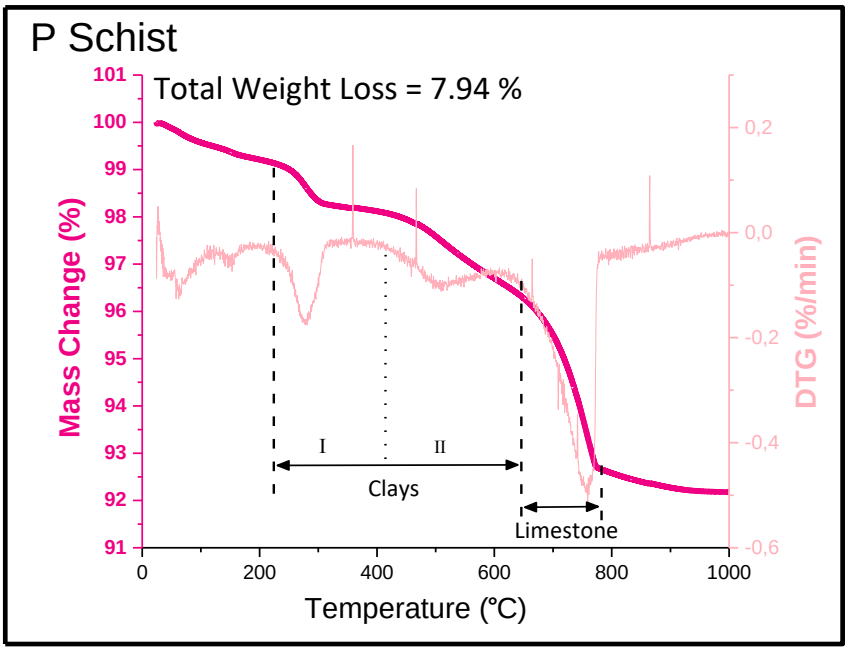

Figure 19. TGA/DTG analysis of P schist powder (as-received) – Left axis: TGA (mass change), Right axis: DTG

As it can be seen in figure 19, the total weight loss due to the decomposition of clay and carbonate phases in the P sample was around 7.94 wt%. The first weight loss (up to ~250°C) in the TGA graph was related to the evaporation of non-structural water. The de-hydroxylation of clayey phases including kaolinite (I) and muscovite (II) took place between 250-650°C. At the end of this temperature range, decomposition of the calcium carbonate phase started and continued till 800°C.

Figure 20 illustrates the TGA diagram of untreated virgin and limestone augmented P schist sample.

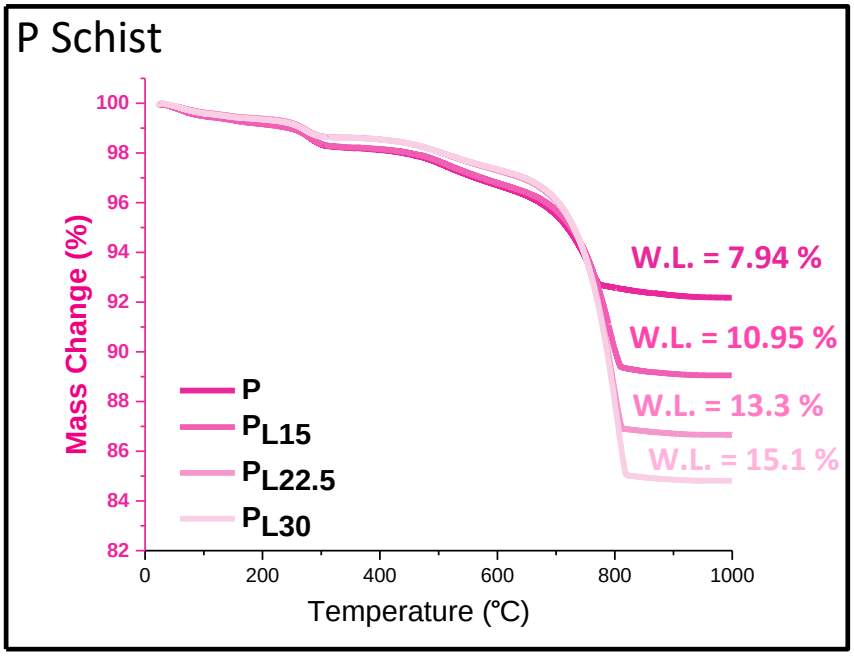

Figure 20. TGA diagram of P: P schist (as-received), P_{L15}: P schist with 15 wt% $C\bar{C}$ addition, $P_{L22.5}$: P schist with 22.5 wt% $C\bar{C}$ addition, and P_{L30}: P schist with 30 wt% $C\bar{C}$ addition

According to the TG analysis and total weight losses of P schist or limestone augmented P samples, the proper calcination temperatures that would correspond to 80% of the total weight losses due to de-hydroxylation or decomposition reactions were calculated and listed in Table 10.

Table 10. Calcination temperatures and total weight loss for virgin or limestone augmented P schist

Sample	Total weight Loss (wt%)	Calcination Temperature 80% of total weight loss (°C)
P	7.94	740
P_{L15}	10.95	770
$P_{L22.5}$	13.3	790
P_{L30}	15.1	810

3.1.2.4. B Schist

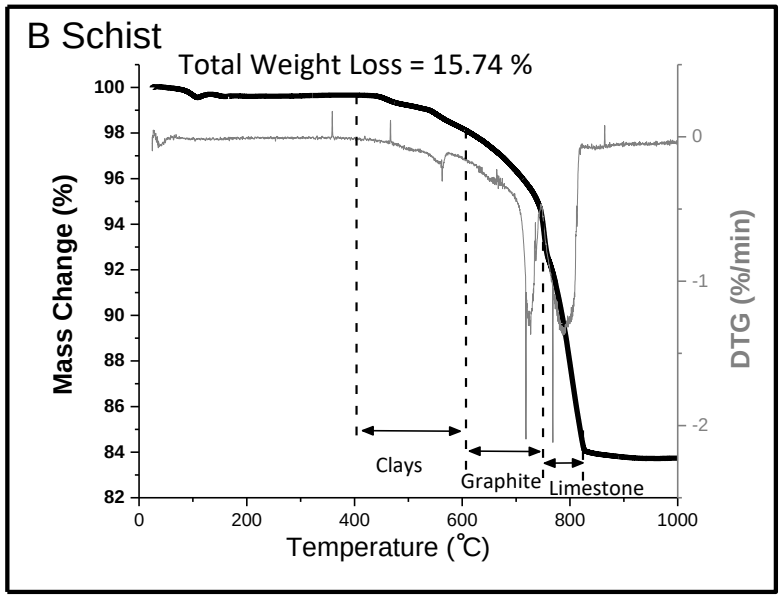

Figure 21. TGA/DTG analysis of B schist powder (as-received) – Left axis: TGA (mass change), Right axis: DTG

As it is visible in figure 21, the total weight loss due to the decomposition of clay and carbonate phases in B sample was 15.74 wt%. The main decomposition in this sample started at around 400°C which was probably related to the de-hydroxylation of clayey materials. Therefore, the clay decomposition starting temperature in this ample was higher than the others. It seemed that the crystal structures of the clayey phases in the B sample were more complex than the other samples. As indicated in the XRD phase analysis, this sample also contained graphite which decomposes around 600°C. Based on the amount of weight loss (about 5 wt%) observed within 600-750°C temperature range which corresponds to the burning temperature of graphite, it was also confirmed that the amount of graphite in this sample was about 5 wt%. Furthermore, there were two different calcium carbonate phases in the B sample; Calcite and Ankerite that were decomposed in the temperature range of 750°C to 830°C.

Figure 22 illustrates the TGA diagram of untreated virgin and limestone augmented B schist sample.

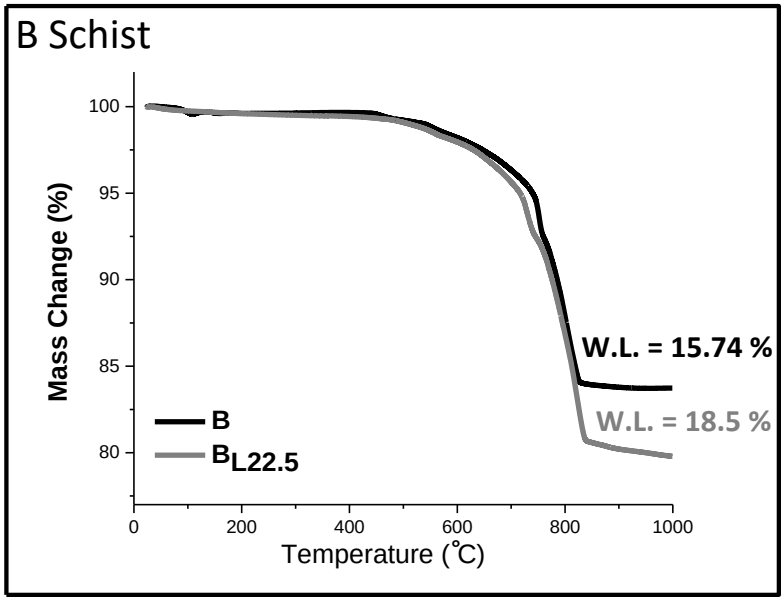

Figure 22. TGA diagram of B: B schist (as-received), and $B_{L22.5}$: B schist with 22.5 wt% $C\bar{C}$ addition

According to the TG analysis of B and limestone augmented B samples, the proper calcination temperatures that would correspond to 80% of the total weight losses due to de-hydroxylation or decomposition reactions were calculated and listed in Table 11.

Table 11. Calcination temperatures and total weight loss for virgin or limestone augmented B schist

Sample	Total weight Loss (wt%)	Calcination Temperature 80% of total weight loss (℃)
B	15.74	770
$B_{L22.5}$	18.5	810

3.1.2.5. L Schist

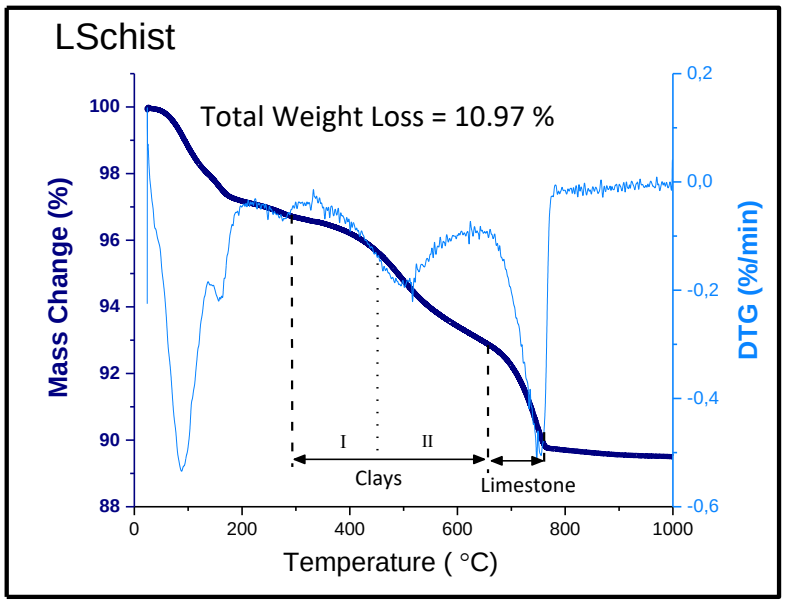

Figure 23. TGA/DTG analysis of L schist powder (as-received) – Left axis: TGA (mass change), Right axis: DTG

As it can be seen in figure 23, the total weight loss due to the decomposition of clay and carbonate phases in the L sample was around 11 wt%. The first weight loss (up to ~250°C) was related to the evaporation of non-structural water (moisture). The de-hydroxylation of complex-structure clayey phases including montmorillonite and clinochlore took place between ~300-650°C. In addition, decomposition of the calcium carbonate phase started at 650°C and lasted till ~800°C.

Figure 24 illustrates the TGA diagram of untreated virgin and limestone augmented L schist sample.

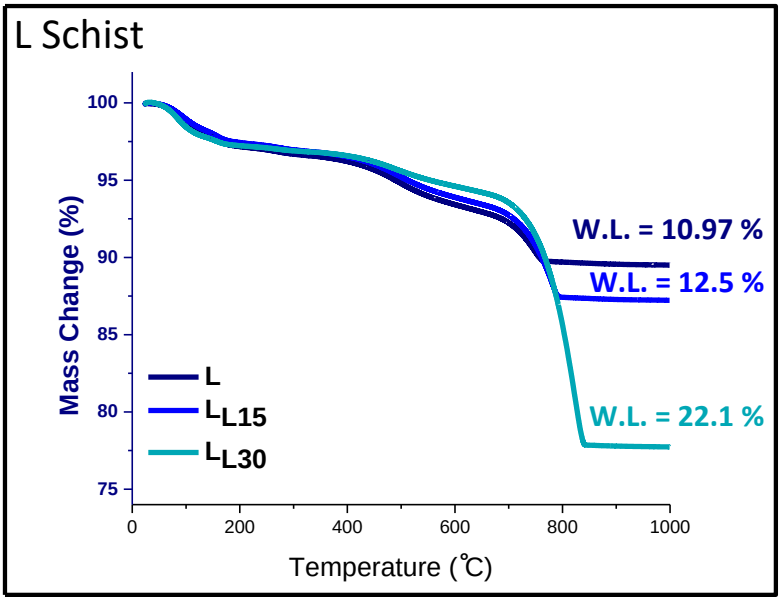

Figure 24. TGA diagram of L: L schist (as-received), L_{L15}: L schist with 15 wt% $C\bar{C}$ addition, and L_{L30}: L schist with 30 wt% $C\bar{C}$ addition

Based on the TG analysis of the L schist or L schist+carbonate mixture, the calcination temperatures that would correspond to 80% of the total weight losses due to de-hydroxylation or decomposition reactions were calculated. These temperature ranges are listed in Table 12.

Table 12. Calcination temperatures and total weight loss for virgin or limestone augmented L schist

Sample	Total weight Loss (wt%)	Calcination Temperature 80% of total weight loss (℃)
L	10.97	740
L_{L15}	12.5	770
L_{L30}	22.1	810

3.1.2.6. Albite

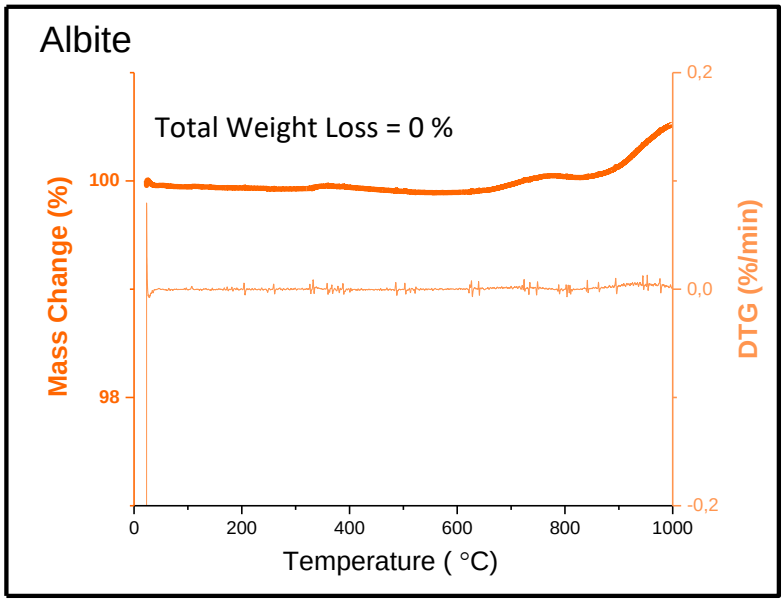

Figure 25. TGA/DTG analysis of Albite powder (as-received) – Left axis: TGA (mass change), Right axis: DTG

Figure 25 shows the TGA diagram of the pure albite sample. The thermal analysis of this sample indicated that it is a stable system in this temperature range (25-1000℃) in terms of decomposition and weight loss. In this sample, there is no decomposable (activatable) phase and therefore, the thermal activation cannot be an effective activation method for albite.

3.1.3. Elemental Analysis

EDX analysis and x-ray mapping were done in order to identify the existing elements in the samples and the portion of each element. In this way, it will be possible to calculate the Ca/Si and Al/Si of the samples which can be an indication of the degree of hydraulicity and pozzolanicity, respectively.

3.1.3.1. G Schist

Figure 26 shows the EDS analysis of untreated G schist sample and table 13 lists the existing elements in the sample and their percentages.

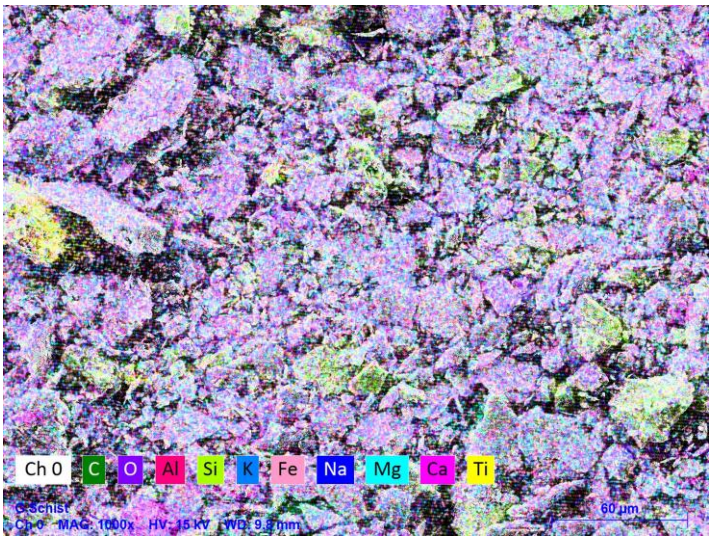

Figure 26. EDS elemental analysis (mapping) of virgin G Schist including Si, Al, Ca, K, Mg, Fe, Na, Ti, C, and O

Table 13. The list and relative amounts (wt% and at%) of the elements existing in virgin G schist EDS mapping analyses

Element	At. NO	Mass (%)	Atom (%)
Sodium	11	0.78	1
Magnesium	12	1.81	2.19
Aluminum	13	24.69	26.91
Silicon	14	57.12	59.82
Potassium	19	6.26	4.71
Calcium	20	1.13	0.83
Iron	26	5.71	3.01
Titanium	22	2.49	1.53
Sum.		100	100

Based on the EDS results of G schist sample, the Ca/Si ratio and the Al/Si ratio was calculated as 0.02 and 0.43, respectively.

3.1.3.2. C Schist

Figure 27 shows the EDS analysis of untreated C schist sample and Table 14 lists the existing elements in the sample and their percentages.

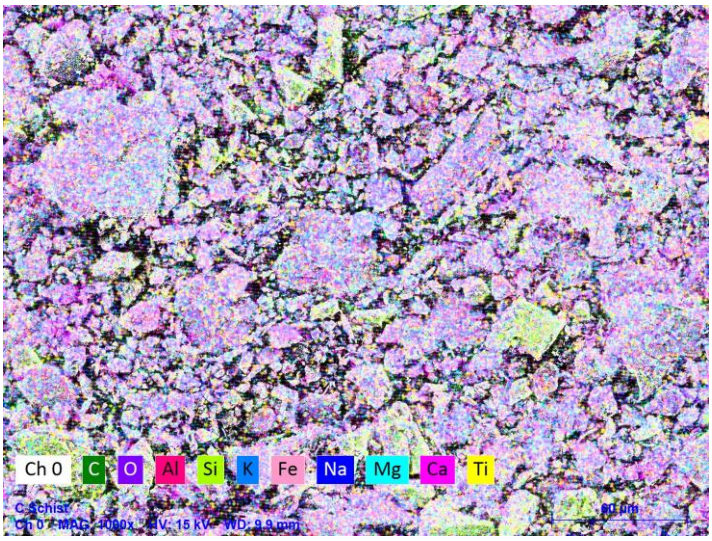

Figure 27. EDS elemental analysis (mapping) of virgin C Schist including Si, Al, Ca, K, Mg, Fe, Na, Ti, C, and O

Table 14. The list and relative amounts (wt% and at%) of the elements existing in virgin C schist EDS mapping analyses

Element	At. NO	Mass (%)	Atom (%)
Sodium	11	0.74	0.94
Magnesium	12	1.7	2.05
Aluminum	13	25.38	27.57
Silicon	14	57.17	59.66
Potassium	19	6.08	4.56
Calcium	20	2.29	1.68
Iron	26	5.97	3.13
Titanium	22	0.67	0.41
Sum.		100	100

In the C schist sample, the Ca/Si ratio was calculated as 0.04 and the Al/Si ratio was calculated as 0.44.

3.1.3.3. P Schist

Figure 28 shows the EDS analysis of the untreated P schist sample and Table 15 lists the existing elements in the sample and their percentages.

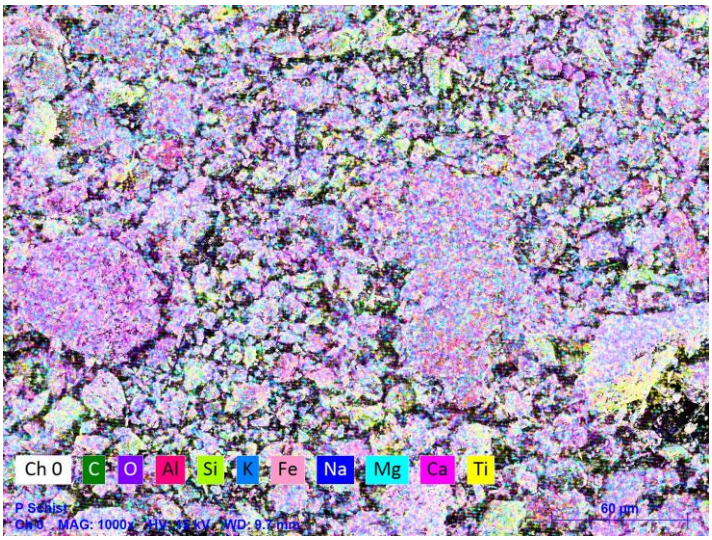

Figure 28. EDS elemental analysis (mapping) of virgin P Schist including Si, Al, Ca, K, Mg, Fe, Na, Ti, C, and O

Table 15. The list and relative amounts (wt% and at%) of the elements existing in virgin P schist EDS mapping analyses

Element	At. NO	Mass (%)	Atom (%)
Sodium	11	0.78	1
Magnesium	12	1.01	1.22
Aluminum	13	29.08	31.59
Silicon	14	53.47	55.8
Potassium	19	3.04	2.28
Calcium	20	6.9	5.04
Iron	26	5	2.63
Titanium	22	0.72	0.44
Sum.		100	100

According to the EDS results, the Ca/Si ratio in the P sample is 0.13 and the Al/Si ratio is 0.54.

3.1.3.4. B Schist

Figure 29 shows the EDS analysis of the untreated B schist sample and Table 16 lists the existing elements in the sample and their percentages.

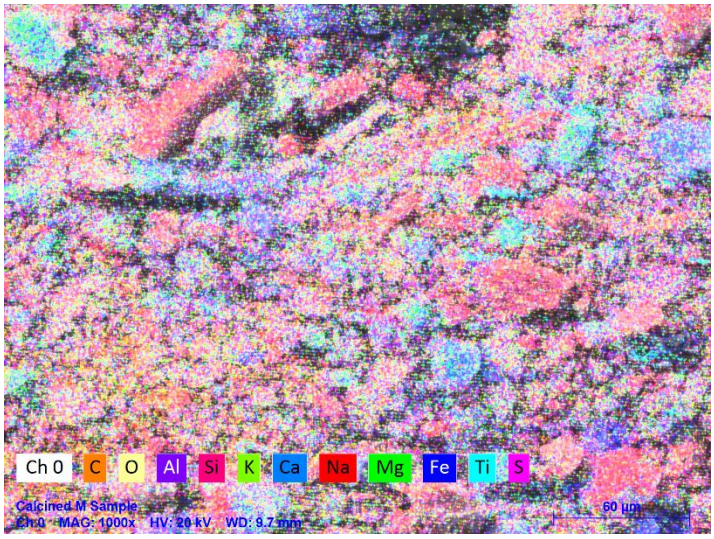

Figure 29. EDS elemental analysis (mapping) of virgin B Schist including Si, Al, Ca, K, Mg, Fe, Na, Ti, C, O, and S

Table 16. The list and relative amounts (wt% and at%) of the elements existing in virgin B schist EDS mapping analyses

Element	At. NO	Mass (%)	Atom (%)
Sodium	11	0.88	1.18
Magnesium	12	4.59	5.84
Aluminum	13	15.99	18.33
Silicon	14	46.77	51.51
Potassium	19	3.3	2.61
Calcium	20	20.78	16.04
Iron	26	6.45	3.57
Sulfur	16	0.39	0.37
Titanium	22	0.87	0.56
Sum.		100	100

The EDS analysis of this sample shows that the Ca/Si ratio is 0.45 and the Al/Si ratio is 0.35.

3.1.3.5. L Schist

Figure 30 shows the EDS analysis of the untreated L schist sample and Table 17 lists the existing elements in the sample and their percentages.

Figure 30. EDS elemental analysis (mapping) of virgin L Schist including Si, Al, Ca, Mg, Fe, Na, Ti, C, and O

Table 17. The list and relative amounts (wt% and at%) of the elements existing in virgin L schist EDS mapping analyses

Element	At. NO	Mass (%)	Atom (%)
Sodium	11	0.68	0.88
Magnesium	12	2.61	3.19
Aluminum	13	19.88	21.85
Silicon	14	59.41	62.73
Calcium	20	9.58	7.09
Iron	26	6.61	3.51
Titanium	22	1.22	0.76
Sum.		100	100

The EDS results indicated the Ca/Si ratio of 0.16 and the Al/Si 0.33 ratio of L sample.

3.2. Thermally Activated Materials

According to the results obtained from the characterization of virgin schist samples, all of the schist type materials have the possibility to be activated by a thermal activation process i. e. heat-treatment. These materials then could be used as a cement partial substitute. Therefore, a

calcination (heat-treatment) process was performed on the schists as it was described in the experimental procedures section. Moreover, in order to investigate the effect of activated calcia additions to activated schists on composite cement hydration, strength and durability, the limestone augmented samples were also calcined and used as cement partial substitutes. In the upcoming sections, a comparison between the untreated and calcined materials (both virgin and limestone augmented samples) will be represented. This comparison includes phase analysis, thermal analysis, microstructure, and strength measurements.

3.2.1. Phase Analysis

In order to investigate the effects of the calcination process on the phase distribution of each schist sample, X-ray analyses were performed on all calcined powders and the results were compared to the un-treated powders' XRD spectra. For the limestone augmented samples, the comparison was performed between schist+calcium carbonate and the same mixtures after calcination.

3.2.1.1. G schist

As it was shown in table 18, the amount of calcium carbonate in the virgin G schist powder was about 0.9 at%. This carbonate content was then topped off to 15, 22.5, and 30%. X-ray diffractograms of each untreated virgin or limestone augmented sample were compared to the same heat-treated samples. Figures 31-34 show the comparison of x-ray diffractograms. As it was mentioned in experimental procedures, the virgin and 15% limestone augmented G samples were calcined up to 80, 100, and 110% of their total weight losses. The other samples were calcined only up to 80% of the total weight losses.

Figure 31 shows the virgin and calcined (80%, 100%, and 110%) powders spectra on the same graph.

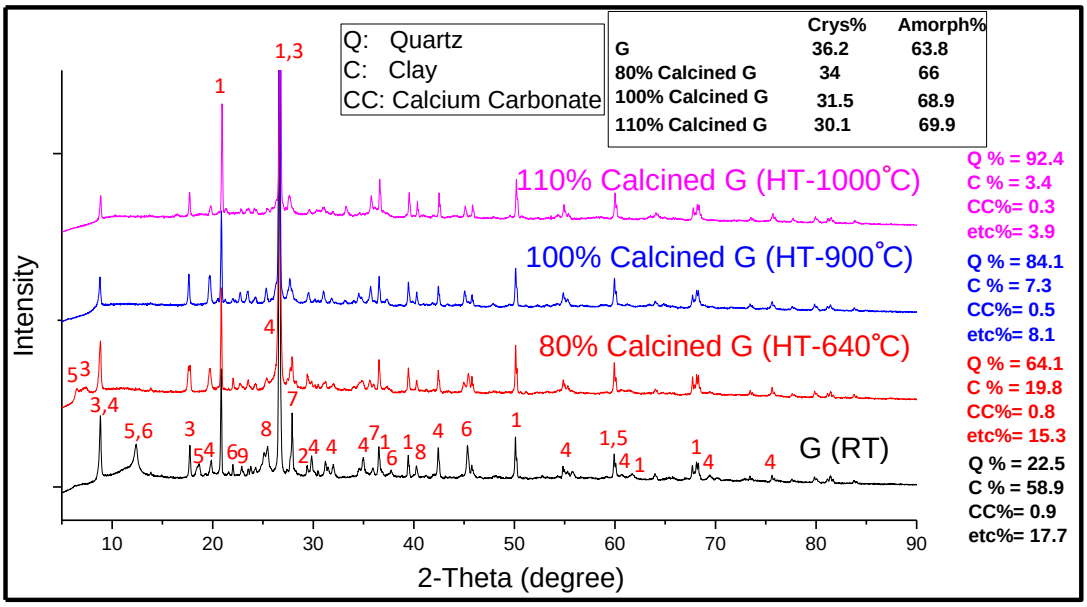

Figure 31. X-ray spectrum of virgin vs. 80%, 100%, and 110% calcined G schist powder. The numbers at the peaks correspond to phases listed in table 18.

Table 18. The phase distribution, chemical formula of each phase, and information about the crystal structure of G powder

Peak Number	Chemical Phases	Crystal Structure	Chemical Formula
1	Quartz	Hexagonal	SiO_2
2	Calcite	Rhombo	$CaCO_3$
3	illite	Monoclinic	$(K, H_3O)Al_2Si_3AlO_{10}(OH)_2$
4	Muscovite	Monoclinic	$KAl_2Si_3AlO_{10}(OH)_2$
5	Clinochlore	Monoclinic	$(Mg_{2.96}\,Fe_{1.55}\,Fe_{1.36}\,Al_{1.275})(Si_{2.622}\,Al_{1.376}O_{10})(OH)_8$
6	Dickite	Monoclinic	$Al_2Si_2O_5(OH)_4$
7	Anorthite	Triclinic	$Na_{0.25}Ca0_{.71}(Al_2Si_2O_8)$
8	Titanium Oxide	Monoclinic	Ti_3O_5
9	Albite	Triclinic	$(Na\ ,Ca)(Si,\ Al)_4O_8$

According to the XRD analyses, the crystalline phase amount decreased from 36.2% to 34%, 31.5%, and 30.5% after heat-treatment to the temperature associated with 80%, 100%, and 110% of total weight loss, respectively. The quantification software calculates the total atomic percentage of all crystalline phases to 100%. Therefore, the relative amount of the stable crystalline phases such as quartz (as an inert phase) increases due to the decomposition of non-stable crystalline phases like clays. After calcination at 640°C, 900°C, and 1000°C for 2 hours, the clay

content of G sample changed from 58.9 to 19.8 at%, 7.3 at% and 3.4 at%, respectively. Therefore, the clay decomposition percentage was about 67% (not 80%) as estimated from XRD results ($\frac{\mathbf{58.9 - 19.8}}{\mathbf{58.9}}$ = 67%). Moreover, the carbonate amount changed from 0.9 to 0.8, 0.5 and 0.3 at%, respectively.

Figure 32 shows the x-ray spectra of the G_{L15} sample before and after heat treatment up to 80%, 100%, and 110% of its total weight loss.

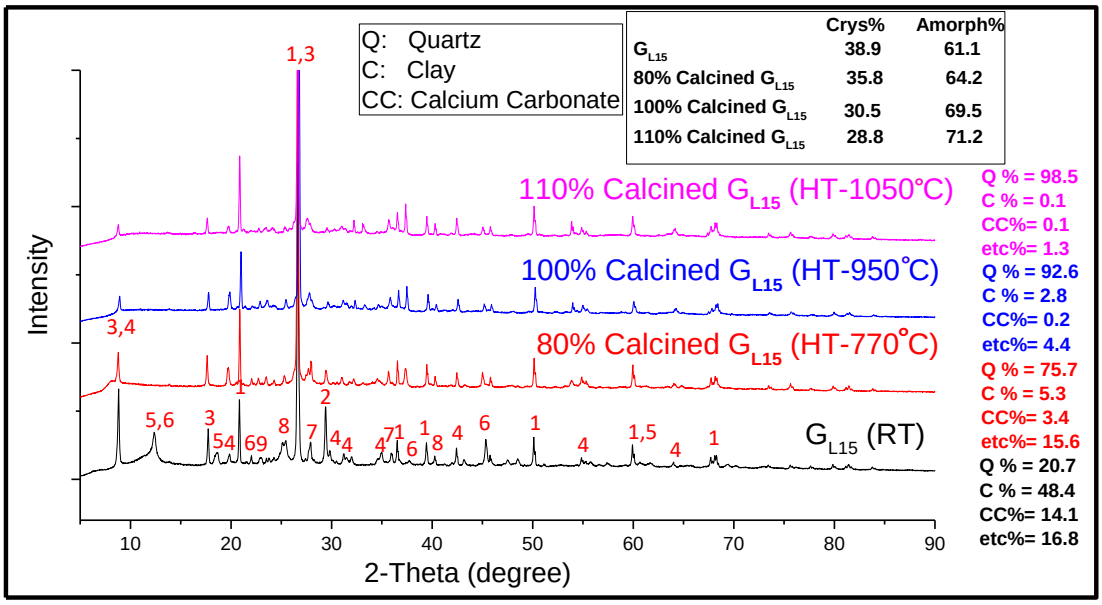

Figure 32. X-ray spectrum of untreated vs. 80%, 100% and 110% calcined G_{L15} schist powder (G schist with 15 wt% $C\bar{C}$ addition). The numbers at the peaks correspond to phases listed in table 18.

Similar to the untreated and calcined G sample, the crystallinity of untreated G_{L15} powder was changed from 38.9% to 35.8%, 30.5%, and 28.8% after 80%, 100%, and 110% calcination, respectively. The clay phase weight percentage changed from 48.4 to 5.3%, 2.8%, and 0.1%, meaning that a noticeable portion of the total clay amount has decomposed during calcination. In addition, more than 75% ($\frac{\mathbf{14.1 - 3.4}}{\mathbf{14.1}}$) of carbonate phase decomposed after 80% calcination.

Figures 33 and 34 represent the x-ray spectra of $G_{L22.5}$ and G_{L30} samples before and after heat treatment up to 80% of their total weight loss. Based on the phase amounts before and after calcination, the clay decomposition percentage during calcination was ~79% for 22.5% $C\bar{C}$ augmented sample and ~84% for 30% $C\bar{C}$ augmented sample. In addition, the calcium carbonate

decomposition was ~52% for 22.5% $C\bar{C}$ augmented sample and ~40% for 30% $C\bar{C}$ augmented sample

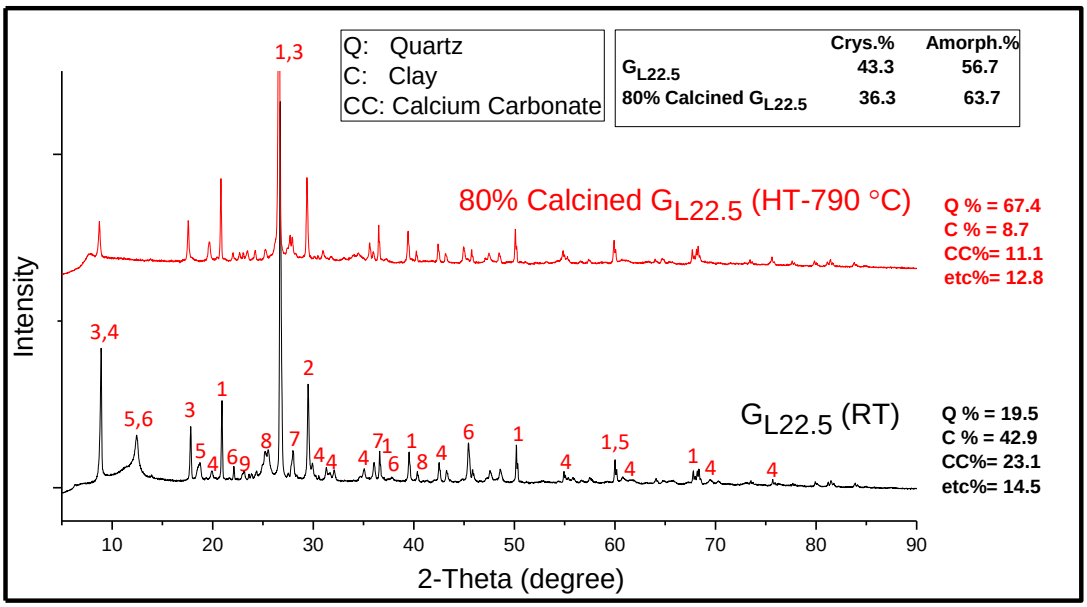

Figure 33. X-ray spectrum of untreated vs. 80% calcined $G_{L22.5}$ schist powder (G schist with 22.5 wt% $C\bar{C}$ addition). The numbers at the peaks correspond to phases listed in table 18.

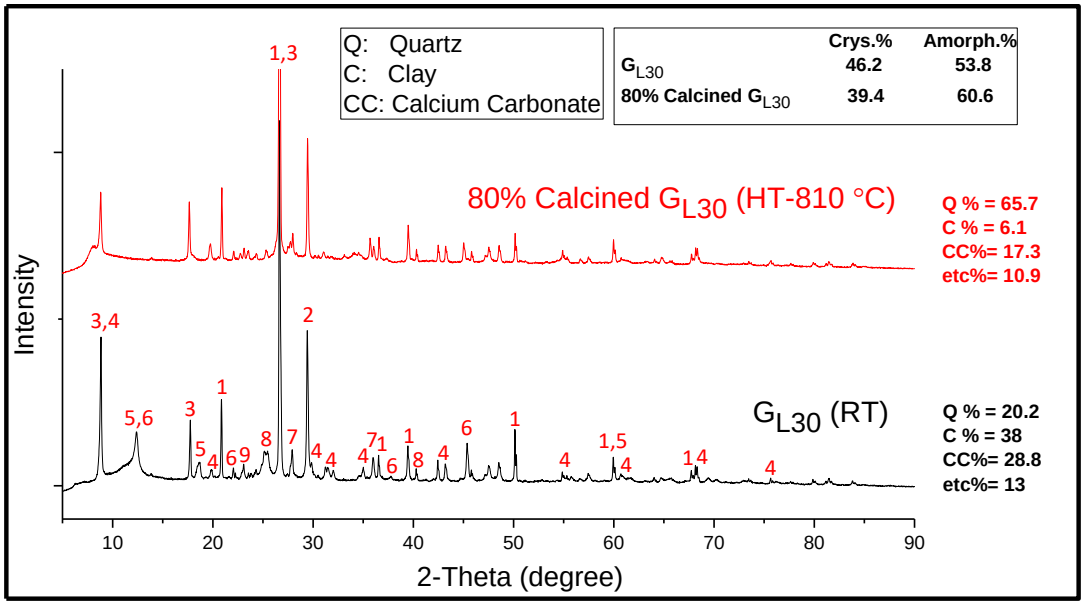

Figure 34. X-ray spectrum of untreated vs. 80% calcined G_{L30} schist powder (G schist with 30 wt% $C\bar{C}$ addition). The numbers at the peaks correspond to phases listed in table 18.

3.2.1.2. C Schist

Based on the initial x-ray analyses on the C schist powder (as-received), this schist type material contains 3.8 at% calcium carbonate. C_{L15}, $C_{L22.5,}$ and C_{L30} samples were generated by adding limestone to this powder such that the total carbonate amount in the schist reaches 15%, 22.5%, and 30%.

Figure 35 shows both virgin and up to 80% calcined C powders spectra (without carbonate additions). After the calcination process, the crystallinity of C powder decreased from 39 to 33.7%. During de-hydroxylation of the clayey materials, the amount of clay decreased from 51.3 at% to 21.8 at%. This means that the achieved decomposition was ~58%. In addition, there was no difference in the calcium carbonate amount before and after the calcination.

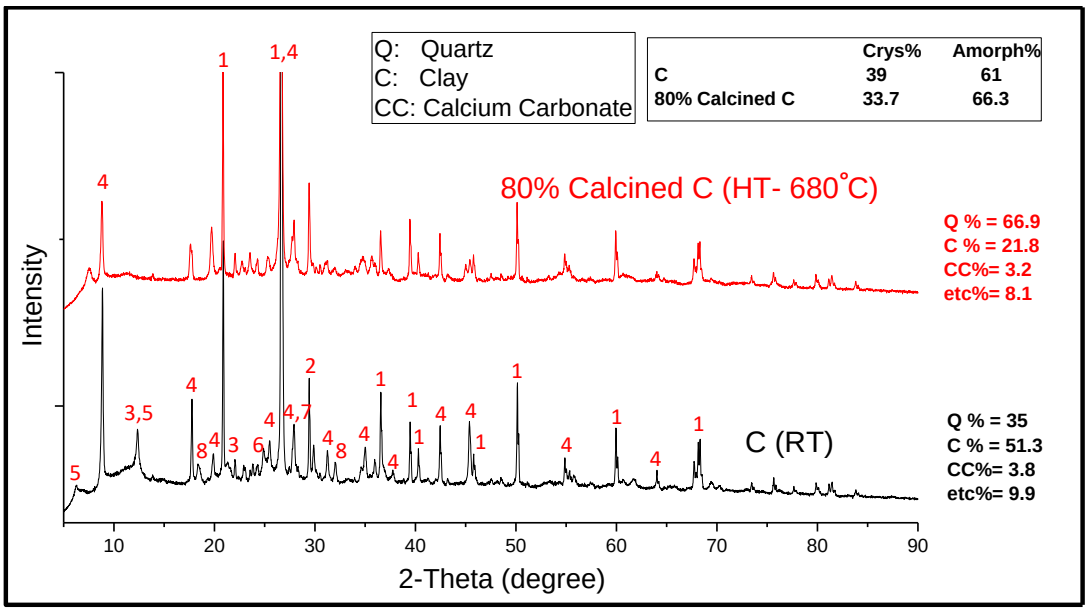

Figure 35. X-ray spectrum of virgin vs. 80% calcined C schist powder. The numbers at the peaks correspond to phases listed in table 19.

Table 19. The phase distribution, chemical formula of each phase, and information about the crystal structure of C powder

Peak Number	Chemical Phases	Crystal Structure	Chemical Formula
1	Quartz	Hexagonal	SiO_2
2	Calcite	Rhombo	$CaCO_3$
4	Muscovite I	Monoclinic	$KAl_2(AlSi_3O_{10})(OH)_2$
4	Muscovite II	Hexagonal	$(K, Na)(Al, Mg, Fe)_2(Si_{3.1}Al_{0.9})O_{10}(OH)_2$
9	Albite	Triclinic	$(Na, Ca)(Si, Al)_4O_8$
5	Clinochlore	Monoclinic	$(Mg_5Al)(Si, Al)_4O_{10}(OH)_8$
3	Kaolinite	Triclinic	$Al_2(Si_2O_5)(OH)_4$
7	Anorthite	Triclinic	$Ca(Al_2Si_2O_8)$
8	Titanium Oxide	Orthorhombic	Ti_3O_5

Figure 36 shows the x-ray spectra of untreated and calcined C_{L15} sample (C with 15% $\overline{CC}$ addition) to compare the decomposition magnitude of clayey and carbonate phases. The amount of clay components changed from 49.7% to 11.3% during de-hydroxylation reactions ($\frac{\mathbf{49.7 - 11.3}}{\mathbf{49.7}} = 77\%$). In addition, 80% of the carbonate content was decomposed.

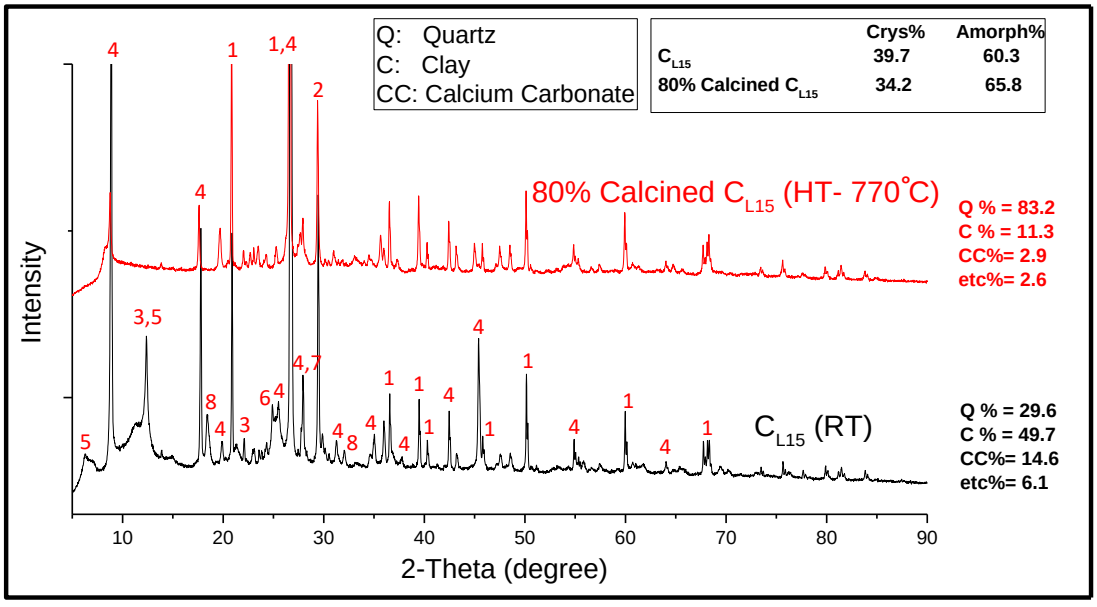

Figure 36. X-ray spectrum of untreated vs. 80% calcined C_{L15} schist powder (C schist with 15 wt% $C\bar{C}$ addition). The numbers at the peaks correspond to phases listed in table 19.

Figures 37 and 38 illustrate the x-ray spectra of $C_{L22.5}$ and C_{L30} schist samples before and after calcination up to 80%. The quantitative x-ray analyses show that during calcination, the clayey components were decomposed ~73% for 22.5% $C\bar{C}$ augmented sample and ~76% for 30% $C\bar{C}$ augmented sample. Furthermore, the calcium carbonate decomposition percentage was ~50% for both samples.

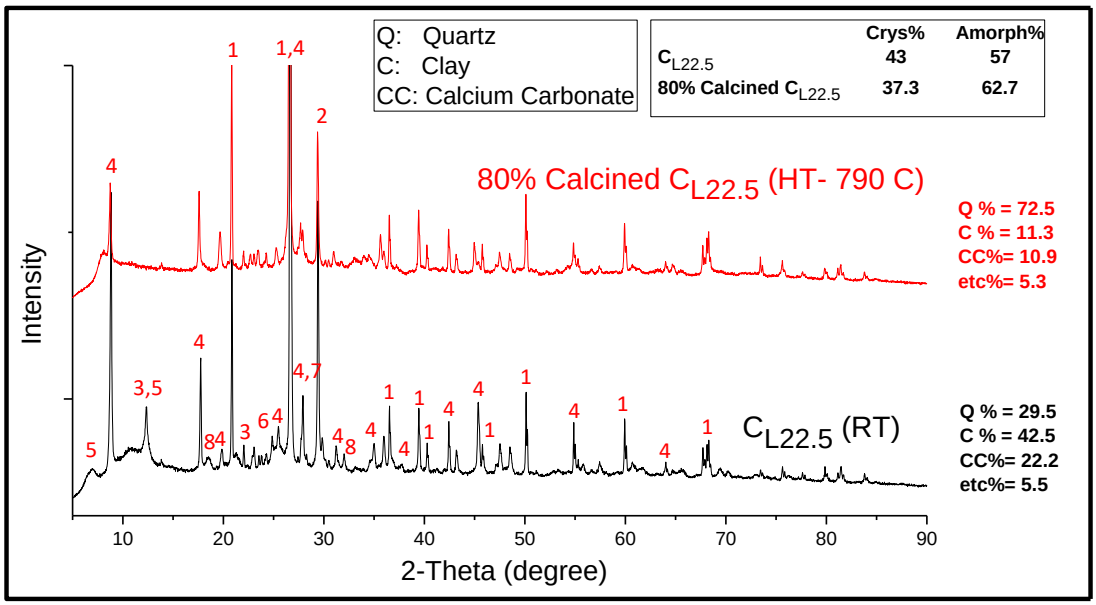

Figure 37. X-ray spectrum of untreated vs. 80% calcined $C_{L22.5}$ schist powder (C schist with 22.5 wt% $C\bar{C}$ addition). The numbers at the peaks correspond to phases listed in table 19.

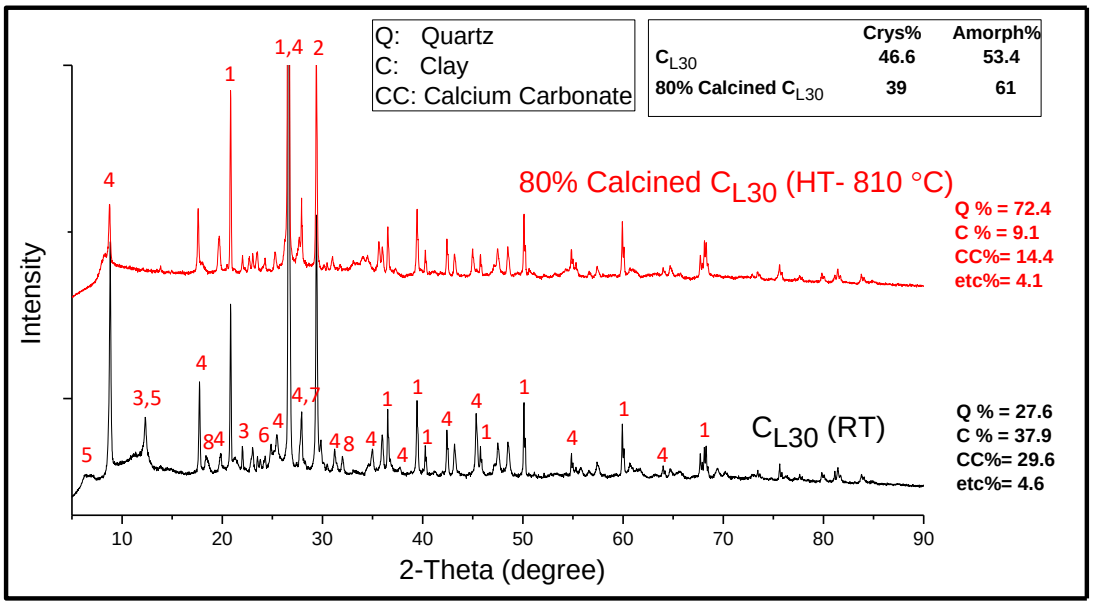

Figure 38. X-ray spectrum of untreated vs. 80% calcined C_{L30} schist powder (C schist with 30 wt% $C\bar{C}$ addition). The numbers at the peaks correspond to phases listed in table 19.

3.2.1.3. P Schist

In order to control the changes in the phase composition of the P sample due to heat treatment at 770 ºC for two hours, the quantitative X-ray analyses were carried out on the untreated and calcined powders. Figure 39 illustrates the x-ray spectra of virgin and calcined P without carbonate additions.

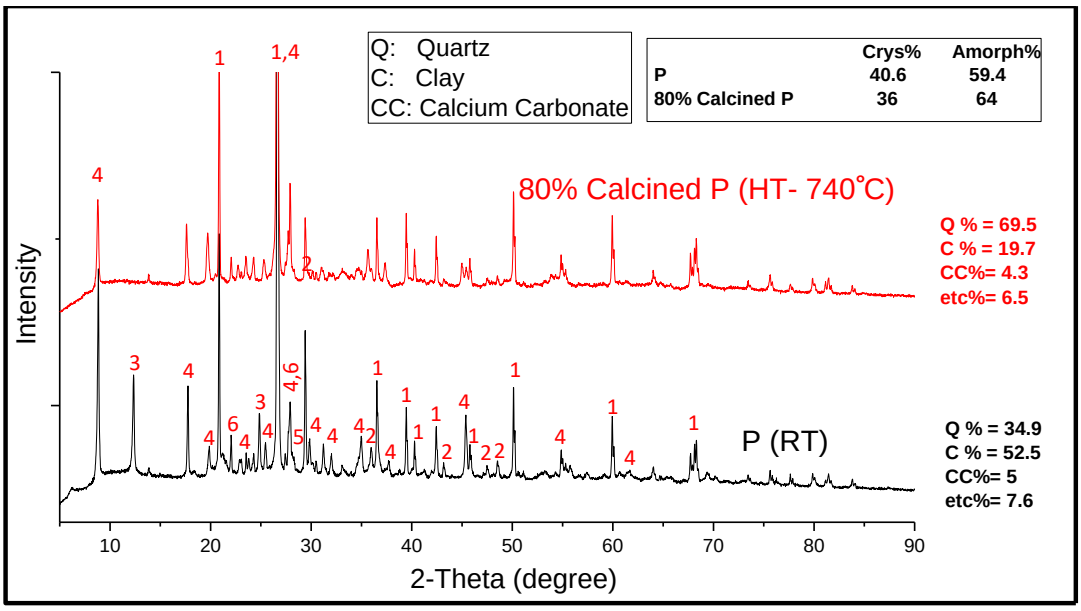

Figure 39. X-ray spectrum of virgin vs. 80% calcined P schist powder. The numbers at the peaks correspond to phases listed in table 20.

Table 20. The phase distribution, chemical formula of each phase, and information about the crystal structure of P powder

Peak Number	Chemical Phases	Crystal Structure	Chemical Formula
1	Quartz	Hexagonal	SiO_2
2	Calcite	Rhombo	$CaCO_3$
3	Kaolinite	Triclinic	$Al_2(Si_2O_5)(OH)_4$
4	Muscovite I	Monoclinic	$K(Al_{1.88}Fe_{0.12})(Si_3Al)O_{10}(OH)_2$
4	Muscovite II	Hexagonal	$(K, Na)(Al, Mg, Fe)_2(Si_{3.1}Al_{0.9})O_{10}(OH)_2$
8	Rutile	Tetragonal	Ti_3O_5
9	Albite	Triclinic	$NaAlSi_3O_8$

The quantitative phase analyses show that 62% of clayey content was decomposed during the calcination of P schist sample. The carbonate phases decomposed for 14% and other phases decomposed for 15%. In addition, the crystallinity decreased from 40.6 to 36%.

Figure 40 shows the XRD spectra of the untreated and calcined P_{L15} schist.

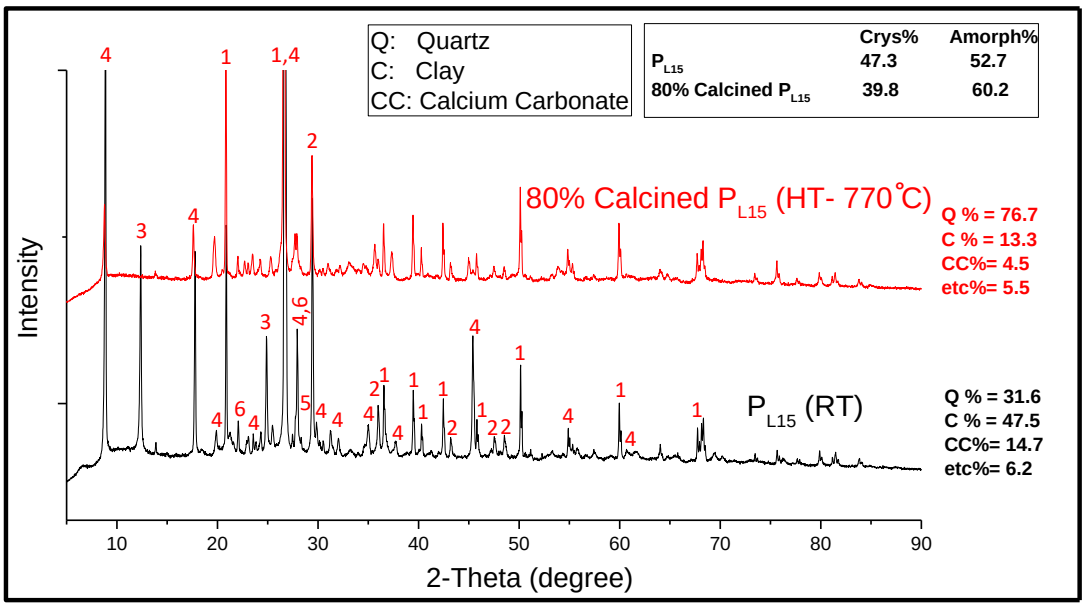

Figure 40. X-ray spectrum of untreated vs. 80% calcined P_{L15} schist powder (P schist with 15 wt% $C\bar{C}$ addition). The numbers at the peaks correspond to phases listed in table 20.

X-ray analyses of untreated and calcined P_{L15} sample show that the crystallinity of this sample decreased from 47.3 to 39.8% due to calcination. The atomic percentage of clayey phases changed from 47.5 to 4.3%. It means that 90% of clayey content was decomposed. In addition, 70% of the carbonate content was also decomposed.

Figures 41 and 42 show a comparison between the x-ray spectra of $P_{L22.5}$ and P_{L30} schist samples before and after calcination. The x-ray analyses results show that during calcination, the clayey components were decomposed ~75% for 22.5% $C\bar{C}$ augmented sample and ~78% for 30% $C\bar{C}$ augmented sample. Moreover, the calcium carbonate decomposition percentage was ~70% for both samples.

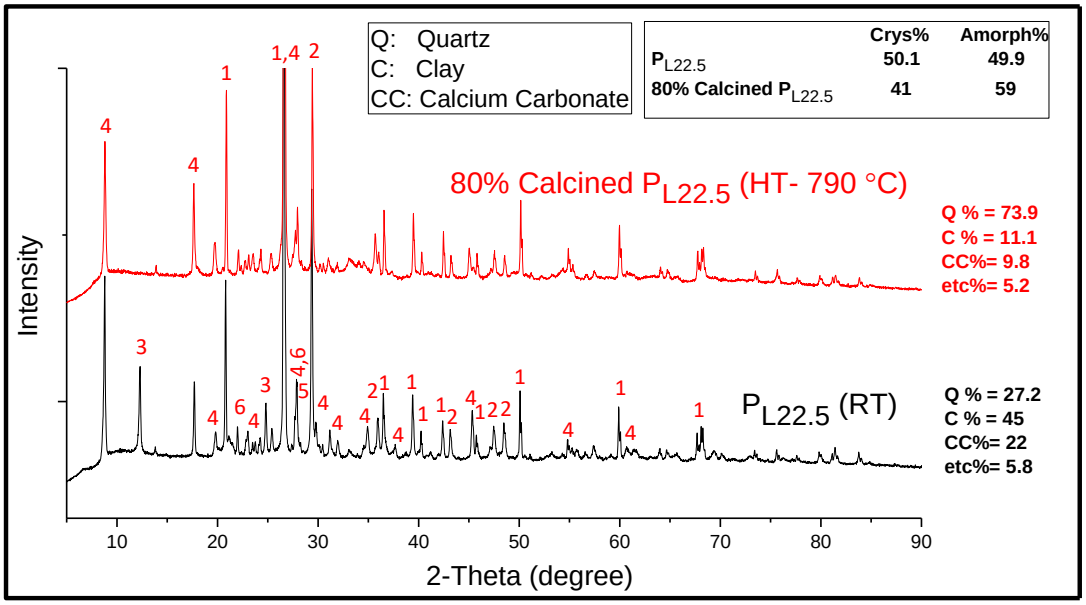

Figure 41. X-ray spectrum of untreated vs. 80% calcined $P_{L22.5}$ schist powder (P schist with 22.5 wt% $C\bar{C}$ addition). The numbers at the peaks correspond to phases listed in table 20.

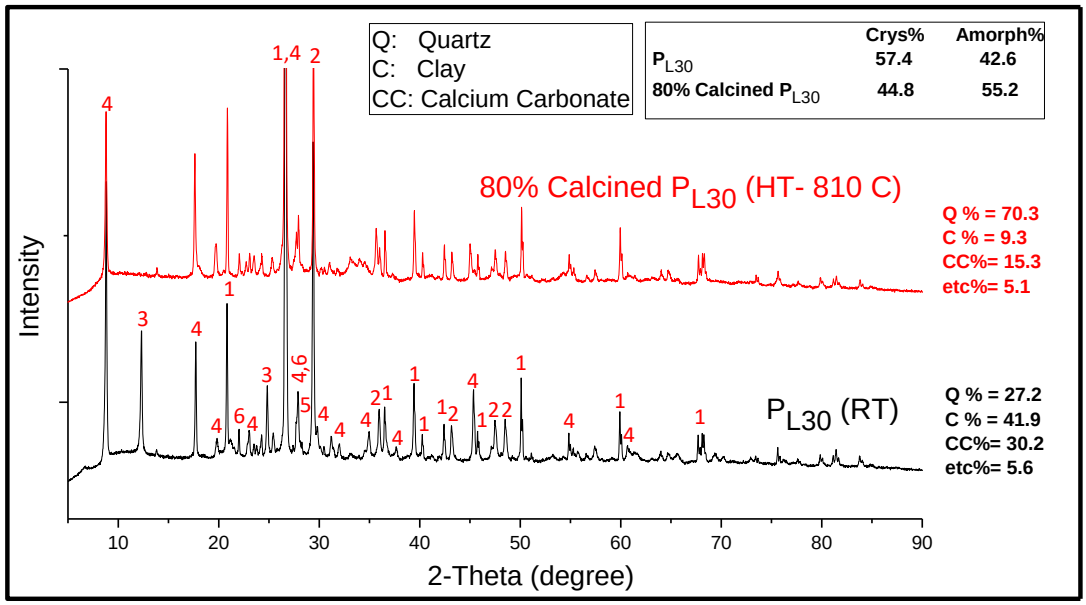

Figure 42. X-ray spectrum of untreated vs. 80% calcined P_{L30} schist powder (P schist with 30 wt% $C\bar{C}$ addition). The numbers at the peaks correspond to phases listed in table 20.

3.2.1.4. B Schist

The X-ray analyses were carried out for the untreated and calcined B schist with and without carbonate additions. Figure 43 shows the x-ray spectra of virgin and calcined B sample without any modification in its calcium carbonate amount. The powder was calcined at 770 ºC for two hours which will correspond to 80% of decomposition. The calcination was done in a box furnace on a 500 g of powder batch.

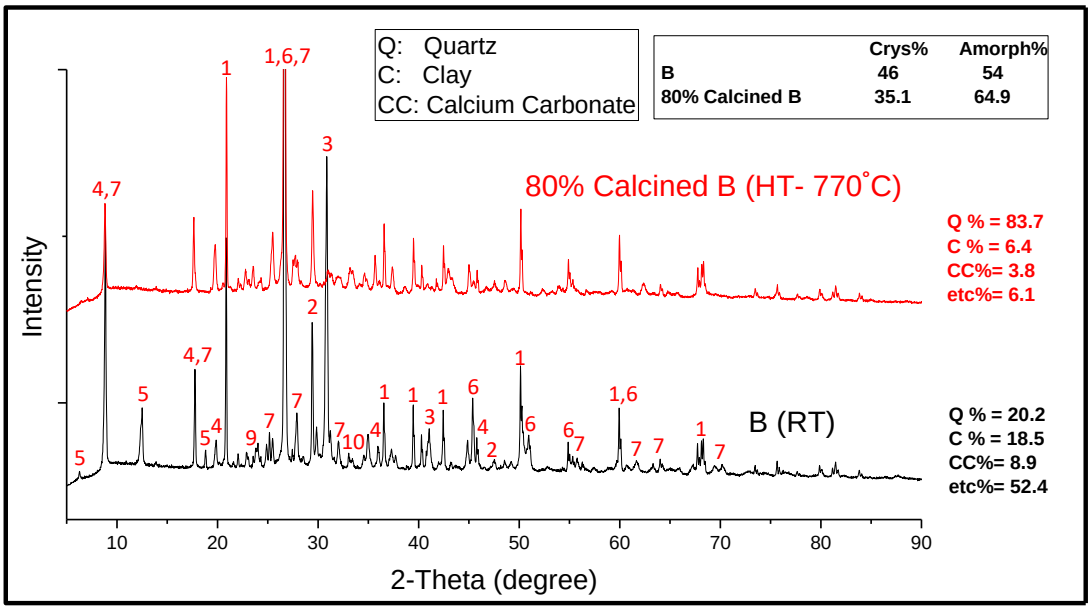

Figure 43. X-ray spectrum of virgin vs. 80% calcined B schist powder. The numbers at the peaks correspond to phases listed in table 21.

Based on the quantitative phase analyses, the amount of clay in B schist sample decreased from 32 at% to 6.4 at% during calcination. Therefore, the clay decomposition percentage due to calcination was 80%. This is a marked difference in the decomposition behavior of this schist in comparison to the rest of the samples. The carbonate phase decomposed ~7% of the initial carbonate amount. The calculated crystallinity of the sample decreased from 46 to 35.1%.

Table 21. The phase distribution, chemical formula of each phase, and information about the crystal structure of B powder

Peak Number	Chemical Phases	Crystal Structure	Chemical Formula
1	Quartz	Hexagonal	SiO_2
2	Calcite	Rhombo	$CaCO_3$
3	Ankerite	Rhombo	$Ca(Mg_{0.67}Fe^{+2}_{0.33})(CO_3)_2$
4	Muscovite I	Hexagonal	$(K, Na)(Al, Mg, Fe)_2(Si_{3.1}Al_{0.9})O_{10}(OH)_2$
5	Clinochlore	Monoclinic	$(Mg_{2.8}Fe_{1.7}Al_{1.2})(Si_{2.8}Al_{1.2})O_{10}(OH)_8$
6	Graphite	Hexagonal	C
7	Mg-Annite	Monoclinic	$K(Mg, Al)_{2.04}(Si_{3.34}A_{l0.66})O_{10}(OH)_2$
8	Rutile	Tetragonal	TiO_2
9	Albite	Triclinic	$NaAlSi_3O_8$
10	Pyrite	Cubic	FeS_2

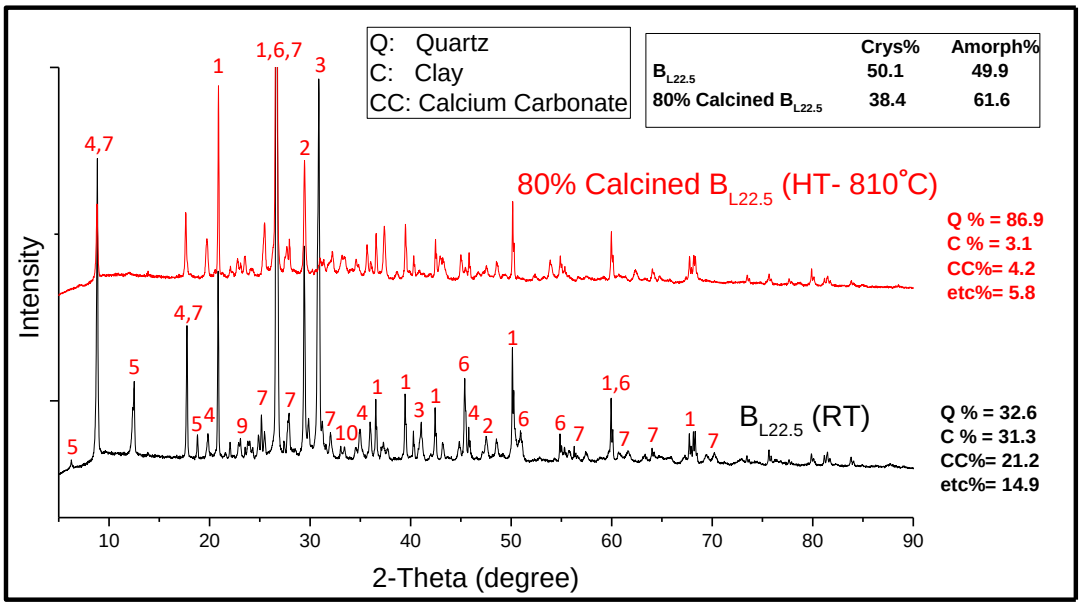

Figure 44. X-ray spectrum of untreated vs. 80% calcined $B_{L22.5}$ schist powder (B schist with 22.5 wt% $C\bar{C}$ addition). The numbers at the peaks correspond to phases listed in table 21.

Figure 44 illustrates the x-ray spectra of untreated and calcined $B_{L22.5}$ sample in which the original amount of carbonate phase was increased from 12 to 21.2 at% by adding calcite powders. The quantitative x-ray diffraction analyses indicated that the crystallinity of $B_{L22.5}$ powder with modified carbonate amount decreased from 50.1 to 38.4%. Almost 90% of clayey components and 80% of carbonate phase decomposed during calcination.

3.2.1.5. L Schist

Similar to the previous samples, the X-ray diffractogram of calcined L powders were also analyzed and compared to the phase distributions of untreated powders to observe the effects of the calcination process.

Figure 45 shows the x-ray spectra of virgin and calcined L sample without any modification in its carbonate amount. The powder was calcined at 740 ºC for two hours. Based on the quantitative x-ray analysis, the crystalline phase amount changed from 30 to 24.8% by heat treatment. After a calcination at 770°C, the clay content of the L sample changed from 26.8 to 3.1 at% and the carbonate amount changed from 8.7 to 4.1 at%. Therefore, the clay decomposition percentage due to calcination was ~88% and this percentage for calcium carbonate was ~53%.

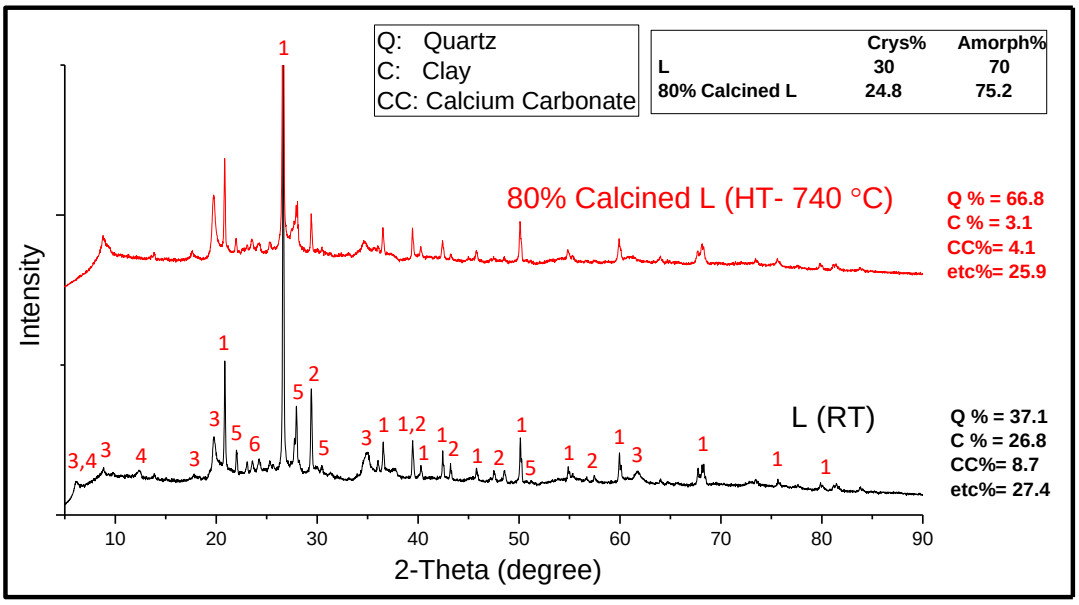

Figure 45. X-ray spectrum of virgin vs. 80% calcined L schist powder. The numbers at the peaks correspond to phases listed in table 22.

Table 22. The phase distribution, chemical formula of each phase, and information about the crystal structure of L powder

Peak Number	Chemical Phases	Crystal Structure	Chemical Formula
1	Quartz	Hexagonal	SiO_2
2	Calcite	Rhombo	$CaCO_3$
3	Montmorillonite	Monoclinic	$(Na, Ca)_{0.3}(Al, Mg)_2Si_4O_{10}(OH)_2.xH_2O$
3	Montmorillonite-22A	Monoclinic	$Na_{0.3}(Al, Mg)_2Si_4O_{10}(OH)_2.8H_2O$
4	Clinchlore	Monoclinic	$(Mg_{2.96}Fe_{1.55}\ Fe_{0.136}Al_{1.275})(\ Si_{2.622}Al_{1.376}O_{10})(OH)_8$
5	Albite	Triclinic	$(Na, Ca)\ (Si, Al)_4\ O_8$
6	Titanium Oxide	Orthorhombic	Ti_3O_5

Figure 46 illustrates the x-ray spectra of untreated and calcined L_{L15} sample (in which the amount of carbonate phase in powder was increased to ~15% by adding limestone).

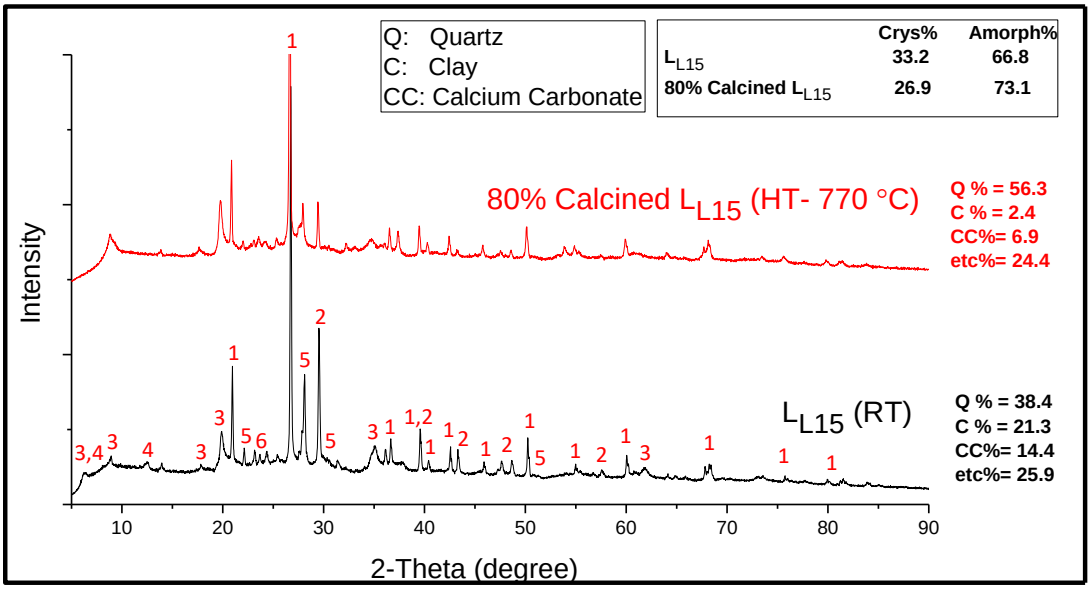

Figure 46. X-ray spectrum of untreated vs. 80% calcined L_{L15} schist powder (L schist with 15 wt% $C\bar{C}$ addition). The numbers at the peaks correspond to phases listed in table 22.

The quantitative x-ray diffraction analyses indicated that the crystallinity of L_{L15} powder with modified carbonate amount decreases from 33.2 to 26.9%. The atomic percentage of clayey phases changed from 21.3 to 2.4% (89% clay decomposition). Moreover, 52% of the carbonate content was also decomposed.

Figure 47 illustrates a comparison between the x-ray spectra of untreated and calcined L_{L30} powder.

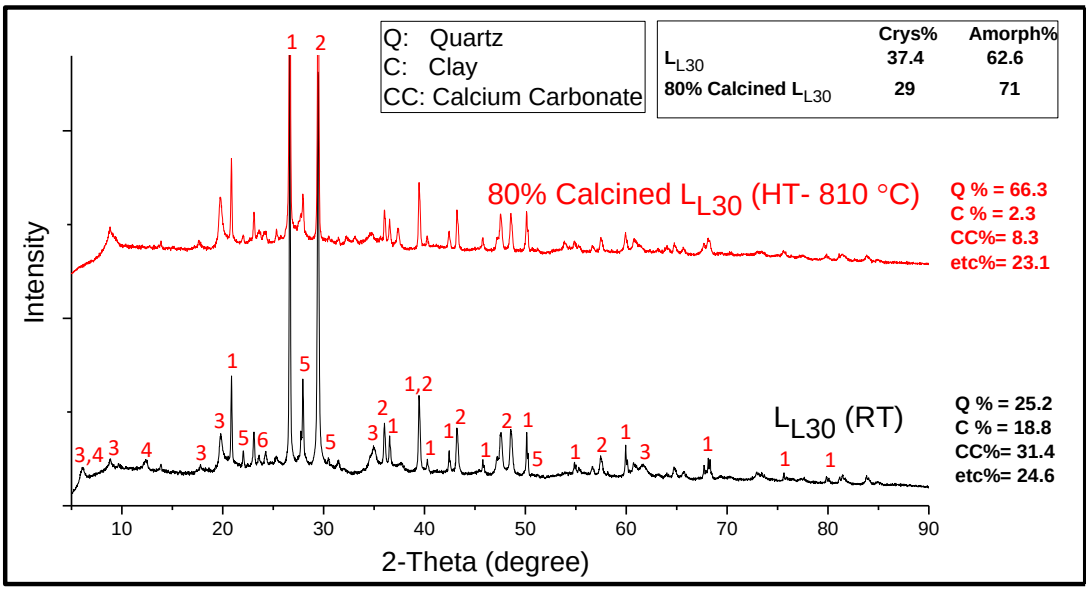

Figure 47. X-ray spectrum of untreated vs. 80% calcined L_{L30} schist powder (L schist with 30 wt% $C\bar{C}$ addition). The numbers at the peaks correspond to phases listed in table 22.

After the calcination process, the amount of clayey components decreased from 18.8 to 2.3 at% and the amount of calcium carbonate changed from 31.4 to 8.3 at%. It means that clay decomposed by 87% and calcium carbonate decomposed by 73% during calcination.

3.2.2. Nuances in Scaling up the Activation Process

In order to check the accuracy of the calcination process, powders heat-treated in the box furnaces were re-evaluated by thermo-gravimetric analysis. The graphs in this section include the TG diagrams illustrating the weight losses of untreated powders (before calcination) and weight losses indicating the remaining activation potential in calcined powders after being heat-treated to the temperatures that would correspond to 80%, 100%, or 110% of activation as estimated by TGA curves.

3.2.2.1. G Schist

The thermo-gravimetric analysis of virgin G schist material (50 mg) revealed that the temperatures that would ensure 80%, 100%, and 110% of weight loss were 640, 900, and 1000ºC respectively.

Figure 48 shows the TG diagrams of virgin and calcined G powders in a laboratory box furnace at 640, 900, and 1000°C for two hours.

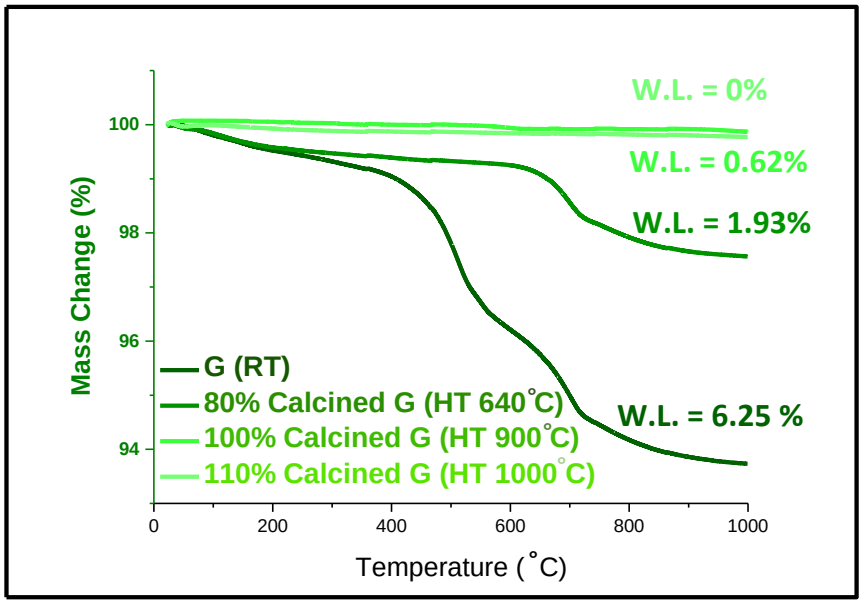

Figure 48. Thermo-gravimetric analysis of virgin vs. 80%, 100%, and 110% calcined G schist powder

As it is visible in the TGA diagram, the total weight loss of the virgin G schist was about 6.25 wt% while this amount dropped down to 1.93 wt% after 80% calcination. The total weight losses after 100% and 110% calcination were calculated as 0.62% and 0%, respectively, both of which should have been 0%. The amount of weight loss related to the decomposition of calcium carbonate in the 80% calcined G powder was almost 1.5 wt%.

Figure 49 illustrates the same comparison for the untreated and 80%, 100%, and 110% heat-treated G_{L15} samples. In the case of G_{L15} (G with 15% $\overline{CC}$), the total weight loss was 10.89 wt% while the 80% calcined sample's weight loss was around 2.72 wt%. The calcium carbonate weight loss in the 80% calcined sample was ~1 wt%. For the 100% and 110% calcined G_{L15} samples, the total weight loss amount was 0.65% and 0%, respectively.

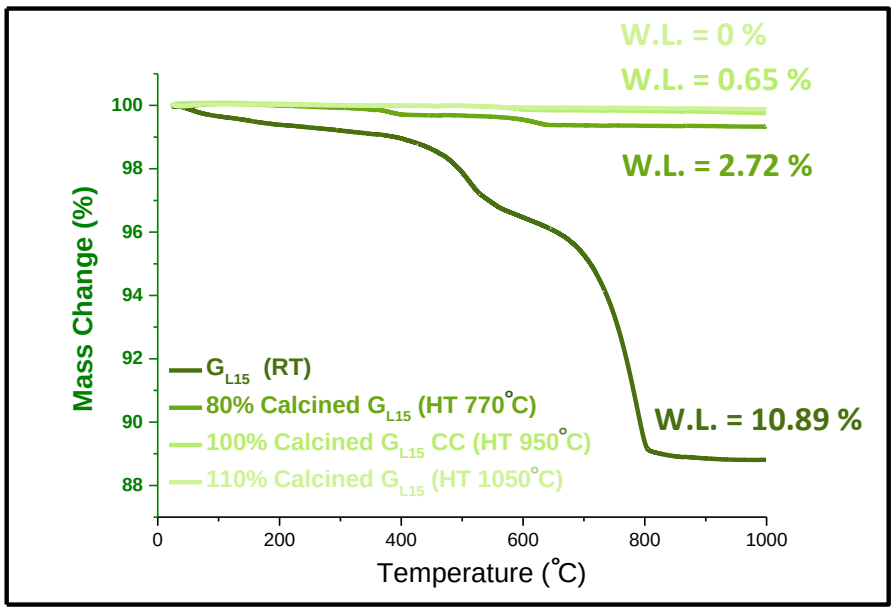

Figure 49. Thermo-gravimetric analysis of untreated vs. 80%, 100% and 110% calcined G_{L15} schist powders (G schist with 15 wt% $C\bar{C}$ addition).

Figures 50 and 51 illustrate the TGA diagrams and total weight losses of the untreated and 80% calcined $G_{L22.5}$ and G_{L30} schist powders, respectively.

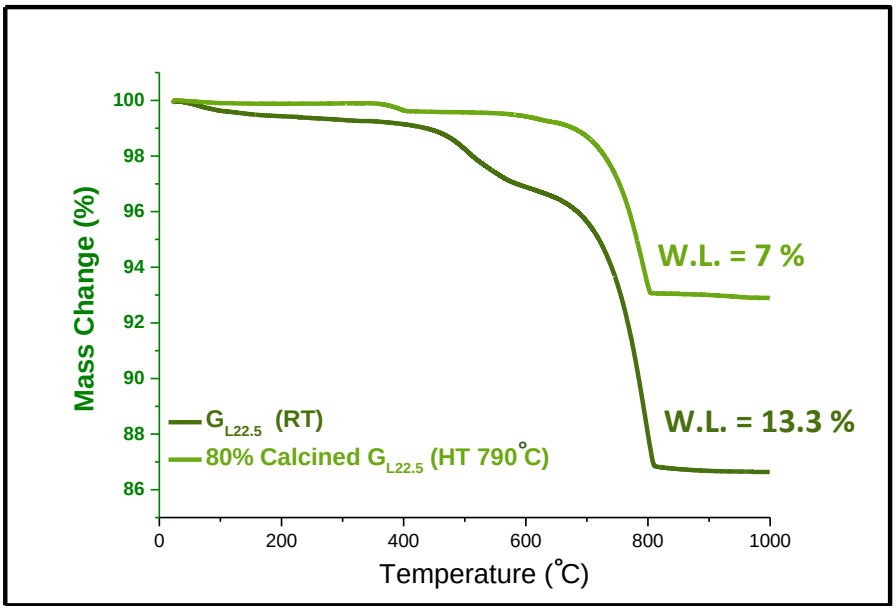

Figure 50. Thermo-gravimetric analysis of untreated vs. 80% calcined $G_{L22.5}$ schist powders (G schist with 22.5 wt% $C\bar{C}$ addition).

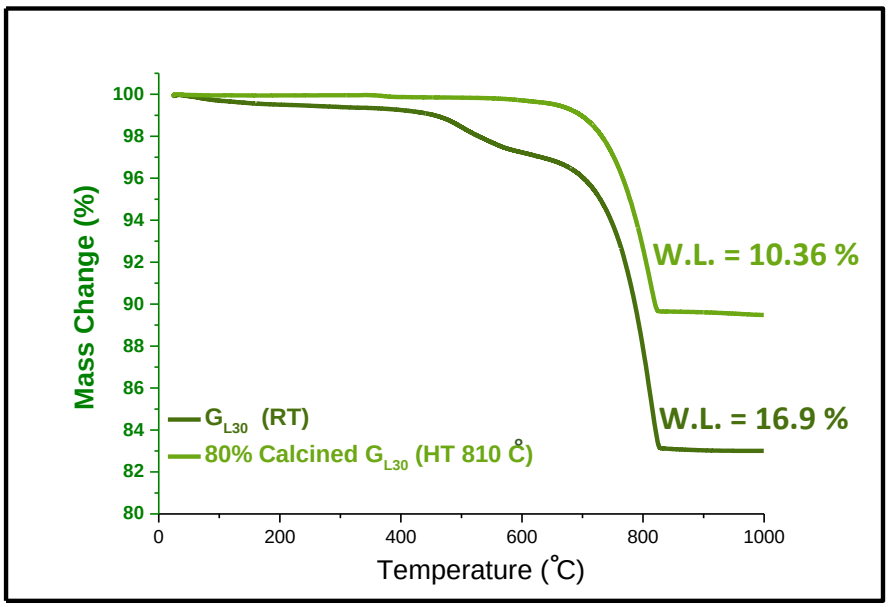

Figure 51. Thermo-gravimetric analysis of untreated vs. 80% calcined G_{L30} schist powders (G schist with 30 wt% $C\bar{C}$ addition).

The amount of calcium carbonate decomposition in the $G_{L22.5}$ sample changed from around 10 wt% to 6 wt%. For the G_{L30} sample, this value changed from 15 wt% to 9%.

3.2.2.2. C Schist

The calcination temperature (680ºC) which was calculated for 80% activation of virgin C schist, was applied to this sample for 2 hours. Figure 52 shows the TGA diagram of virgin and 80% calcined (activated at 680°C) C schist powders. The amount of total weight loss in the 80% calcined C sample was 2.58 wt% and the amount of calcium carbonate weight loss was around 1.5 wt%.

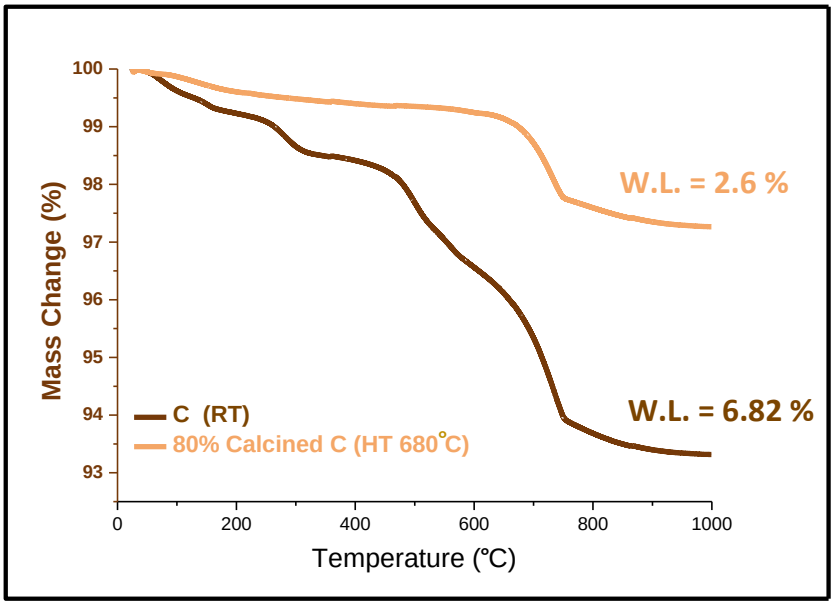

Figure 52. Thermo-gravimetric analysis of virgin vs. 80% calcined C schist powder

Figure 53 shows the TGA results of the untreated and calcined C_{L15} sample (C with 15% $\overline{CC}$ additions).

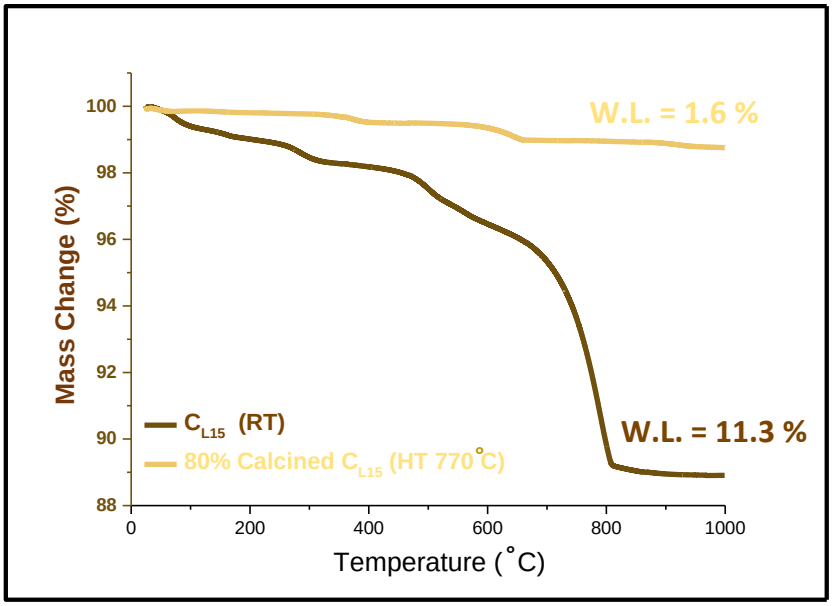

Figure 53. Thermo-gravimetric analysis of untreated vs. 80% calcined C_{L15} schist powders (C schist with 15 wt% $C\bar{C}$ addition).

The weight loss values of untreated and 80% calcined C_{L15} samples were about 11.3 wt% and 1.6 wt%, respectively. The calcination temperature was 770 ºC. This temperature range includes the

decomposition of clayey minerals and carbonate in the mixture as well. The weight loss value related to the decomposition of calcium carbonate in the untreated and calcined sample was about 7 wt% and 1 wt%, respectively.

Figures 54 and 55 show the TGA diagrams and total weight losses of the untreated and 80% calcined $C_{L22.5}$ and C_{L30} schist powders, respectively. The total weight loss of the $C_{L22.5}$ sample changed from 13.5 wt% to 7.55 wt% due to calcination. The amount of calcium carbonate decomposition in the heat-treated $C_{L22.5}$ sample was 6 wt%.

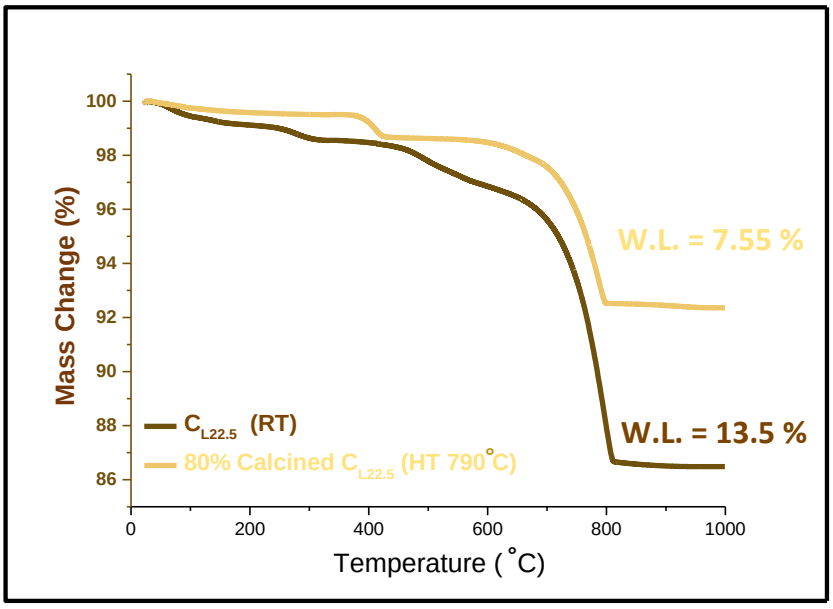

Figure 54. Thermo-gravimetric analysis of untreated vs. 80% calcined $C_{L22.5}$ schist powders (C schist with 22.5 wt% $C\bar{C}$ addition).

In the case of C_{L30} sample, the total weight loss of untreated and 80% calcined powders was 15.35 wt% and 9.2 wt%, respectively. In addition, the calcium carbonate decomposition amount for heat-treated C_{L30} was around 8 wt%

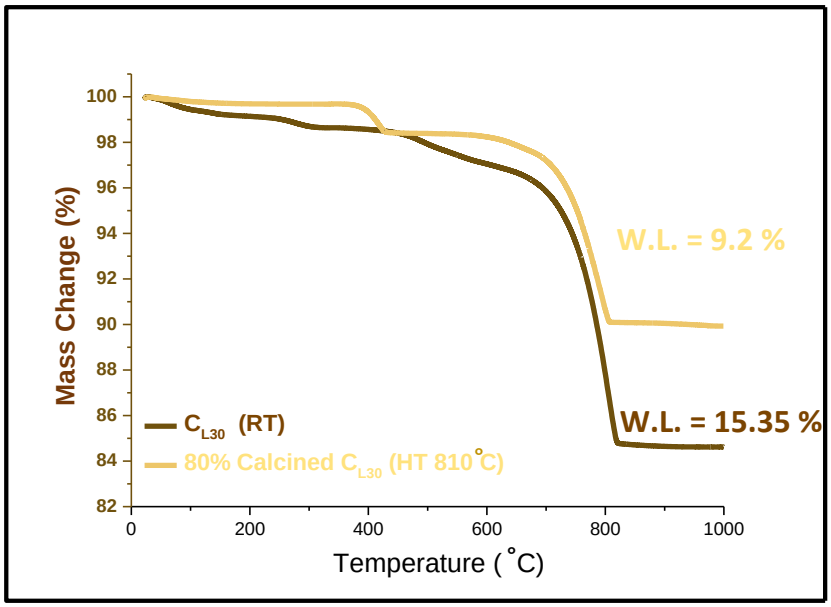

Figure 55. Thermo-gravimetric analysis of untreated vs. 80% calcined C_{L30} schist powders (C schist with 30 wt% $C\bar{C}$ addition).

3.2.2.3. P Schist

Figure 56 shows the TG diagram of virgin and heat-treated (80% activated) P schist powders.

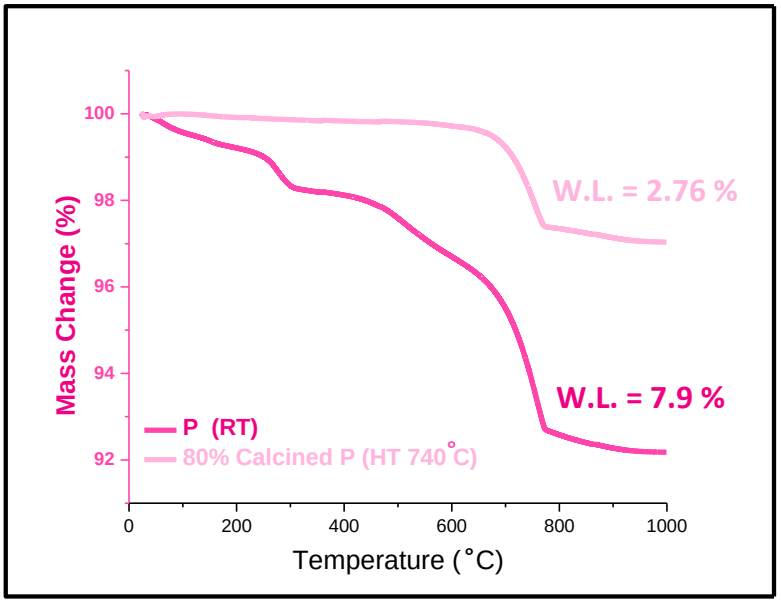

Figure 56. Thermo-gravimetric analysis of virgin vs. 80% calcined P schist powder

The TGA results showed that the 80% calcined P schist powder's weight loss was 2.76 wt%. The calcium carbonate weight loss in untreated and 80% calcined P powders was around 4 wt% and 2.5 wt%, respectively.

Figure 57 illustrates the TG curves of the untreated and calcined P_{L15} schist powders.

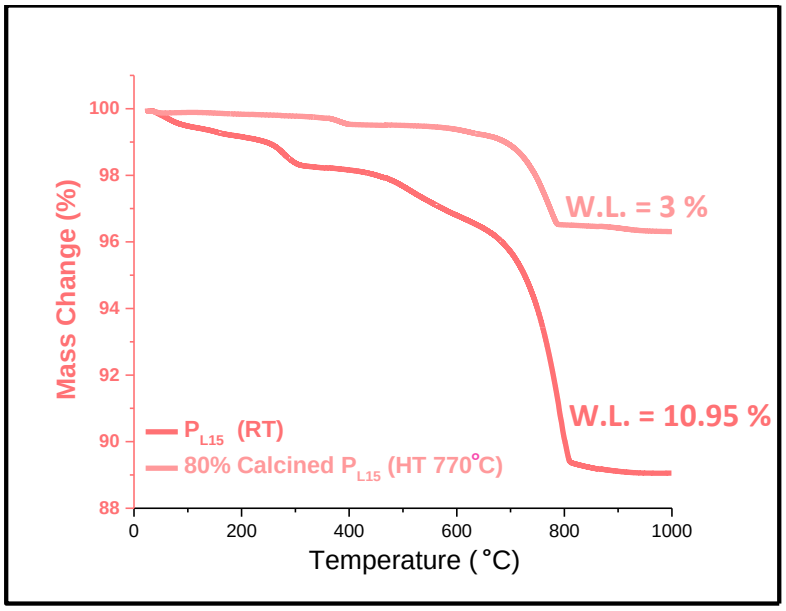

Figure 57. Thermo-gravimetric analysis of untreated vs. 80% calcined P_{L15} schist powders (P schist with 15 wt% $C\bar{C}$ addition).

The temperature that would achieve 80% activation for P_{L15} sample (P schist powder with 15% $\overline{CC}$) was estimated from TG analysis as around 770ºC. The associated remaining weight loss for 80% activated P_{L15} powder was around 3 wt%. In addition, the amount of weight loss related to calcium carbonate decomposition in 80% calcined sample was ~2.5 wt%.

Figure 58 shows a comparison between the TGA diagrams of untreated and 80% calcined $P_{L22.5}$ samples. Figure 59 illustrates the same comparison for the P_{L30} sample.

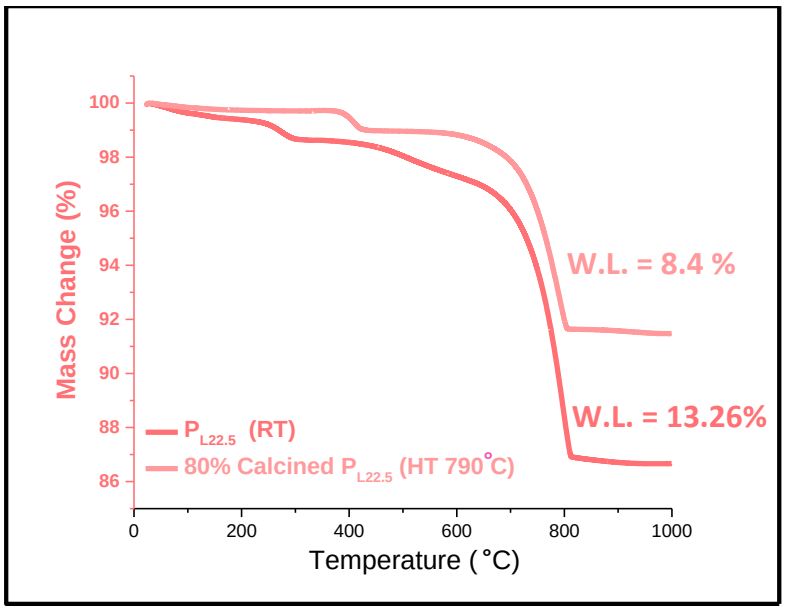

Figure 58. Thermo-gravimetric analysis of untreated vs. 80% calcined $P_{L22.5}$ schist powders (P schist with 22.5 wt% $C\bar{C}$ addition).

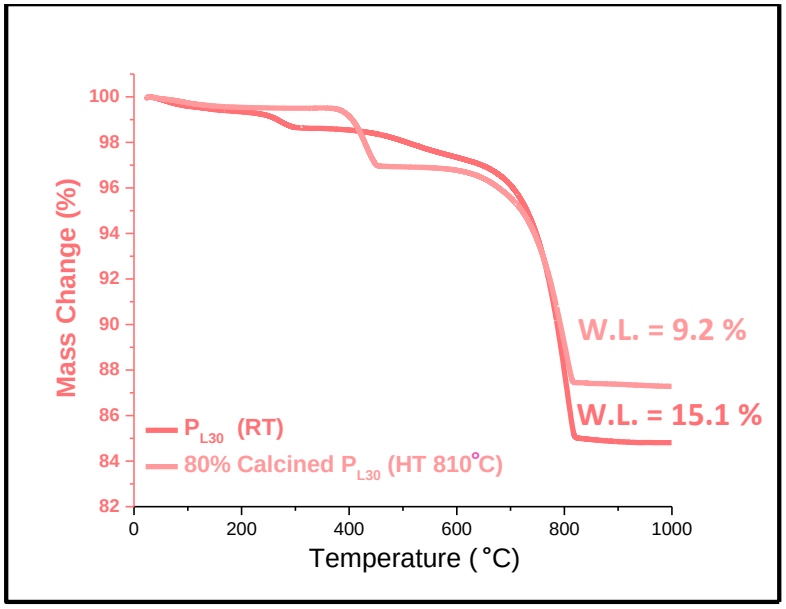

Figure 59. Thermo-gravimetric analysis of untreated vs. 80% calcined P_{L30} schist powders (P schist with 30 wt% $C\bar{C}$ addition).

According to the weight loss amounts in figures 58 and 59, the calcium carbonate weight loss percentage in 80% calcined $P_{L22.5}$ and P_{L30} samples was 5wt% and 8wt%, respectively.

3.2.2.4. B Schist

Figure 60 compares the TG analysis results of virgin and 80% activated B schist powders. This sample had a significant amount of carbon (graphite~ 5 wt%) in its mineral blend. The calculated theoretical weight loss for a sample activated to 80 wt% of its potential should be around 3.2 wt% and the obtained experimental value which is shown in the figure is very close to it.

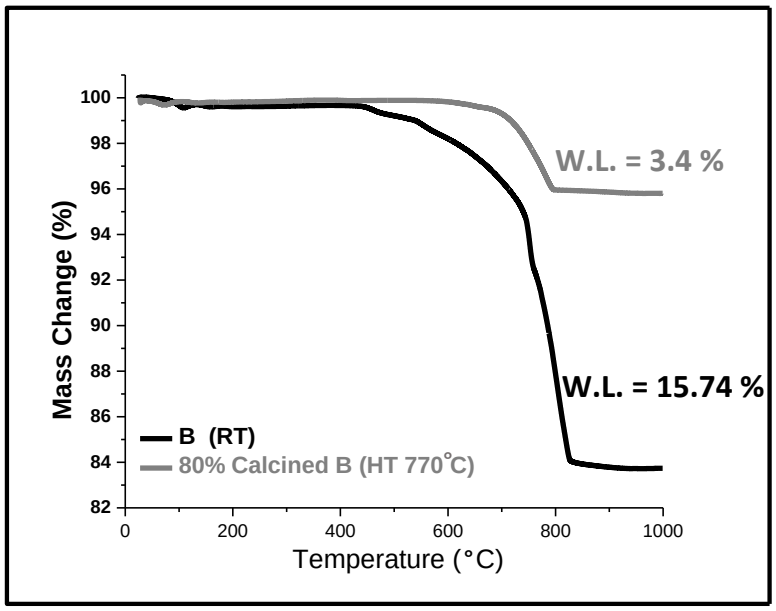

Figure 60. Thermo-gravimetric analysis of virgin vs. 80% calcined B schist powder

Figure 61 illustrates the TGA diagrams of $B_{L22.5}$ (B with 22.5% calcium carbonate in its composition) before and after the 80% thermal activation process. The 80% activated powder would have had 3.7 wt% remaining weight loss (potential for further activation). The TGA results showed 3 wt% which is very close to the expected value.

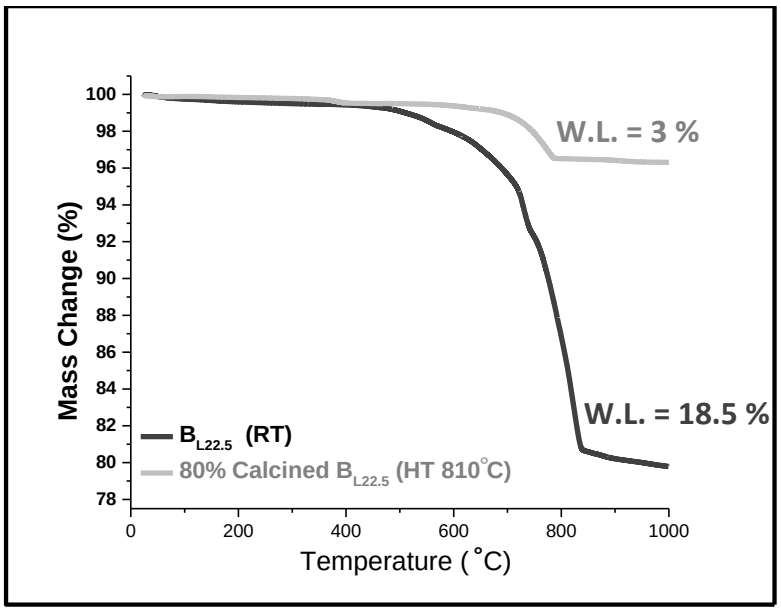

Figure 61. Thermo-gravimetric analysis of untreated vs. 80% calcined $B_{L22.5}$ schist powders (B schist with 22.5 wt% $C\bar{C}$ addition).

3.2.2.5. L Schist

Figure 62 compares the TG analysis results of the virgin and 80% activated L schist powders. The weight loss amount of L sample activated to 80 wt% of its potential was 2.7 wt%.

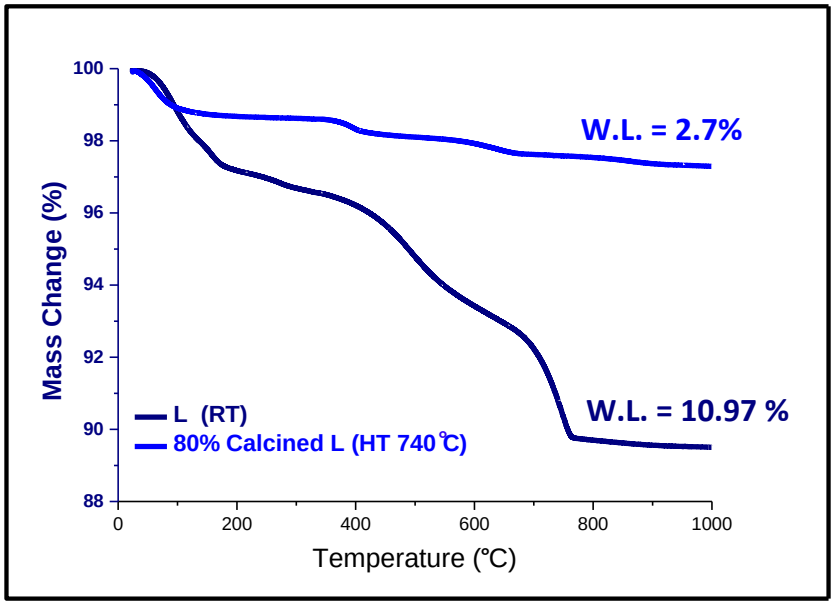

Figure 62. Thermo-gravimetric analysis of virgin vs. 80% calcined L schist powder

Figures 63 and 64 illustrate the TGA diagrams of untreated and 80% calcined L_{L15} and L_{L30} samples, respectively. For the L_{L15} sample, the 80% activated powder showed 4.1 wt% remaining weight loss (potential for further activation), and this value for the L_{L30} sample was around 5.9 wt%. Moreover, the amount of calcium carbonate decomposition weight loss for the 80% calcined L_{L15} and L_{L30} samples was around 2.5 wt% and 4 wt%, respectively.

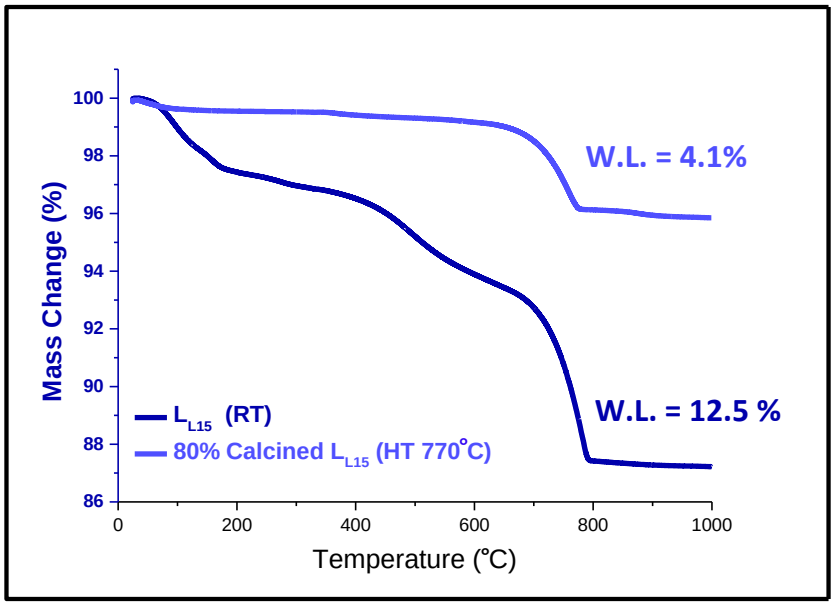

Figure 63. Thermo-gravimetric analysis of untreated vs. 80% calcined L_{L15} schist powders (L schist with 15 wt% $C\bar{C}$ addition).

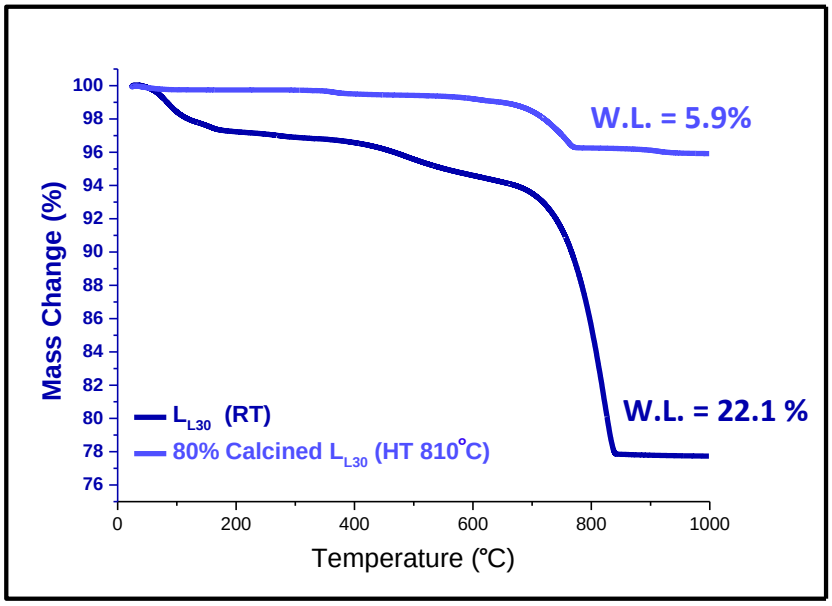

Figure 64. Thermo-gravimetric analysis of untreated vs. 80% calcined L_{L30} schist powders (L schist with 30 wt% $C\bar{C}$ addition).

3.2.3. Microstructure Analysis

Scanning electron microscopy was performed on all untreated and calcined materials to investigate the changes in the microstructure during calcination. In addition, the changes in the chemistry of the phases which were caused by heat treatment were observed with the help of EDS mapping.

3.2.3.1. G Schist

The micrographs of the virgin (left) and calcined (right) G schist sample are shown in Figure 65. The SEM images are only provided for virgin-untreated and calcined schist in their original composition without any modification in the calcium carbonate amount.

(Virgin) **(Calcined)**

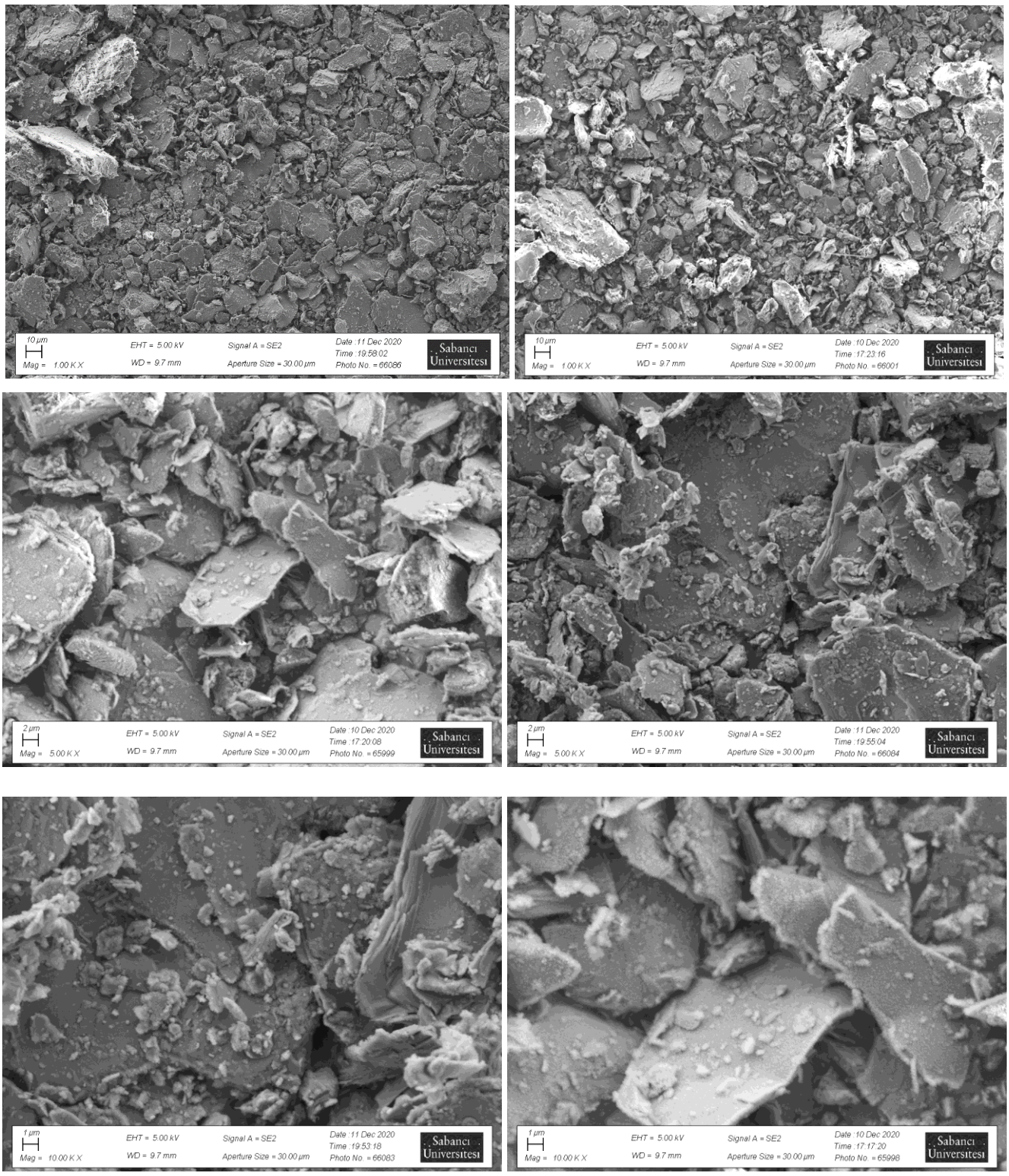

Figure 65. G schist micrographs for Virgin (Left) and Calcined (Right) Powders at the same magnification. First row: mag. = 1KX, second row: mag = 5KX, and third row: mag = 10KX

The SEM micrographs illustrated the particle morphological changes and reduction in size in some parts and de-crystallization (the disappearance of prisms was interpreted as such).

3.2.3.2. C Schist

Figure 66 illustrates the SEM micrographs taken from virgin and calcined C schist samples.

(Virgin) **(Calcined)**

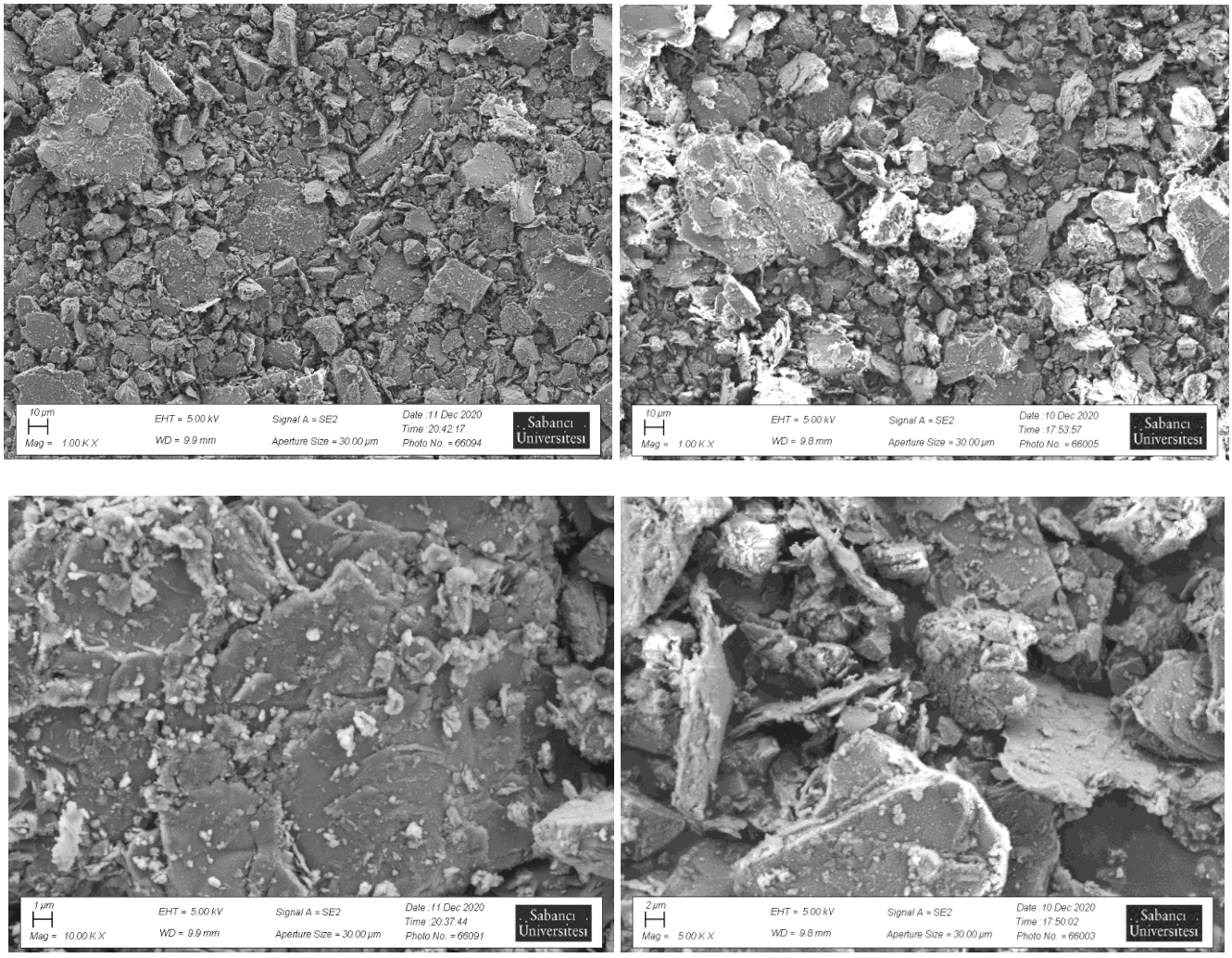

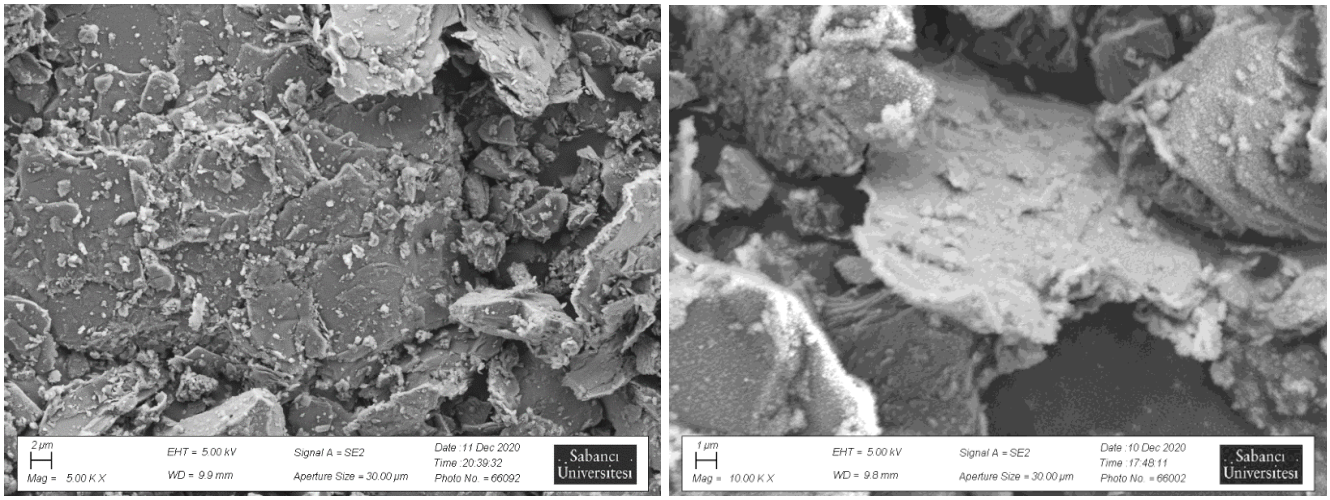

Figure 66. C schist micrographs for Virgin (Left) and Calcined (Right) Powders at the same magnification. First row: mag. = 1KX, second row: mag = 5KX, and third row: mag = 10KX

Similar to the G schist sample, the calcination process changed the microstructure of some platy particles in the C schist as well. Calcined powder particles had ruffled edges of the plate clay particles.

3.2.3.3. P Schist

Figure 67 shows the micrographs of the virgin (left) and calcined (right) P schist sample.

(Virgin) **(Calcined)**

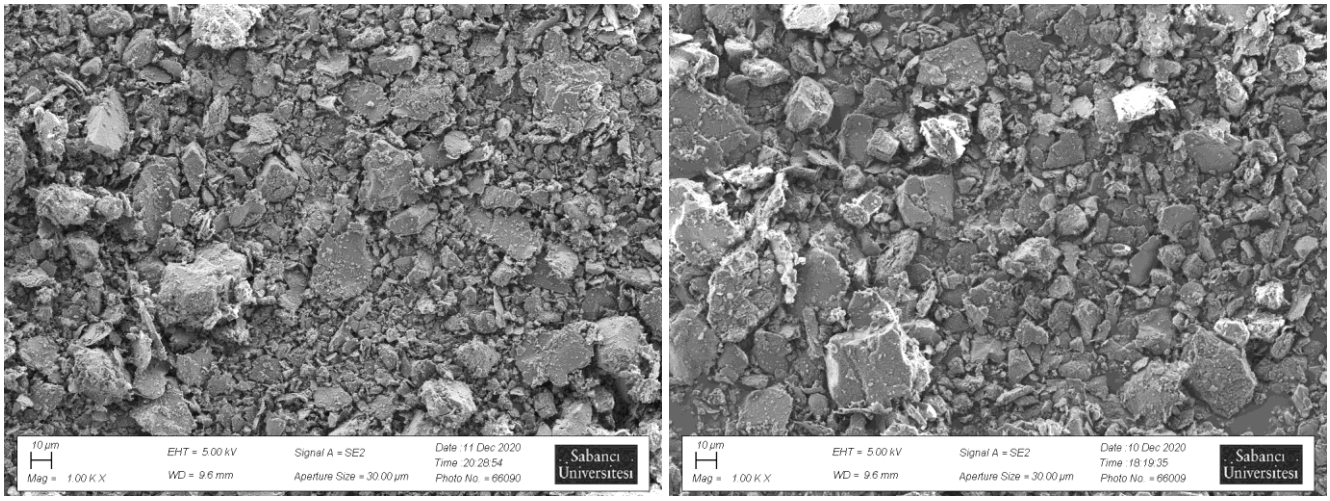

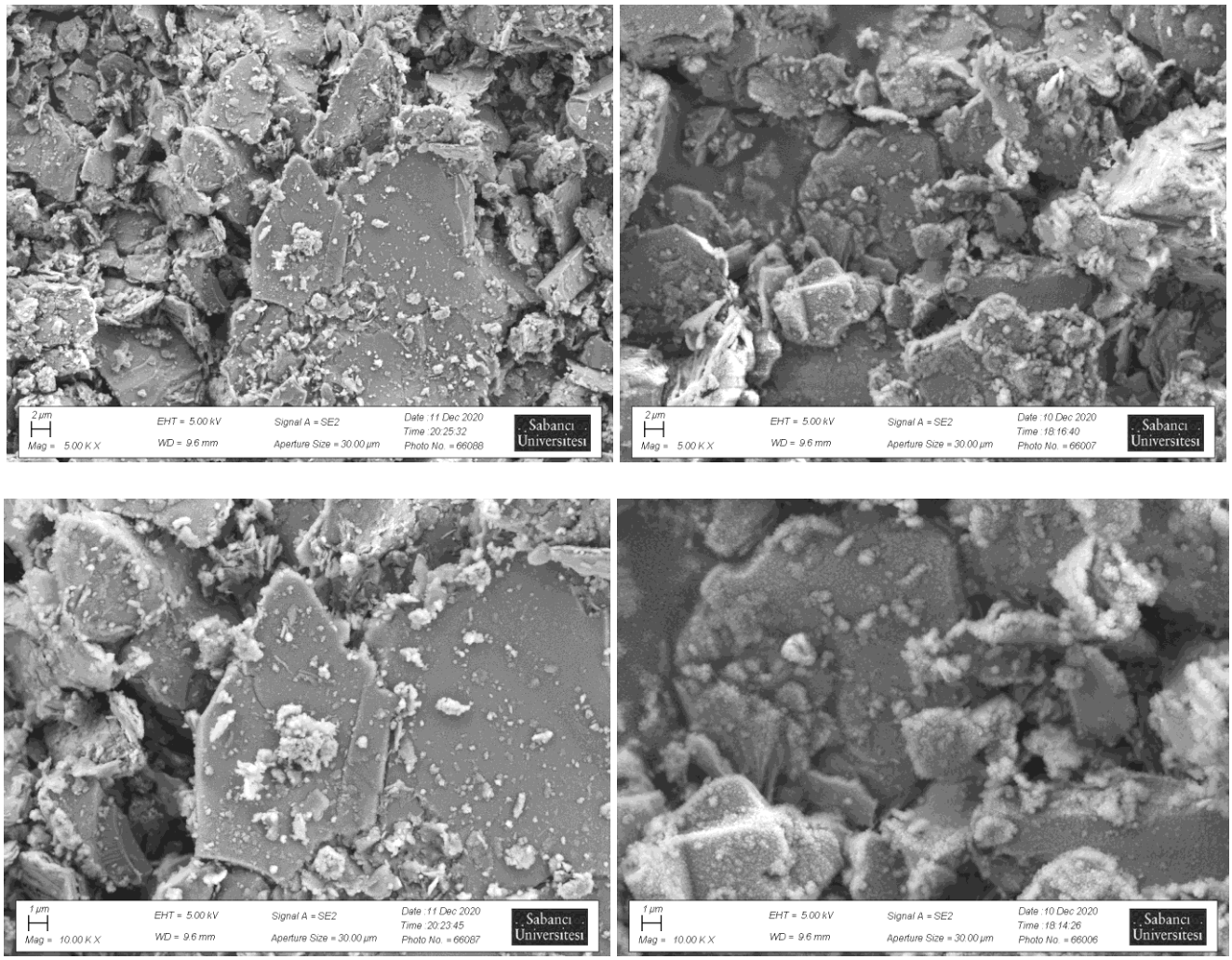

Figure 67. P schist micrographs for Virgin (Left) and Calcined (Right) Powders at the same magnification. First row: mag. = 1KX, second row: mag = 5KX, and third row: mag = 10KX

As it can be seen in the SEM images, the particles of the P sample were destroyed and the edges were ruffled after calcination.

3.2.3.4. B Schist

Figure 68 represents the SEM micrographs of B schist powder before and after the heat treatment.

(Virgin) **(Calcined)**

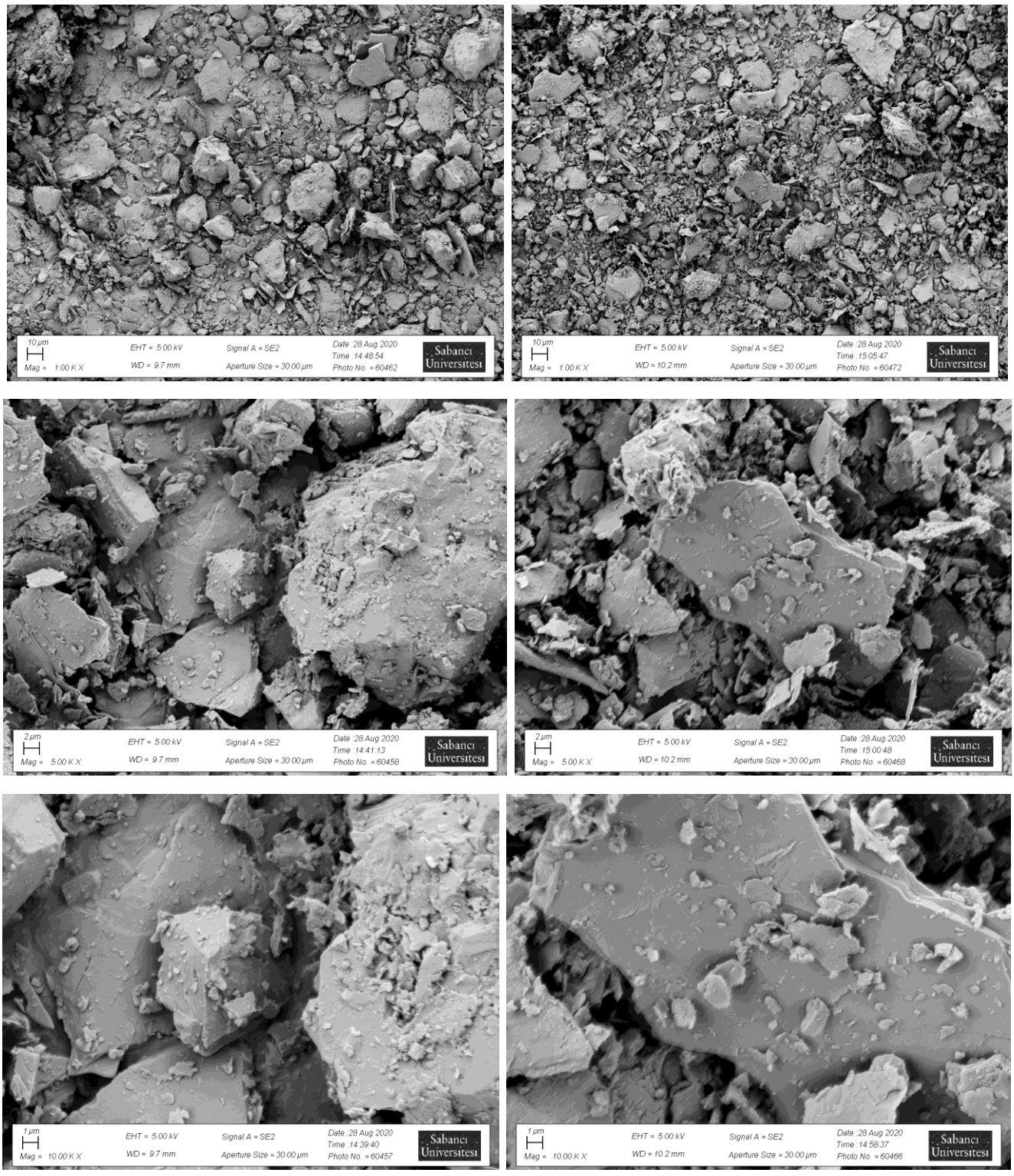

Figure 68. B schist micrographs for Virgin (Left) and Calcined (Right) Powders at the same magnification. First row: mag. = 1KX, second row: mag = 5KX, and third row: mag = 10KX

The de-hydroxylated clayey particles can be seen as ruffled edge sheety particles in some parts of the B micrograph. The ruffled edged particles are more obvious in this sample after calcination. Moreover, there is an obvious reduction in average particle size during the heat-treatment process.

3.2.3.5. L Schist

Figure 69 represents the SEM micrographs of L schist powder before and after the heat treatment.

(Virgin) **(Calcined)**

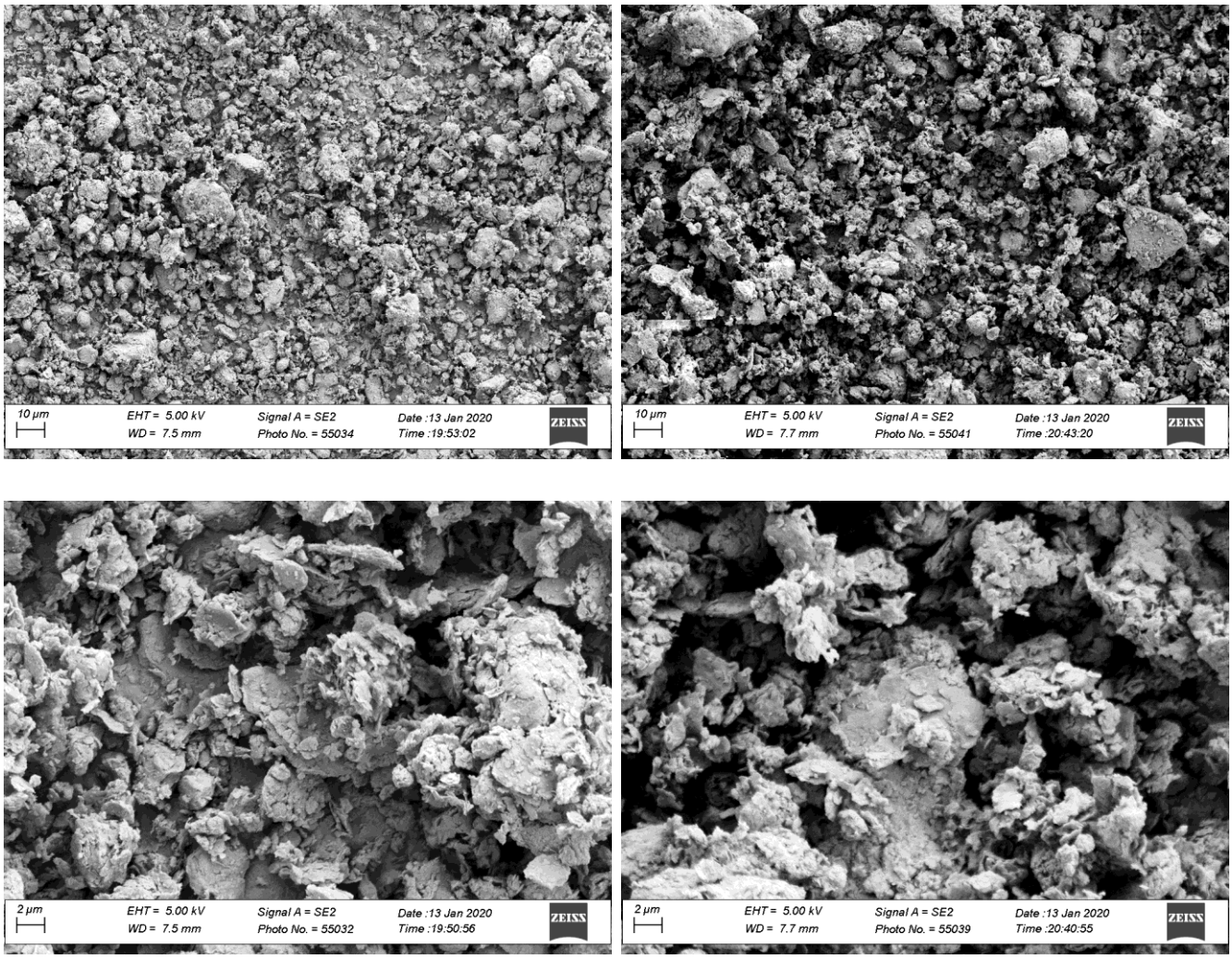

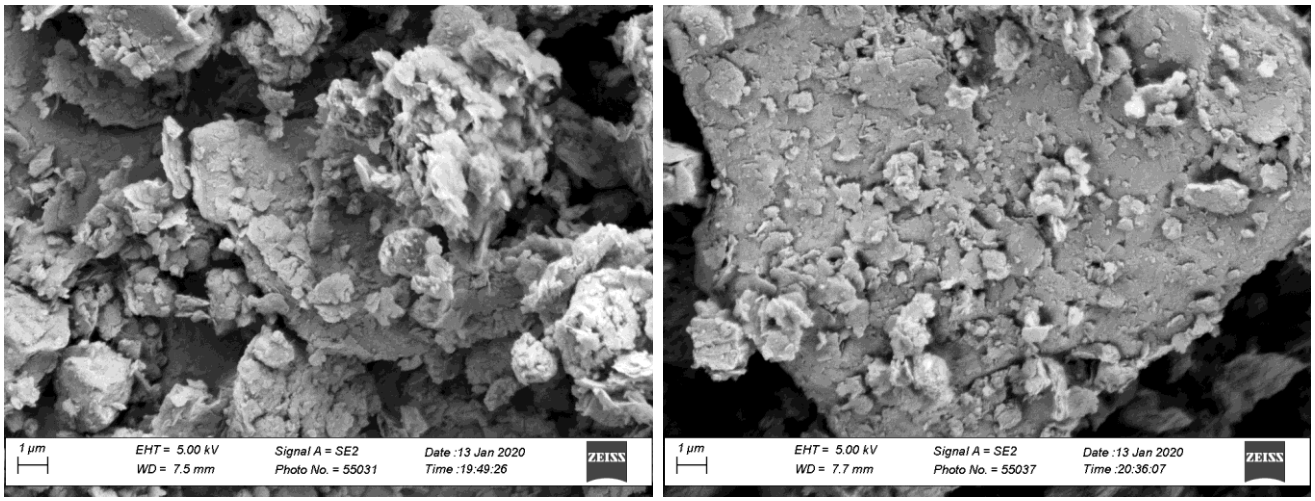

Figure 69. L schist micrographs for Virgin (Left) and Calcined (Right) Powders at the same magnification. First row: mag. = 1KX, second row: mag = 5KX, and third row: mag = 10KX

As it can be seen in the SEM micrographs of L schist, there is a considerable reduction in particle size after calcination. In addition, there is a very rare amount of plate-like structures in this sample, compared to the previous samples.

3.2.4. DSC Analysis

With the help of DSC analysis, we determined the exact energy amount needed for each clay/carbonate composition of L schist to be calcined. This energy amount differs based on the portion of calcium carbonate to clay.

Figures 70, 71, 72, and 73 illustrate the DSC/TGA curves of the kaolinite, L, $L_{L15,}$ and L_{L30} samples, respectively. Additionally, for each weight loss step, the area under the curve was integrated. This integral is equivalent to the energy consumption during calcination.

3.2.4.1. Kaolinite

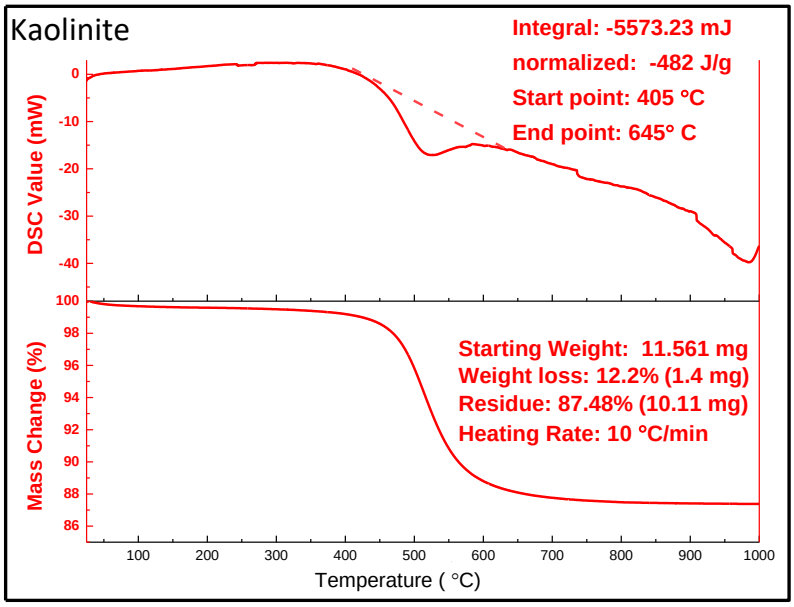

Figure 70. DSC/TGA curve of kaolinite sample in the temperature range of 25-1000°C

3.2.4.2. L Schist

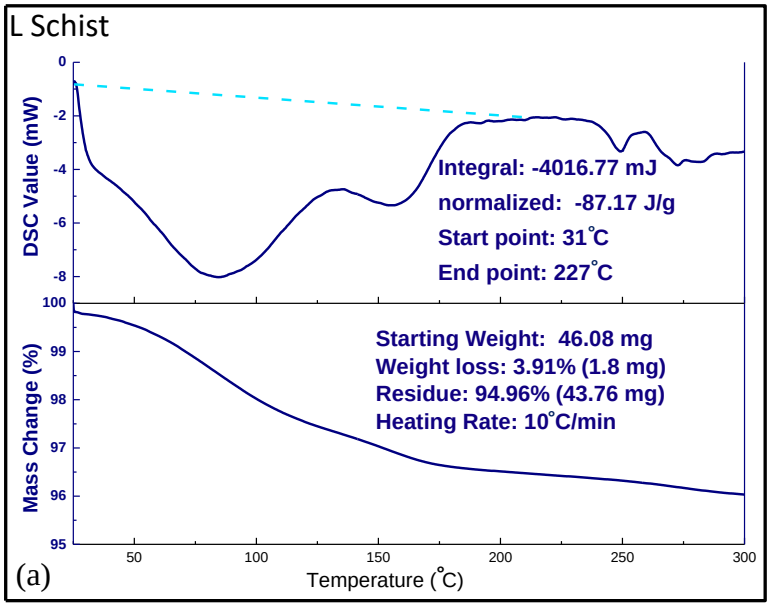

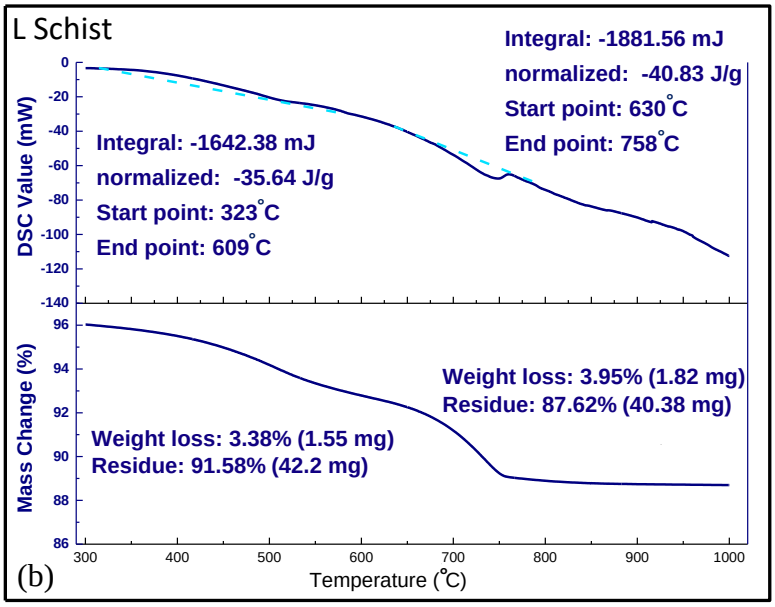

Figure 71. DSC/TGA curve of L schist sample in the temperature range of (a) 25-300°C and (b) 300-1000°C

3.2.4.3. L_{L15} Schist

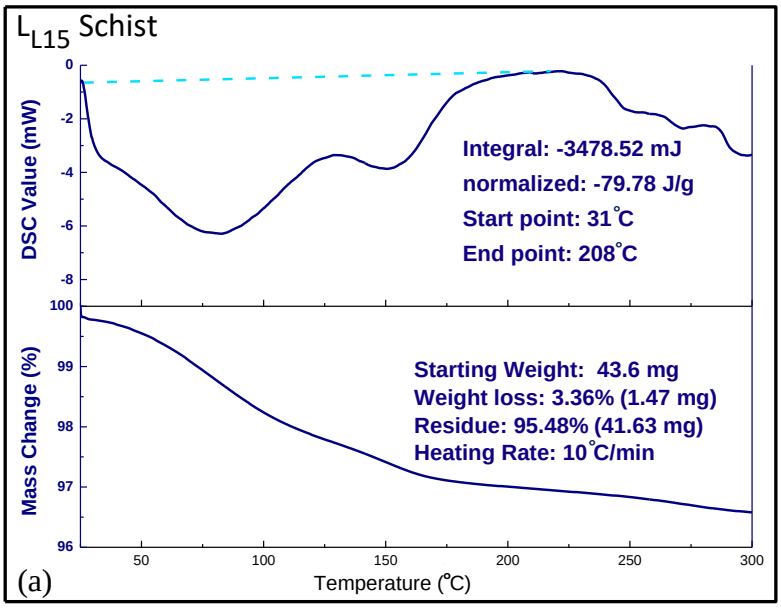

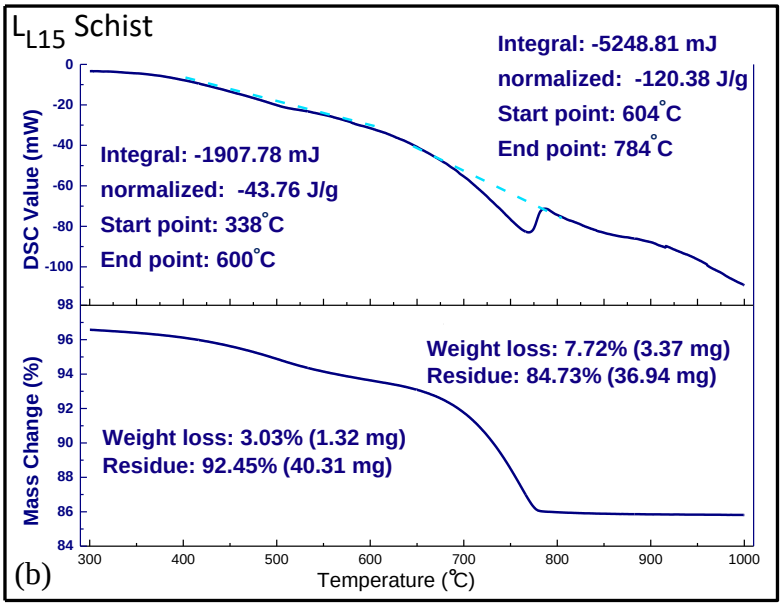

Figure 72. DSC/TGA curve of L_{L15} schist sample in the temperature range of (a) 25-300°C and (b) 300-1000°C

3.2.4.4. L_{L30} Schist

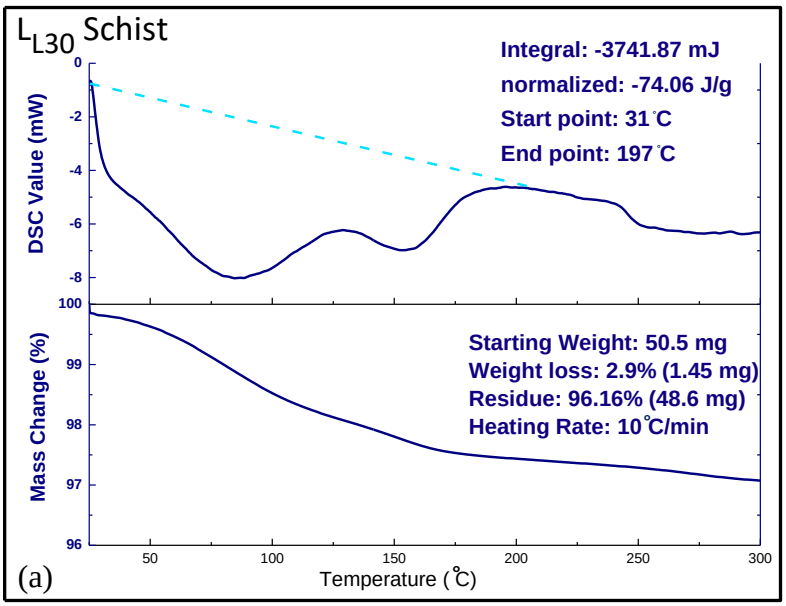

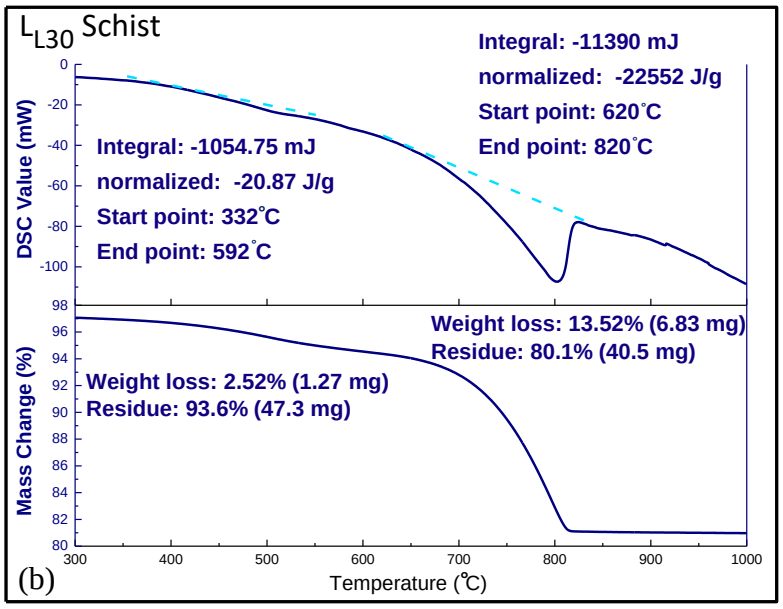

Figure 73. DSC/TGA curve of L_{L30} schist sample in the temperature range of (a) 25-300℃ and (b) 300-1000℃

3.2.5. Compressive Strength Measurement of Composite Cement

The compressive strength measurement is the best way to evaluate the potential candidates for cement substitution. The compressive strength of all of the thermally activated schist samples with several amounts of $C\bar{C}$ were compared. In such a way, the effect of limestone addition either as calcined carbonate (i.e. CaO) or untreated limestone ($CaCO_3$) and also the pozzolanic reactivity of the thermally activated schist samples were investigated. The compressive strength of 70 wt% of cement and 30 wt% hypothetical inert filler powder is chosen as a benchmark to evaluate the role of calcined clay as cement substitution. The targeted compressive strength criteria for the composite cement in this study was 90% of the pure cement paste after 28 days of hydration when 30 wt% of cement is replaced by SCMs. In addition, the composite cement samples were also compared to 70% of pure OPC strength.

3.2.5.1. G Schist

Figure 74 and Table 23 illustrate the 80%, 100% and 110% calcined G schist compressive strength results when it is substituted 30 wt% of the cement.

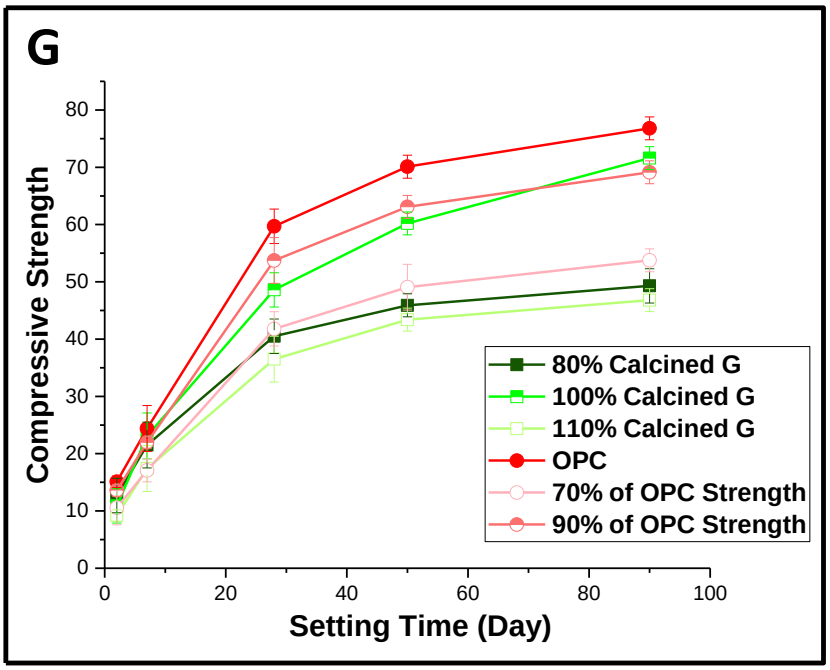

Figure 74. Compressive strength of OP cement blended with 30 wt% of calcined G schist, compared to pure cement

Table 23. Compressive strength of OP cement blended with 30 wt% of calcined G schist, compared to pure cement

Setting Time (Day)	80% Calcined G	100% Calcined G	110% Calcined G	OPC	70% of OPC Strength	90% of OPC Strength
2	12.7	10.9	9.2	15.1	10.57	13.59
7	21.5	23.1	17.4	24.4	17.08	21.96
28	40.5	48.6	36.5	59.7	41.79	53.73
50	45.9	60.2	43.4	70.1	49.07	63.09
90	49.3	71.6	46.8	76.8	53.76	69.12

As it can be seen in the compressive strength test results, the 80% and 110% calcined G sample could not reach the 70% of pure OPC strength. However, the 100% calcined sample of G schist was very close to the criteria which was 90% of pure OPC strength.

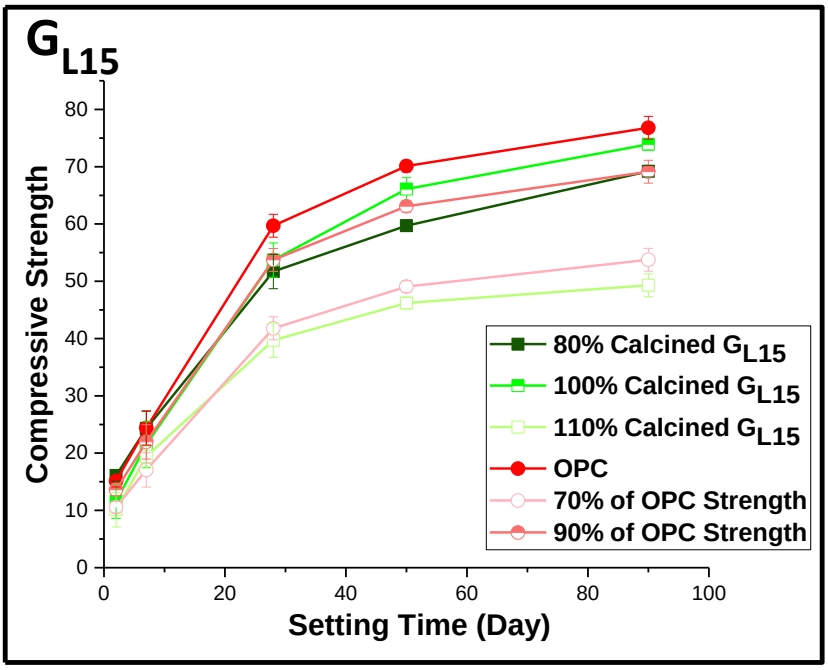

Figure 75. Compressive strength of OP cement blended with 30 wt% of calcined G_{L15} schist (G schist with 15 wt% $C\bar{C}$ addition), compared to pure cement

Table 24. Compressive strength of OP cement blended with 30 wt% of calcined GL15 schist (G schist with 15 wt% $C\bar{C}$ addition), compared to pure cement

Setting Time (Day)	80% Calcined G_{L15}	100% Calcined G_{L15}	110% Calcined G_{L15}	OPC	70% of OPC Strength	90% of OPC Strength
2	16.1	11.6	10.1	15.1	10.57	13.59
7	24.3	21.5	19.4	24.4	17.08	21.96
28	51.7	53.7	39.7	59.7	41.79	53.73
50	59.7	66.1	46.2	70.1	49.07	63.09
90	69.2	73.9	49.3	76.8	53.76	69.12

Figure 75 and Table 24 illustrate the 80%, 100%, and 110% calcined G_{L15} schist compressive strength results when it is substituted 30 wt% of the cement. Based on the results, the added amount of carbonate to G schist had a drastic effect on composite cement paste hydration even in 80% calcination. Furthermore, among the selected temperatures for calcination of G and G_{L15}, the 100% calcination temperature was the most effective one. Therefore, the optimum calcination

temperature for virgin or carbonate augmented samples is the temperature associated with 100% calcination. The samples which are calcined at higher temperatures (110% calcination) have lower strength values compared to the others.

Figure 76 and Table 25 show the 80% calcined $G_{L22.5}$ schist sample compressive strength results when it is substituted 30 wt% of the cement. It is obvious that this sample's compressive strength does not satisfy the criteria. It did not reach 90% of pure OPC strength.

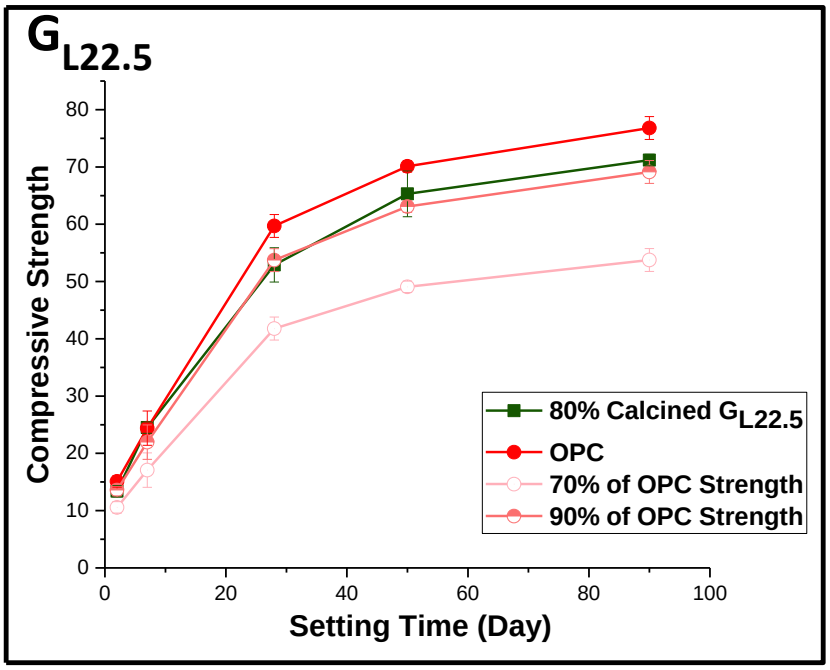

Figure 76. Compressive strength of OP cement blended with 30 wt% of calcined $G_{L22.5}$ schist (G schist with 22.5 wt% $C\bar{C}$ addition), compared to pure cement

Table 25. Compressive strength of OP cement blended with 30 wt% of calcined GL22.5 schist (G schist with 22.5 wt% $C\bar{C}$ addition), compared to pure cement

Setting Time (Day)	80% Calcined $G_{L22.5}$	OPC	70% of OPC Strength	90% of OPC Strength
2	13.4	15.1	10.57	13.59
7	24.5	24.4	17.08	21.96
28	52.9	59.7	41.79	53.73
50	65.3	70.1	49.07	63.09
90	71.2	76.8	53.76	69.12

Figure 77 and Table 26 show the 80% calcined G_{L30} schist sample compressive strength results when it is substituted 30 wt% of the cement. According to the strength values, this sample's compressive strength reaches 70% of pure OPC strength, but still very lower than the 90% of pure OPC strength.

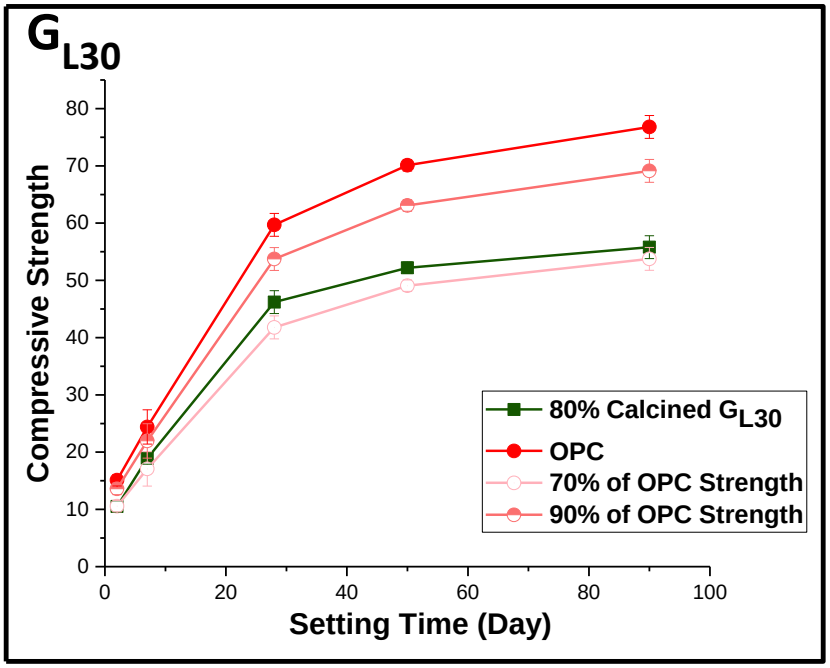

Figure 77. Compressive strength of OP cement blended with 30 wt% of calcined G_{L30} schist (G schist with 30 wt% $C\bar{C}$ addition), compared to pure cement

Table 26. Compressive strength of OP cement blended with 30 wt% of calcined GL30 schist (G schist with 30 wt% $C\bar{C}$ addition), compared to pure cement

Setting Time (Day)	80% Calcined G_{L30}	OPC	70% of OPC Strength	90% of OPC Strength
2	10.5	15.1	10.57	13.59
7	18.9	24.4	17.08	21.96
28	46.2	59.7	41.79	53.73
50	52.2	70.1	49.07	63.09
90	54.2	76.8	53.76	69.12

3.2.5.2. C Schist

Figure 78 and Table 27 show the compressive strength results for the composite cement pastes prepared with 30 wt% of 80% calcined C schist.

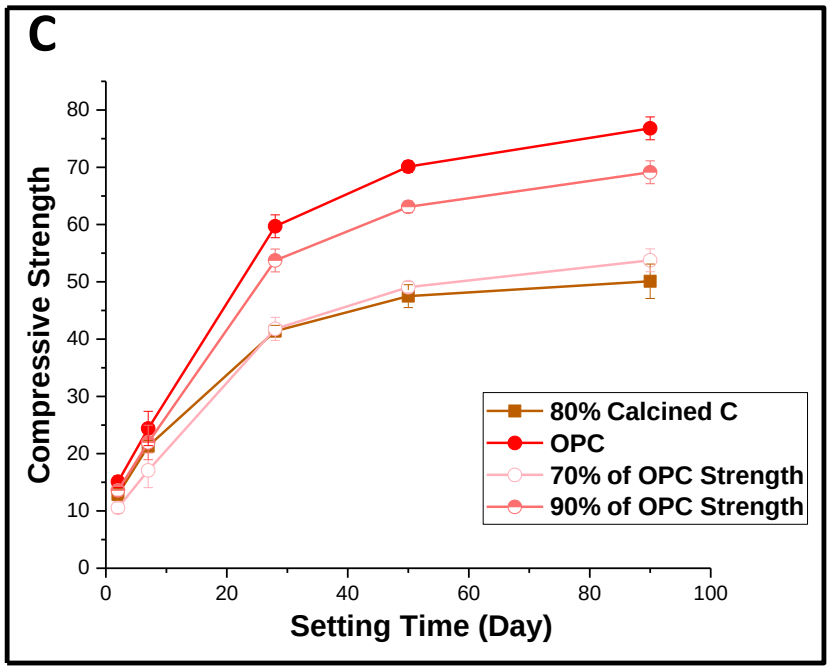

Figure 78. Compressive strength of OP cement blended with 30 wt% of calcined C schist, compared to pure cement

Table 27. Compressive strength of OP cement blended with 30 wt% of calcined C schist, compared to pure cement

Setting Time (Day)	80% Calcined C	OPC	70% of OPC Strength	90% of OPC Strength
2	12.9	15.1	10.57	13.59
7	21.3	24.4	17.08	21.96
28	41.4	59.7	41.79	53.73
50	47.5	70.1	49.07	63.09
90	50.1	76.8	53.76	69.12

Figure 79 and Table 28 show the compressive strength results for the composite cement pastes prepared with 30 wt% of 80% calcined C_{L15} schist.

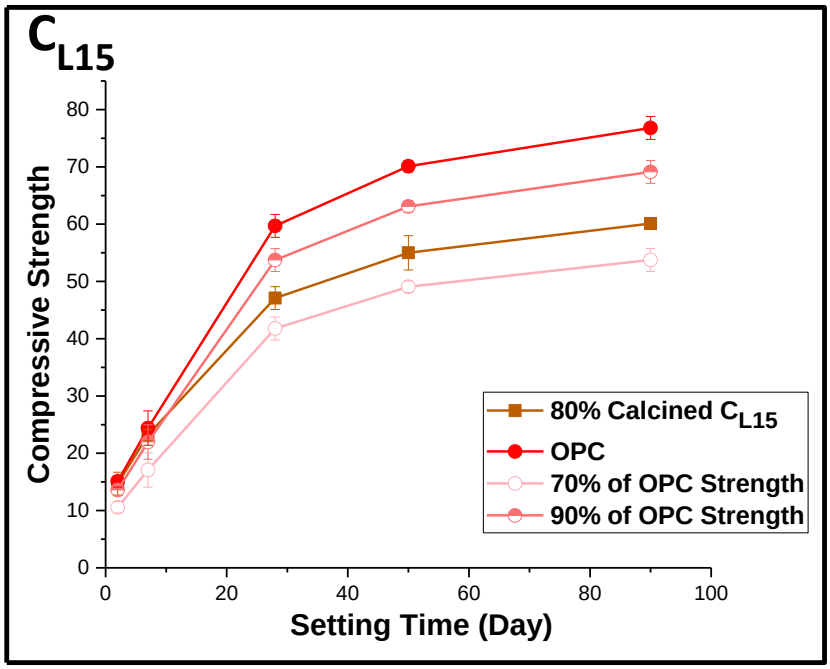

Figure 79. Compressive strength of OP cement blended with 30 wt% of calcined C_{L15} schist (C schist with 15 wt% $C\bar{C}$ addition), compared to pure cement

Table 28. Compressive strength of OP cement blended with 30 wt% of calcined C_{L15} schist (C schist with 15 wt% $C\bar{C}$ addition), compared to pure cement

Setting Time (Day)	80% Calcined C_{L15}	OPC	70% of OPC Strength	90% of OPC Strength
2	13.4	15.1	10.57	13.59
7	24.5	24.4	17.08	21.96
28	52.9	59.7	41.79	53.73
50	65.3	70.1	49.07	63.09
90	71.2	76.8	53.76	69.12

The compressive strength test results for C and C_{L15} samples did not satisfy the set goals. The obtained values are significantly lower than pure cement strength. The achieved strength value for C schist (without the carbonate addition) is almost 70% of cement strength that means the effect of pozzolanic reaction on strength of cement was zero. In the case of composite cement paste sample prepared with C_{L15} (C with 15 wt% of carbonate), the strength was only 80% of the OP cement strength. Therefore, both SCMs could not satisfy the chosen strength criteria. These results will be discussed in detail in the discussion section in the light of all results.

Figure 80 and table 29 illustrate the compressive strength results for the composite cement pastes prepared with 30 wt% of 80% calcined $C_{L22.5}$ schist.

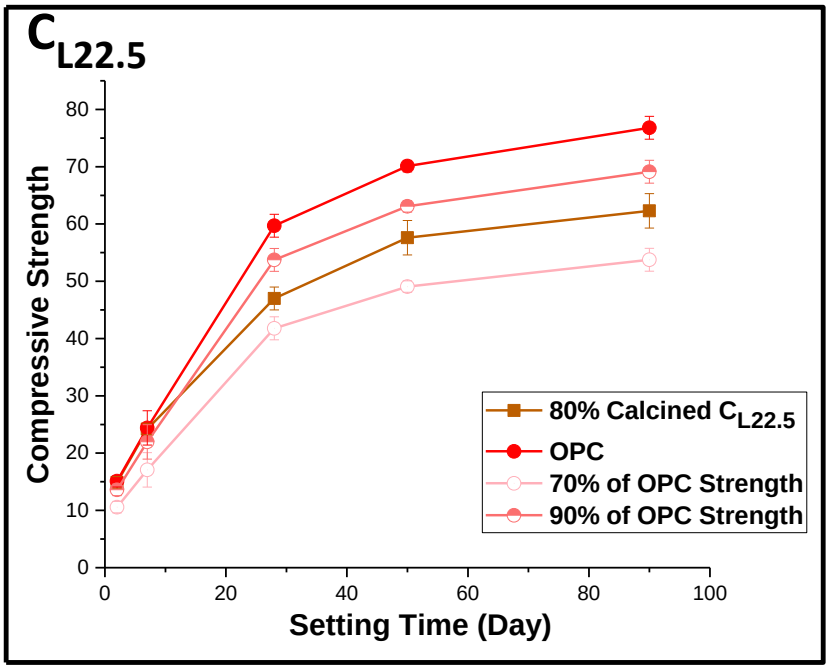

Figure 80. Compressive strength of OP cement blended with 30 wt% of calcined $C_{L22.5}$ schist (C schist with 22.5 wt% $C\bar{C}$ addition), compared to pure cement

Table 29. Compressive strength of OP cement blended with 30 wt% of calcined $C_{L22.5}$ schist (C schist with 22.5 wt% $C\bar{C}$ addition), compared to pure cement

Setting Time (Day)	80% Calcined $C_{L22.5}$	OPC	70% of OPC Strength	90% of OPC Strength
2	14.9	15.1	10.57	13.59
7	24.2	24.4	17.08	21.96
28	47	59.7	41.79	53.73
50	57.6	70.1	49.07	63.09
90	62.3	76.8	53.76	69.12

Figure 81 and Table 30 illustrate the compressive strength results for the composite cement pastes prepared with 30 wt% of 80% calcined C_{L30} schist.

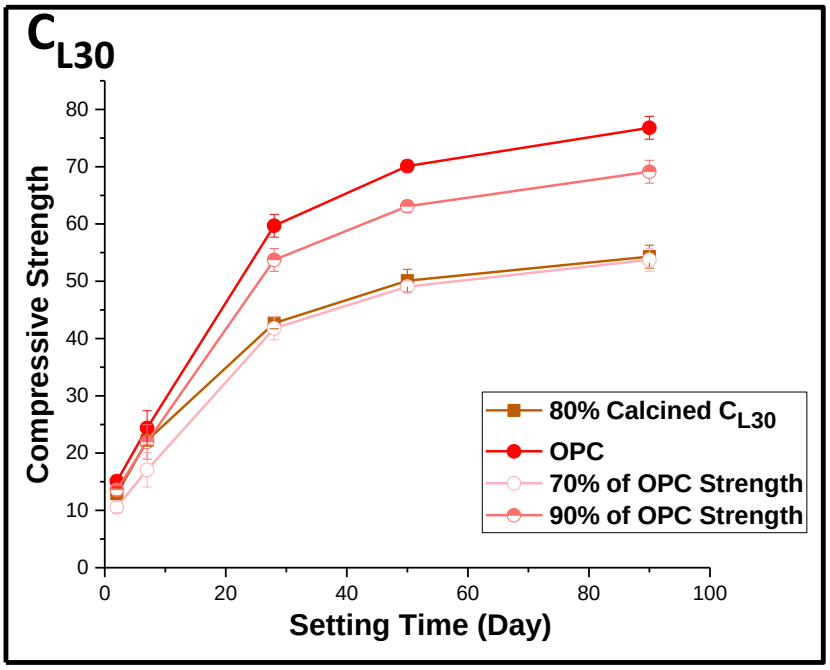

Figure 81. Compressive strength of OP cement blended with 30 wt% of calcined C_{L30} schist (C schist with 30 wt% $C\bar{C}$ addition), compared to pure cement

Table 30. Compressive strength of OP cement blended with 30 wt% of calcined C_{L30} schist (C schist with 30 wt% $C\bar{C}$ addition), compared to pure cement

Setting Time (Day)	80% Calcined C_{L30}	OPC	70% of OPC Strength	90% of OPC Strength
2	12.9	15.1	10.57	13.59
7	22.2	24.4	17.08	21.96
28	42.7	59.7	41.79	53.73
50	50.1	70.1	49.07	63.09
90	54.3	76.8	53.76	69.12

The strength results show that the compressive strength of the 80% calcined $C_{L22.5}$ sample is very similar to the 100% calcined C_{L15} sample. The strength values of the C_{L30} sample is the same as 70% of pure OPC strength which does not satisfy the criteria.

3.2.5.3. P Schist

Figure 82 and Table 31 show the compressive strength results for composite cement paste mixture prepared with 80% calcined P without carbonate additions.

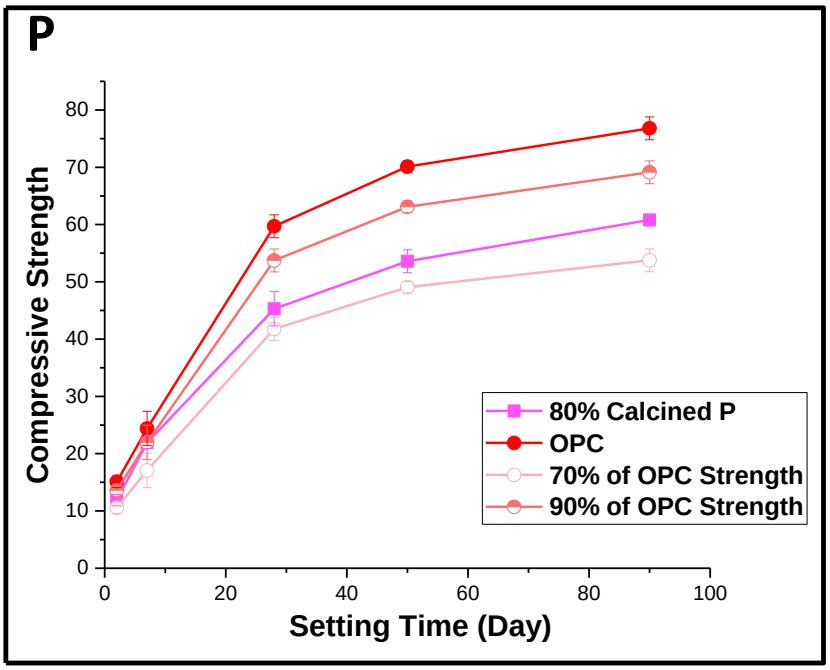

Figure 82. Compressive strength of OP cement blended with 30 wt% of calcined P schist, compared to pure cement

Table 31. Compressive strength of OP cement blended with 30 wt% of calcined P schist, compared to pure cement

Setting Time (Day)	80% Calcined P	OPC	70% of OPC Strength	90% of OPC Strength
2	11.9	15.1	10.57	13.59
7	21.9	24.4	17.08	21.96
28	45.3	59.7	41.79	53.73
50	53.6	70.1	49.07	63.09
90	60.8	76.8	53.76	69.12

Figure 83 and Table 32 show the compressive strength results for composite cement paste mixture prepared with 80% calcined P_{L15} (P with 15% calcium carbonate addition).

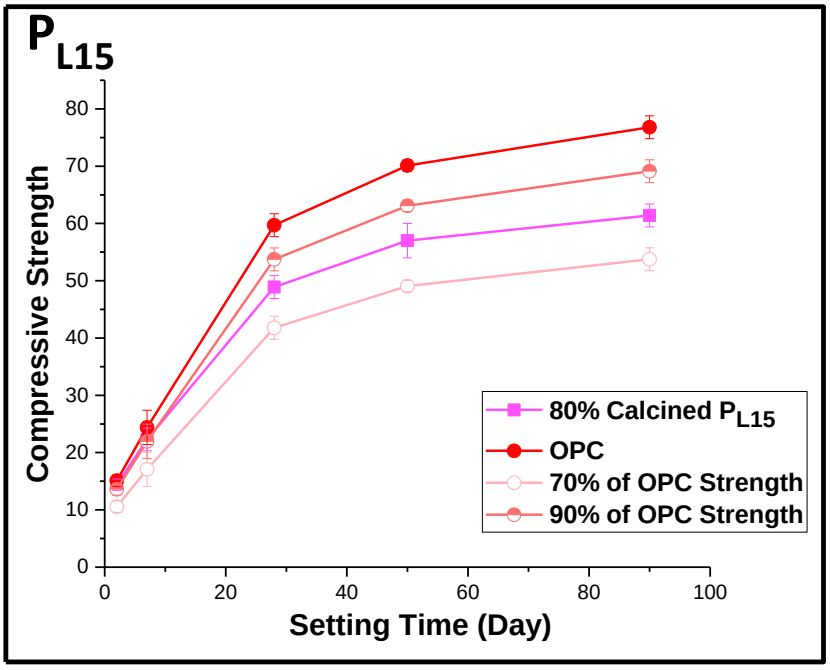

Figure 83. Compressive strength of OP cement blended with 30 wt% of calcined P_{L15} schist (P schist with 15 wt% $C\bar{C}$ addition), compared to pure cement

Table 32. Compressive strength of OP cement blended with 30 wt% of calcined P_{L15} schist (P schist with 15 wt% $C\bar{C}$ addition), compared to pure cement

Setting Time (Day)	80% Calcined P_{L15}	OPC	70% of OPC Strength	90% of OPC Strength
2	14.4	15.1	10.57	13.59
7	22.3	24.4	17.08	21.96
28	48.9	59.7	41.79	53.73
50	57	70.1	49.07	63.09
90	61.4	76.8	53.76	69.12

According to the strength measurements graphs, there is no substantial difference between the strength values of P and P_{L15} calcined schist samples. Both are considerably below the strength of 100 wt% OP cement paste. For both cases, the values are close to 80% of the OP cement strength.

Figure 84 and Table 33 illustrate the compressive strength results for the composite cement pastes prepared with 30 wt% of 80% calcined $P_{L22.5}$ schist.

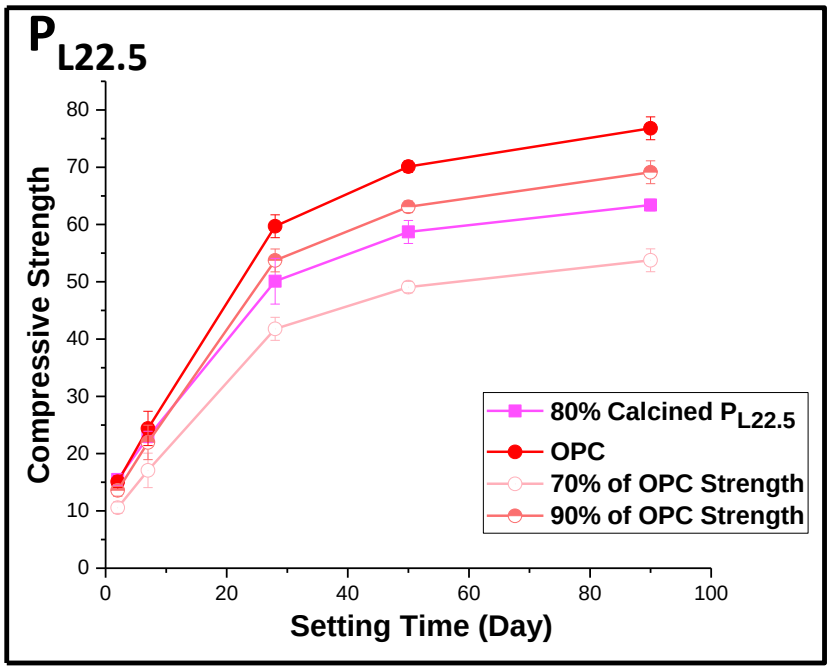

Figure 84. Compressive strength of OP cement blended with 30 wt% of calcined $P_{L22.5}$ schist (P schist with 22.5 wt% $C\bar{C}$ addition), compared to pure cement

Table 33. Compressive strength of OP cement blended with 30 wt% of calcined $P_{L22.5}$ schist (P schist with 22.5 wt% $C\bar{C}$ addition), compared to pure cement

Setting Time (Day)	80% Calcined $P_{L22.5}$	OPC	70% of OPC Strength	90% of OPC Strength
2	15.5	15.1	10.57	13.59
7	22.9	24.4	17.08	21.96
28	50.1	59.7	41.79	53.73
50	58.7	70.1	49.07	63.09
90	63.4	76.8	53.76	69.12

Figure 85 and Table 34 illustrate the compressive strength results for the composite cement pastes prepared with 30 wt% of 80% calcined P_{L30} schist.

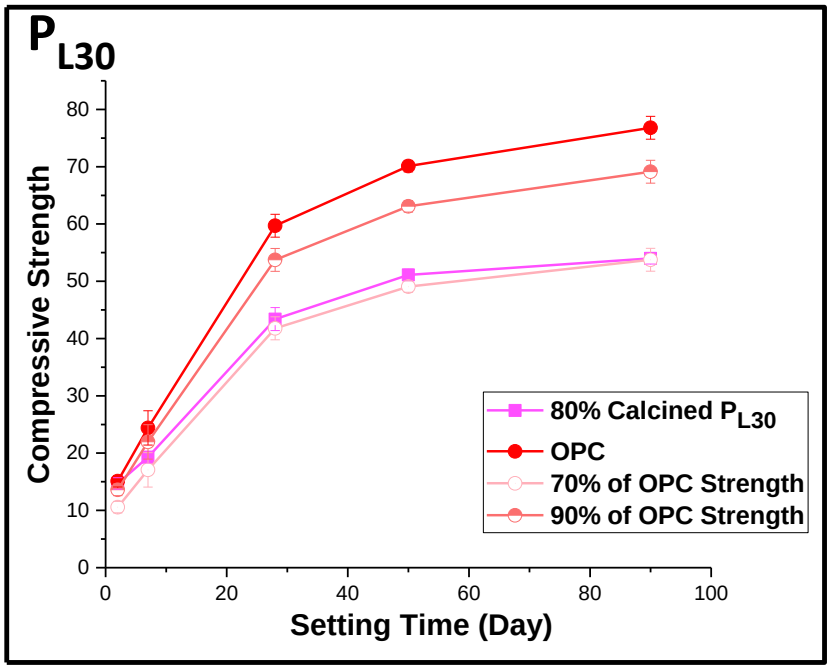

Figure 85. Compressive strength of OP cement blended with 30 wt% of calcined P_{L30} schist (P schist with 30 wt% $C\bar{C}$ addition), compared to pure cement

Table 34. Compressive strength of OP cement blended with 30 wt% of calcined P_{L30} schist (P schist with 30 wt% $C\bar{C}$ addition), compared to pure cement

Setting Time (Day)	80% Calcined P_{L30}	OPC	70% of OPC Strength	90% of OPC Strength
2	14.7	15.1	10.57	13.59
7	19.3	24.4	17.08	21.96
28	43.4	59.7	41.79	53.73
50	51.1	70.1	49.07	63.09
90	54	76.8	53.76	69.12

The strength results show that the compressive strength of the 80% calcined $P_{L22.5}$ sample is very close to the strength values of the P_{L15} sample. The strength values of the P_{L30} sample reached 70% of pure OPC strength which does not satisfy the criteria.

3.2.5.4. B Schist

Figure 86 and Table 35 show the compressive strength of composite cement paste that was prepared with 30 wt% 80% calcined B schist sample without carbonate additions.

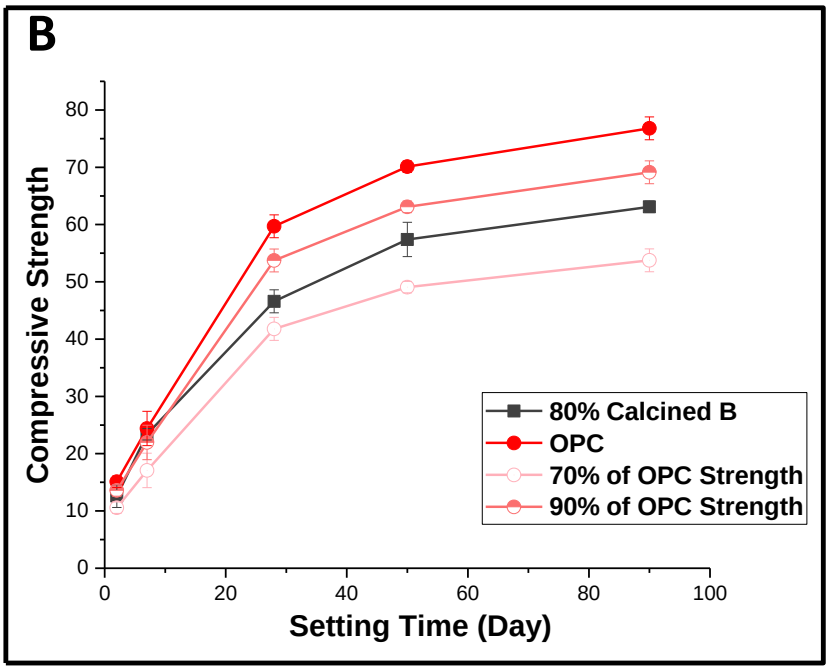

Figure 86. Compressive strength of OP cement blended with 30 wt% of calcined B schist, compared to pure cement

Table 35. Compressive strength of OP cement blended with 30 wt% of calcined B schist, compared to pure cement

Setting Time (Day)	80% Calcined B	OPC	70% of OPC Strength	90% of OPC Strength
2	12.6	15.1	10.57	13.59
7	23.4	24.4	17.08	21.96
28	46.6	59.7	41.79	53.73
50	57.4	70.1	49.07	63.09
90	63.1	76.8	53.76	69.12

Figure 87 and Table 36 show the compressive strength of composite cement paste that was prepared with 30 wt% 80% calcined $B_{L22.5}$ schist sample (B with 22.5% carbonate addition).

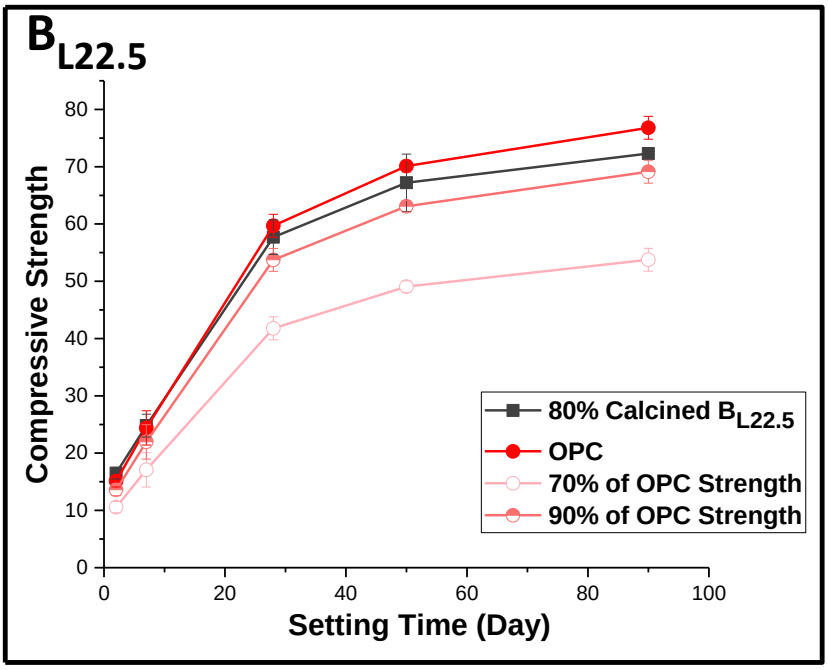

Figure 87. Compressive strength of OP cement blended with 30 wt% of calcined $B_{L22.5}$ schist (B schist with 22.5 wt% $C\bar{C}$ addition), compared to pure cement

Table 36. Compressive strength of OP cement blended with 30 wt% of calcined $B_{L22.5}$ schist (B schist with 22.5 wt% $C\bar{C}$ addition), compared to pure cement

Setting Time (Day)	80% Calcined $B_{L22.5}$	OPC	70% of OPC Strength	90% of OPC Strength
2	16.5	15.1	10.57	13.59
7	24.8	24.4	17.08	21.96
28	57.7	59.7	41.79	53.73
50	67.2	70.1	49.07	63.09
90	72.3	76.8	53.76	69.12

The composite cement pastes which were made with calcined B schist without any modification in carbonate amount could not surpass the acceptable threshold. However, the $B_{L22.5}$ sample astonishingly satisfied the criteria. As it can be seen in this table, the compressive strength of the $B_{L22.5}$ was almost 97% of the pure cement strength. The strength difference between these two samples must have been related to the effect of calcined carbonate.

3.2.5.5. L Schist

Figure 88 and Table 37 show the compressive strength of composite cement paste that was prepared with 30 wt% 80% calcined L schist sample without carbonate additions.

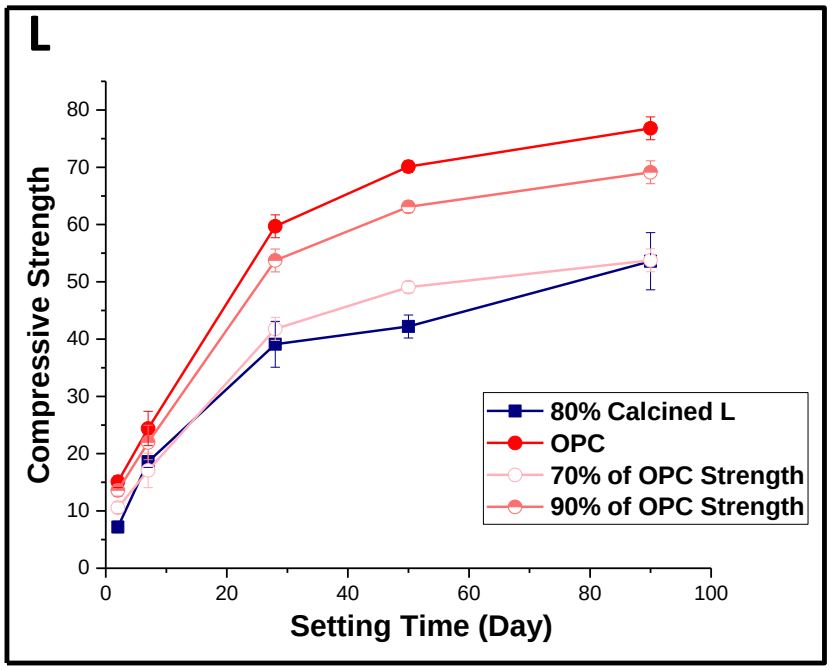

Figure 88. Compressive strength of OP cement blended with 30 wt% of calcined L schist, compared to pure cement

Table 37. Compressive strength of OP cement blended with 30 wt% of calcined L schist, compared to pure cement

Setting Time (Day)	80% Calcined L	OPC	70% of OPC Strength	90% of OPC Strength
2	7.2	15.1	10.57	13.59
7	18.6	24.4	17.08	21.96
28	39.1	59.7	41.79	53.73
50	42.2	70.1	49.07	63.09
90	53.6	76.8	53.76	69.12

Figure 89 and Table 38 show the compressive strength of composite cement paste that was prepared with 30 wt% 80% calcined L_{L15} schist sample (L with 15% carbonate addition).

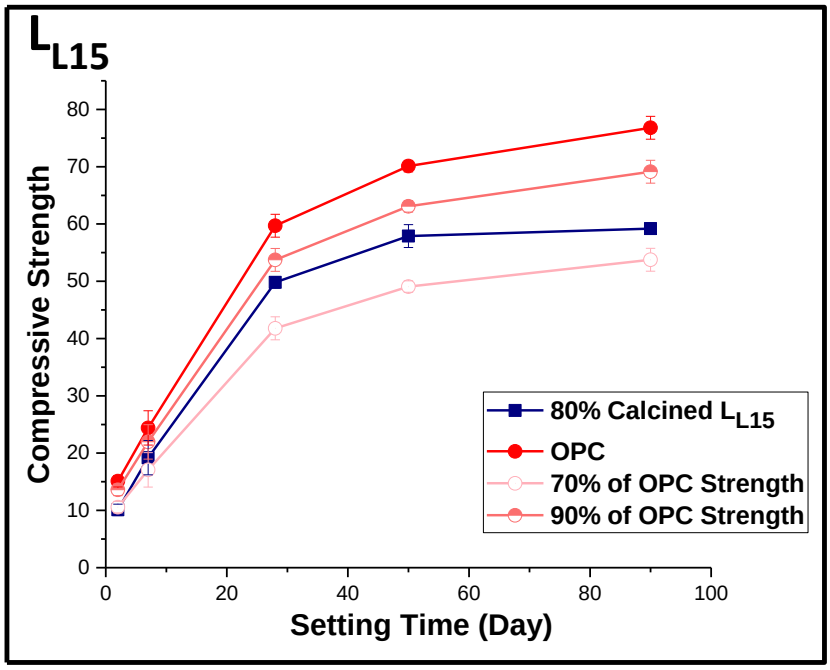

Figure 89. Compressive strength of OP cement blended with 30 wt% of calcined L_{L15} schist (L schist with 15 wt% $C\bar{C}$ addition), compared to pure cement

Table 38. Compressive strength of OP cement blended with 30 wt% of calcined L_{L15} schist (L schist with 15 wt% $C\bar{C}$ addition), compared to pure cement

Setting Time (Day)	80% Calcined L_{L15}	OPC	70% of OPC Strength	90% of OPC Strength
2	10.1	15.1	10.57	13.59
7	19.2	24.4	17.08	21.96
28	49.8	59.7	41.79	53.73
50	57.9	70.1	49.07	63.09
90	59.2	76.8	53.76	69.12

Figure 90 and Table 39 show the compressive strength of composite cement paste that was prepared with 30 wt% 80% calcined L_{L30} schist sample (L with 30% carbonate addition).

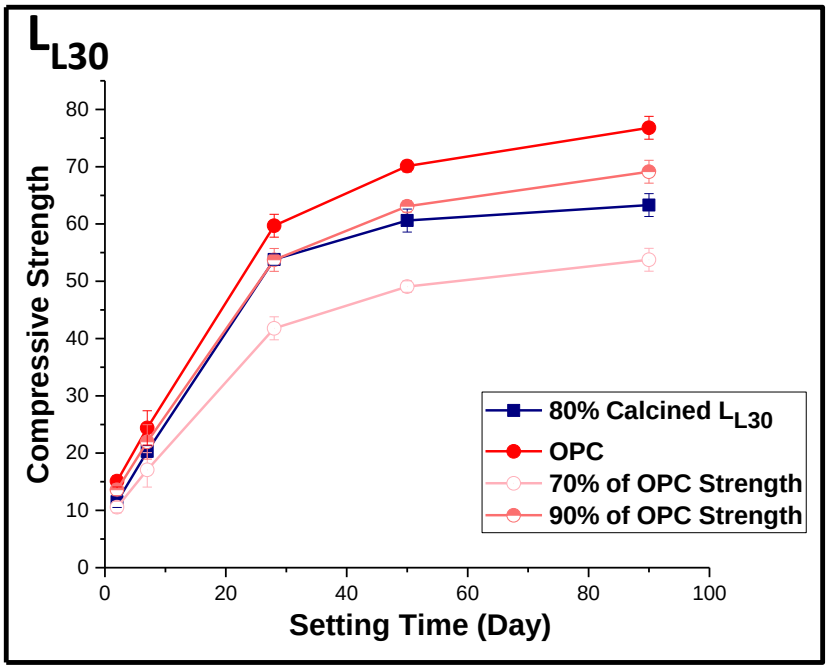

Figure 90. Compressive strength of OP cement blended with 30 wt% of calcined L_{L30} schist (L schist with 30 wt% $C\bar{C}$ addition), compared to pure cement

Table 39. Compressive strength of OP cement blended with 30 wt% of calcined L_{L30} schist (L schist with 30 wt% $C\bar{C}$ addition), compared to pure cement

Setting Time (Day)	80% Calcined L_{L30}	OPC	70% of OPC Strength	90% of OPC Strength
2	11.5	15.1	10.57	13.59
7	20.3	24.4	17.08	21.96
28	53.8	59.7	41.79	53.73
50	60.6	70.1	49.07	63.09
90	63.3	76.8	53.76	69.12

The compressive strength results of 80% calcined L, L_{L15}, and L_{L30} samples indicate that none of these three samples could satisfy the expected criteria. The highest strength value belongs to the L_{L30} sample which is almost 80% of OPC strength after 50 and 90 days.

3.2.6. Phase Analysis of Composite Cement

The phase distribution of the composite cement samples will provide a scientific justification for the different compressive strength values after 2, 7, 28, 50, and 90 days of hydration. To this end, a comparison of XRD spectra of the composite cement samples made up of 30 wt% thermally activated B schist and 70 wt% OPC after each hydration period (2, 7, 28, 50, and 90 days) is illustrated in figures 91 and 92.

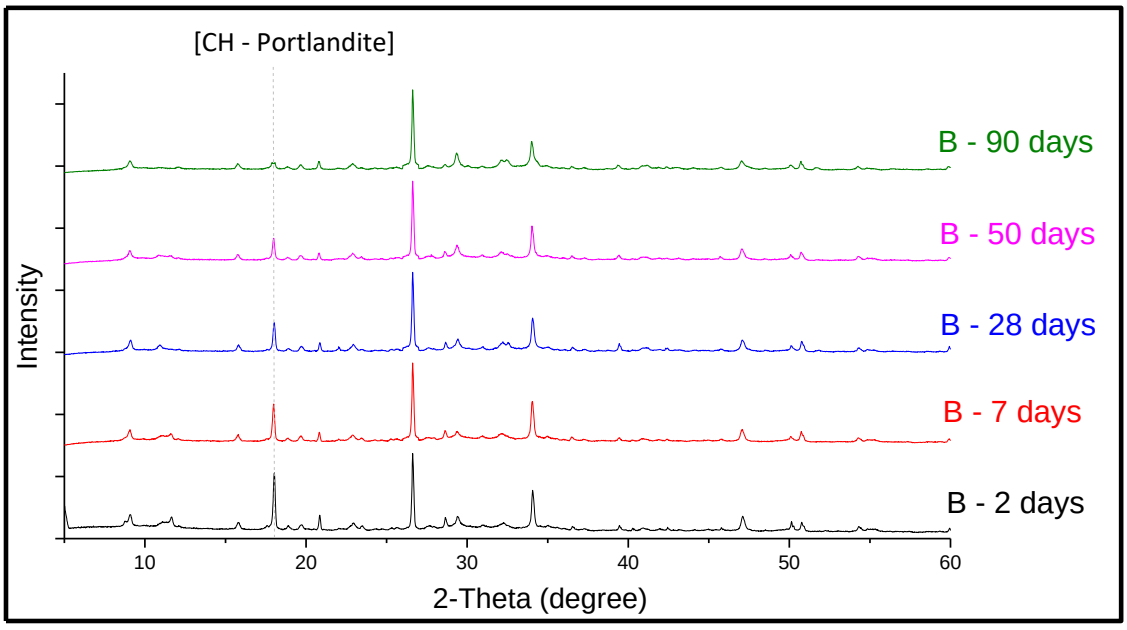

Figure 91. XRD spectra of cement blended with 30 wt% of calcined B schist after 2, 7, 28, 50, and 90 days of hydration

According to figure 91, after 2 and 7 days of hydration, there is a considerable amount of CH (Portlandite) in the phase composition. However, the peak intensity and therefore the portion of CH decreases after 50 days. After 90 days of hydration, there is only a small amount of Portlandite in the composite cement phase distribution. The same results were gained in the B sample with 22.5% of $C\bar{C}$, as it is indicated in figure 92.

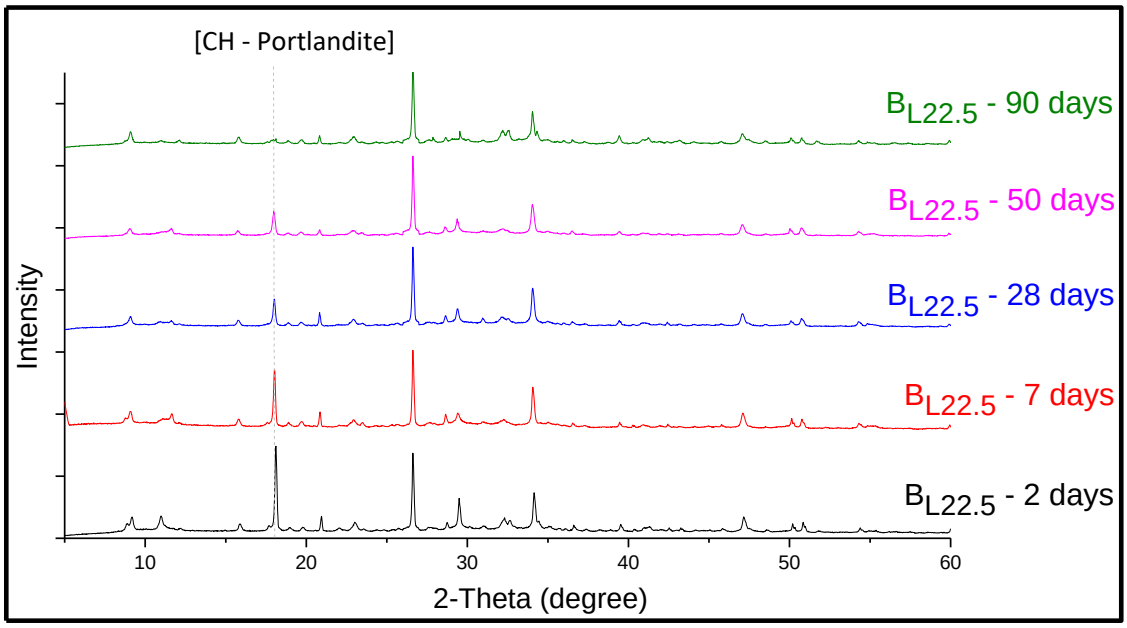

Figure 92. XRD spectra of cement blended with 30 wt% of calcined $B_{L22.5}$ schist (B with 22.5 wt% calcium carbonate) after 2, 7, 28, 50, and 90 days of hydration

3.3. Mechanically Activated Materials

As it was mentioned, the strength values of the thermally activated L samples were not satisfactory. Based on the XRD results of this sample (figures 38, 39, and 40), there was still a significant amount of inactivated aluminosilicates (feldspars) in its phase composition even after heat-treatment. Although a considerable portion of clayey phases decomposed during calcination, the amount of activated aluminosilicate was not adequate for contributing to cement hydration reactions and enhancing the strength of blended cement. Therefore, if we could find a way to benefit from the feldspars as well as the clayey phases, it would be possible to boost the compressive strength of the blended cement. To this end, it was decided to perform some mechanical activation processes on the L schist sample (as described in the experimental section). Besides, the same mechanical activation processes were performed on a pure feldspar material (Albite). The results of phase distribution and evolution, microstructural changes, and the compressive strength during mechanical processes will be represented below.

3.3.1. Phase Distribution

Investigation of the effect of the ball milling process on the decomposition of the existing phases (especially feldspars) was done with the help of XRD analysis. The crystallinity to amorphous ratio and the peak intensities before and after activation will indicate the degree of success of the ball milling process. Note that the decrease in the peak intensity of any phase is an indication of decomposition.

3.3.1.1. L Schist

Figure 93 shows the XRD spectra of the virgin L sample before and after the ball milling process. As it can be seen in the graphs, during mechanical activation the clayey phases' peaks are getting slightly smaller. However, there is no significant change in albite peaks (peak number: 5).

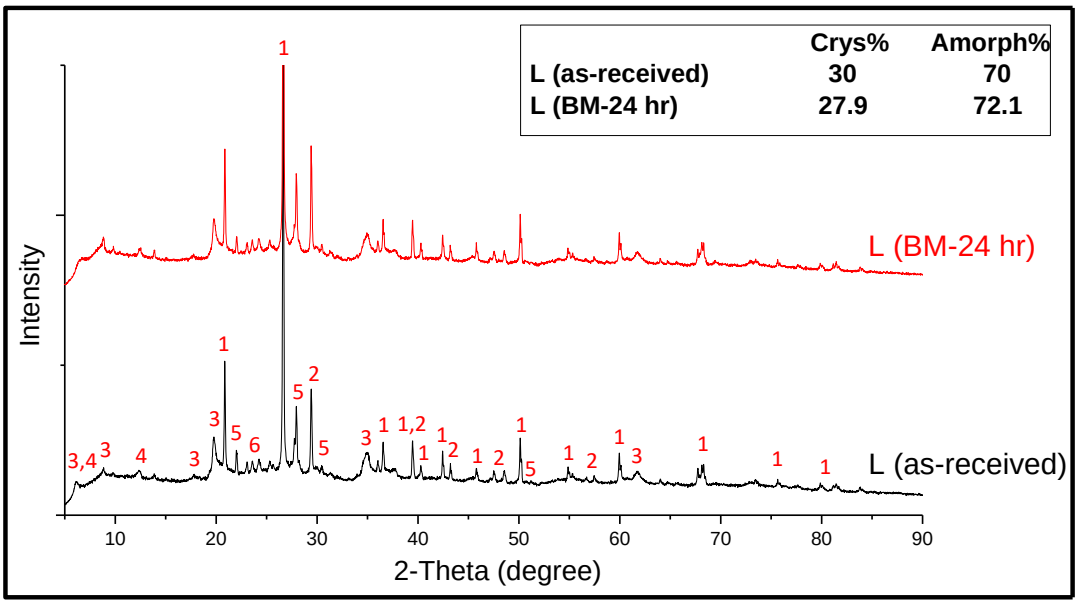

Figure 93. X-ray spectrum of virgin vs. L schist powder ball milled for 24 hours. The numbers at the peaks correspond to phases listed in table 40.

Table 40. The phase distribution, chemical formula of each phase, and information about the crystal structure of L powder

Peak Number	Chemical Phases	Crystal Structure	Chemical Formula
1	Quartz	Hexagonal	SiO_2
2	Calcite	Rhombo	$CaCO_3$
3	Montmorillonite	Monoclinic	$(Na, Ca)_{0.3}(Al, Mg)_2Si_4O_{10}(OH)_2.xH_2O$
3	Montmorillonite-22A	Monoclinic	$Na_{0.3}(Al, Mg)_2Si_4O_{10}(OH)_2.8H_2O$
4	Clinchlore	Monoclinic	$(Mg_{2.96}Fe_{1.55}\ Fe_{0.136}Al_{1.275})(\ Si_{2.622}Al_{1.376}O_{10})(OH)_8$
5	Albite	Triclinic	$(Na, Ca)\ (Si, Al)_4\ O_8$
6	Titanium Oxide	Orthorhombic	Ti_3O_5

Figure 94 illustrates the XRD spectra of the virgin, 80% calcined, and ball-milled L sample. As it is obvious in the ball-milled sample's XRD spectra, there was a decrease in albite peak after performing mechanical activation on the heat-treated L schist sample. Besides the existing phase in L schist (indicated by numbers), there was a new peak (indicated by ∗), which corresponded to "anhydrous mica".

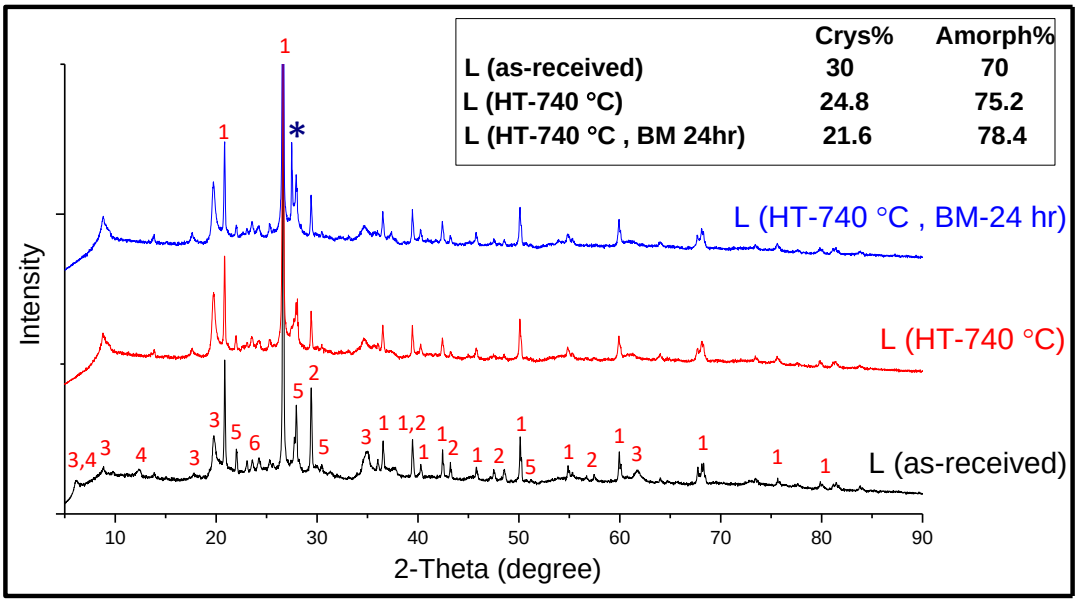

Figure 94. X-ray spectrum of the virgin, 80% calcined and ball milled (for 24 hours) L schist powder. The numbers at the peaks correspond to phases listed in table 40.

Figure 95 illustrates the XRD spectra of inactivated, 80% calcined and ball-milled L_{L30} sample (L sample augmented with 30 wt% calcium carbonate addition).

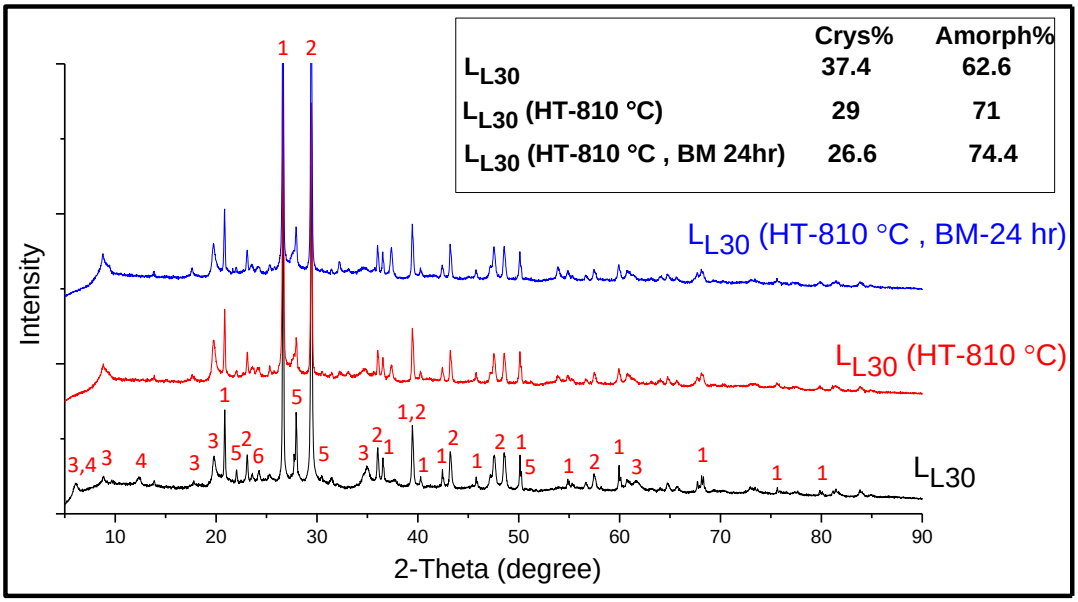

Figure 95. X-ray spectrum of inactivated, 80% calcined and ball milled (for 24 hours) L_{L30} schist powder (L schist with 30 wt% $C\bar{C}$ addition). The numbers at the peaks correspond to phases listed in table 40.

According to the XRD results of the L_{L30} sample before and after activation, there is no significant decrease in albite peak (peak number: 5) intensity. It means that the ball milling process on this sample was not as effective as the one in the calcined L sample (figure 94).

3.3.1.2. Albite Feldspar

Figure 94 shows a comparison among XRD spectra of virgin albite and albite powder ball milled with alumina balls for two different durations (6 and 24 hours). As it was mentioned in the previous sections, the only impurity in the albite sample was quartz phase. The quartz peaks are indicated in figure 94. The rest of the peaks correspond to the albite phase. According to the crystallinity and amorphous amounts (shown in fig. 96, the crystallinity value of albite does not change after even 24 hours of ball milling with alumina balls. The stability of these values indicates that the ball milling process has not been performed successfully.

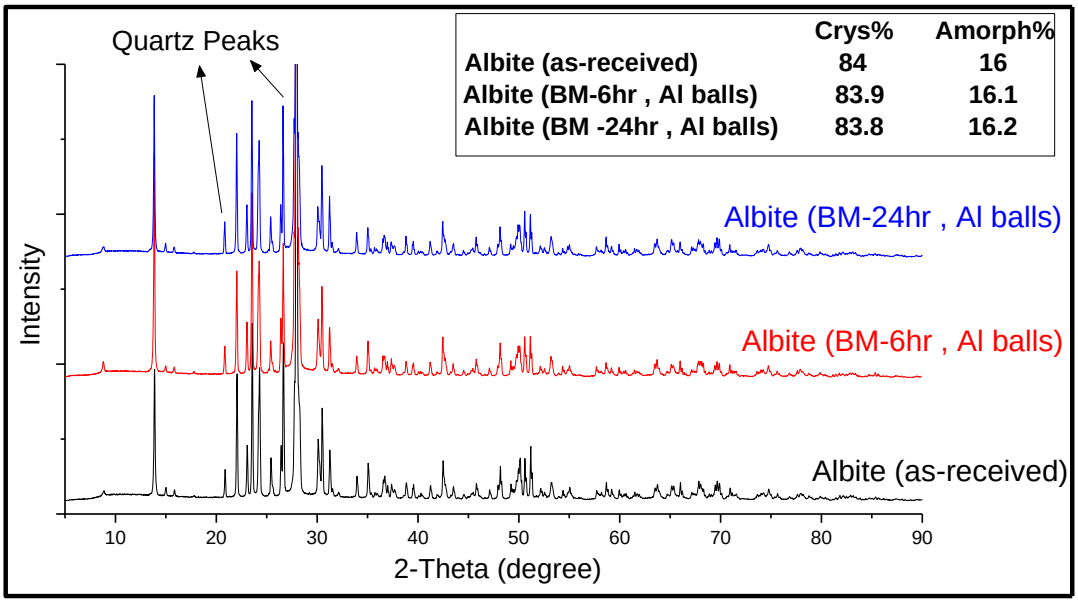

Figure 96. X-ray spectrum of virgin albite sample, albite ball milled with alumina balls for 6 hours, and albite ball milled with alumina balls for 24 hours

Figure 97 illustrates a comparison among XRD spectra of virgin albite and albite powder ball milled with steel balls for two different durations (6 and 24 hours).

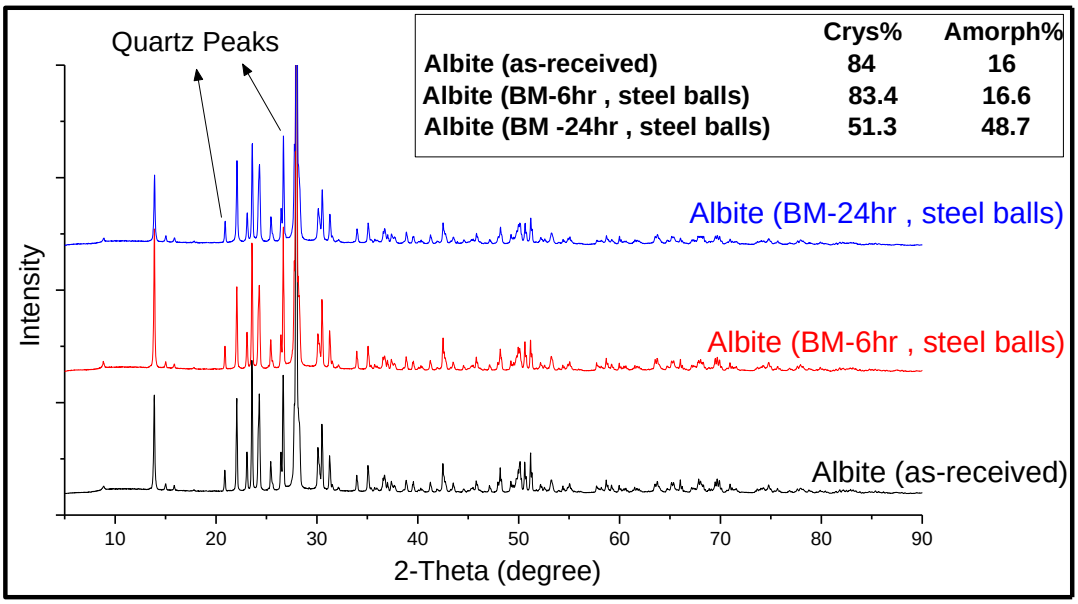

Figure 97. X-ray spectrum of virgin albite sample, albite ball milled with steel balls for 6 hours, and albite ball milled with steel balls for 24 hours

According to the crystallinity and amorphous values, the only effective common ball milling method for decomposing albite is ball milling the powder with steel balls for 24 hours.

Figure 98 illustrates a comparison among XRD spectra of virgin albite and albite powder ball milled with steel balls by planetary method for two different durations (30 minutes and 1 hour).

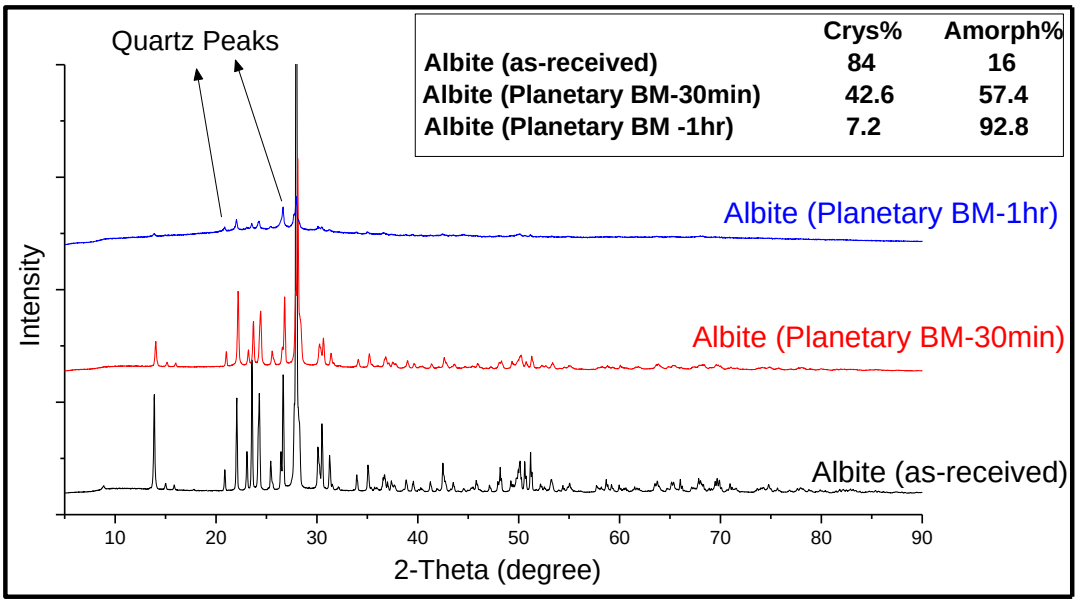

Figure 98. X-ray spectrum of virgin albite sample, albite ball milled (planetary) with steel balls for 30 minutes, and albite ball milled (planetary) with steel balls for 1 hour

It is obvious from the XRD results that the most effective ball milling method for decomposing albite is the planetary ball milling process with steel balls. Nevertheless, there is no trace of mica peak or any other new clayey phases in ball-milled samples.

3.3.2. Microstructure Analysis

Scanning electron microscopy was used to investigate the changes in the microstructure during ball milling processes.

3.3.2.1. L schist

The micrographs of the virgin (left) and ball milled (right) L schist sample are shown in Figure 99. The SEM images are only provided for virgin and ball-milled schist in their original composition without any modification in the calcium carbonate amount.

(Virgin) **(Ball milled)**

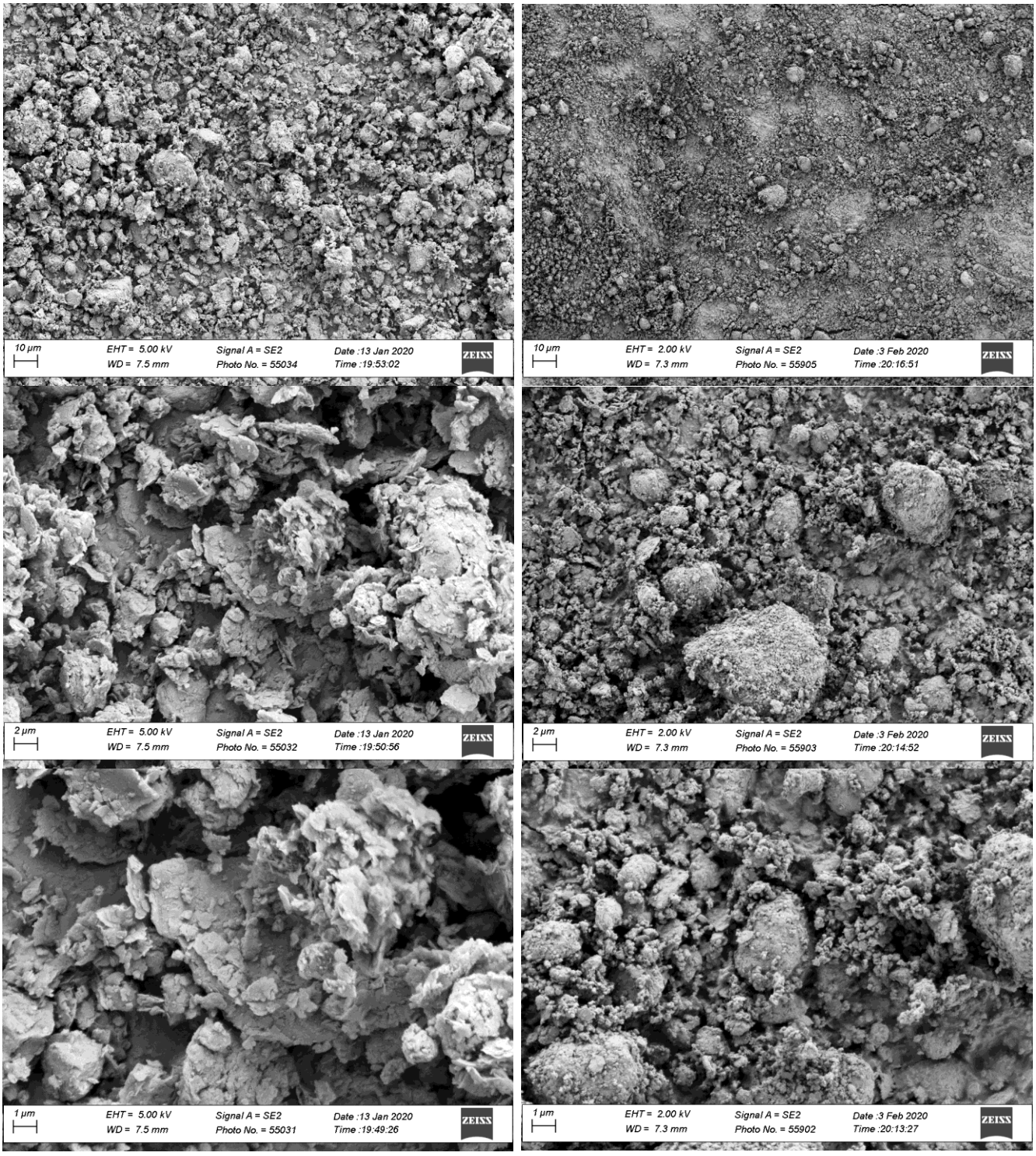

Figure 99. L schist micrographs for Virgin (Left) and ball milled (Right) Powders at the same magnification. First row: mag. = 1KX, second row: mag = 5KX, and third row: mag = 10KX

The SEM micrographs illustrated that there was a reduction in the average particle size of the L sample after the ball milling process.

3.3.2.2. Albite Feldspar

(Virgin) **(Ball milled)**

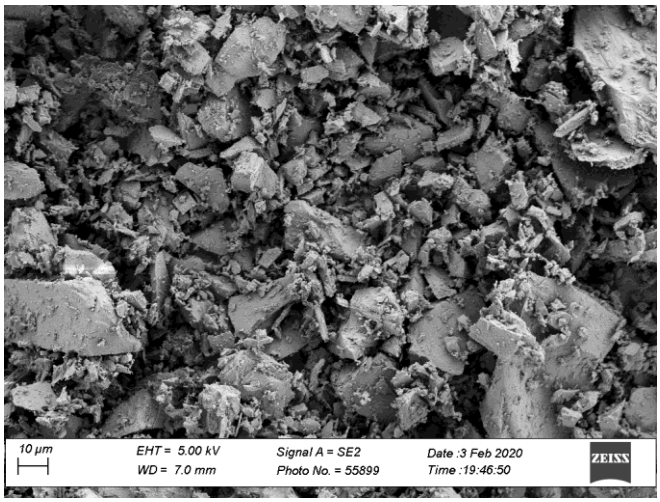

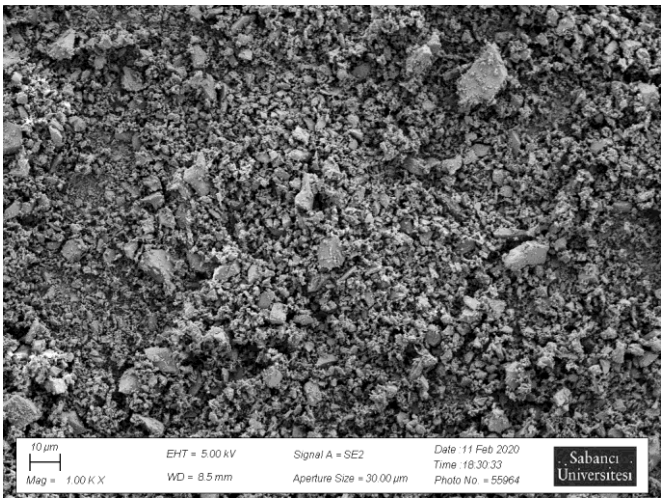

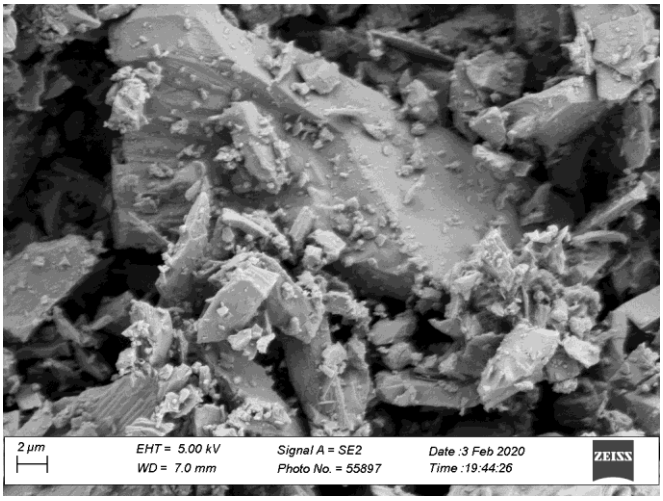

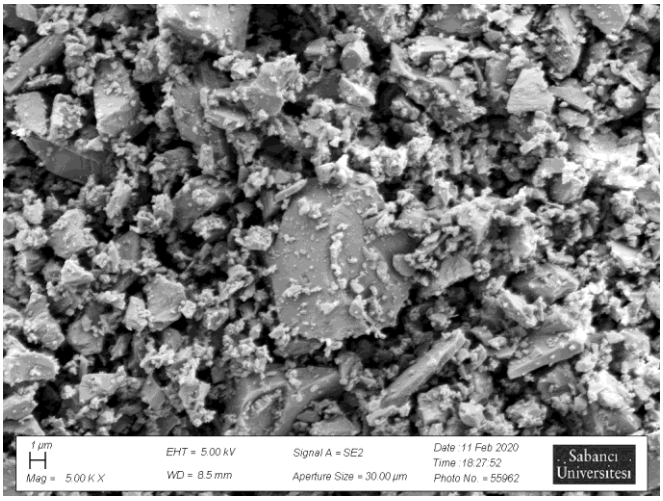

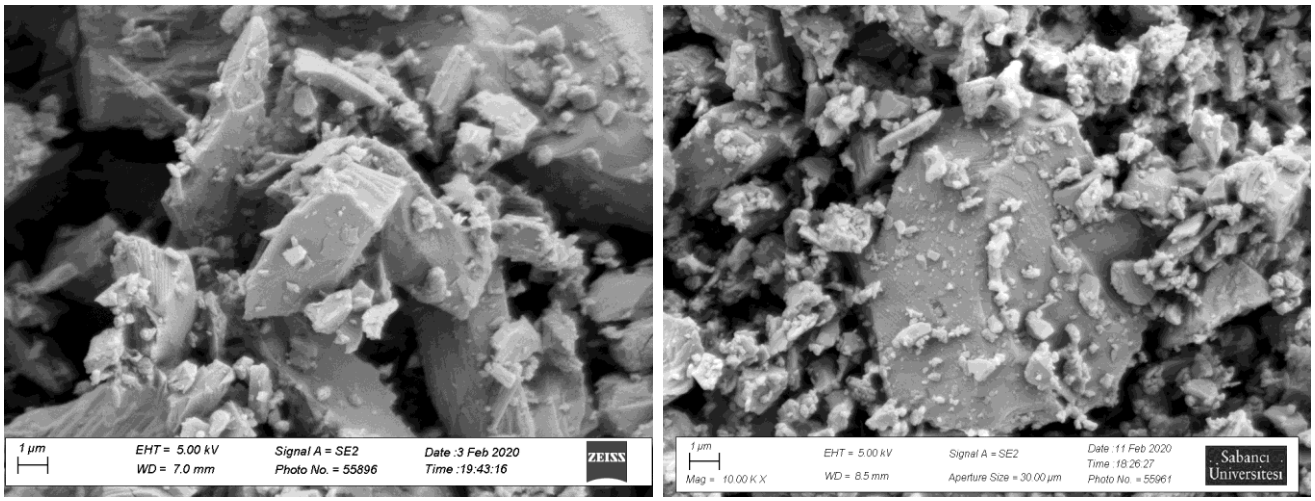

Figure 100. Albite feldspar micrographs for Virgin (Left) and ball milled with steel balls (Right) powders at the same magnification. First row: mag. = 1KX, second row: mag = 5KX, and third row: mag = 10KX

3.3.3. Compressive Strength Measurement

Figure 101 and Table 41 illustrate the mechanical activated L and L_{L30} schist compressive strength results when it is substituted 30 wt% of the cement. It shows a comparison among the compressive strength values of the ball-milled L sample, heat-treated/ball-milled L sample, and heat-treated/ball-milled L_{L30} sample. This comparison was done to discern the effect of the mechanical activation process on either the schist or the limestone augmented schist samples.

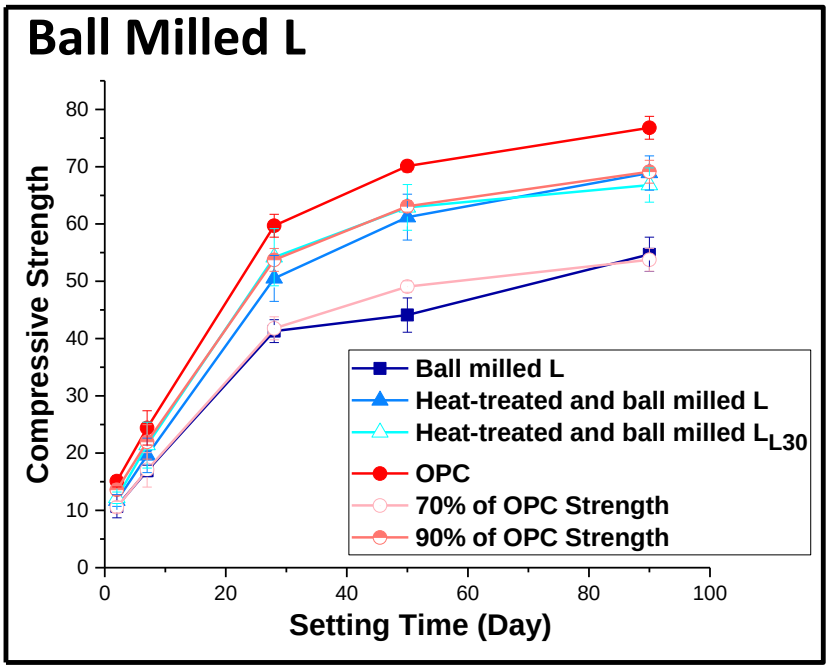

Figure 101. Compressive strength of OP cement blended with 30 wt% of mechanical activated L and L_{L30} schist, compared to pure cement

Table 41. Compressive strength of OP cement blended with 30 wt% of mechanical activated L and L_{L30} schist, compared to pure cement

Setting Time (Day)	Ball milled L	Heat-treated and ball milled L	Heat-treated and ball milled L_{L30}	OPC	70% of OPC Strength	90% of OPC Strength
2	10.7	11.7	12.2	15.1	10.57	13.59
7	16.9	19.6	21.4	24.4	17.08	21.96
28	41.3	50.5	54.2	59.7	41.79	53.73
50	44.1	61.2	62.9	70.1	49.07	63.09
90	54.7	68.9	66.8	76.8	53.76	69.12

The compressive strength test results of the mechanically activated L schist indicated that the heat-treated/ball-milled L and L_{L30} samples reached the criteria. Therefore, the mechanical activation process was successful.

3.4. Mechanochemical Activation Process on Albite

Besides mechanical activation, one more method (mechanochemical activation) was used to decompose the albite sample and convert a part of its phase composition to a clayey phase. To this end, the albite sample was blended with 15 wt% NaOH and 15 wt% CaOH. Subsequently, this mixture was ball milled (with and without water) for 24 hours. The phase composition of obtained samples is represented in figures 102 and 103.

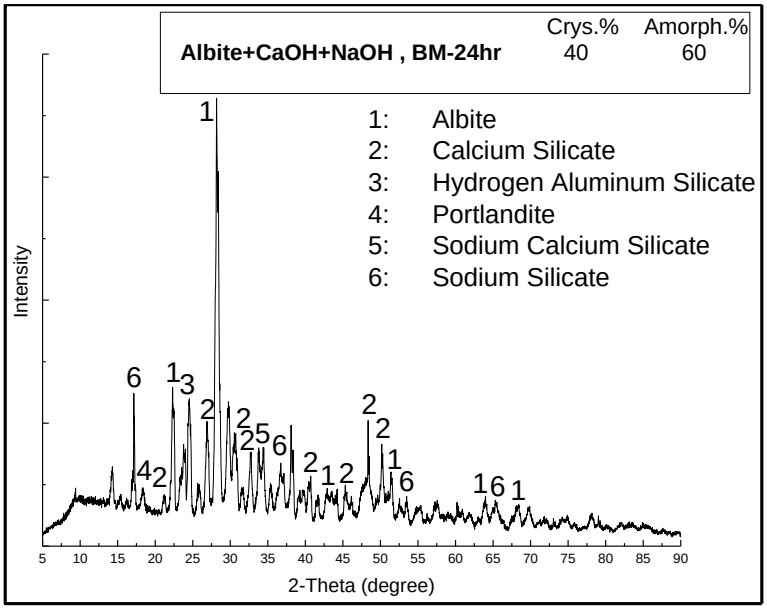

Figure 102. XRD spectra of albite (75 wt%) + NaOH (15 wt%) + CaOH (15 wt%) mixture ball-milled without water

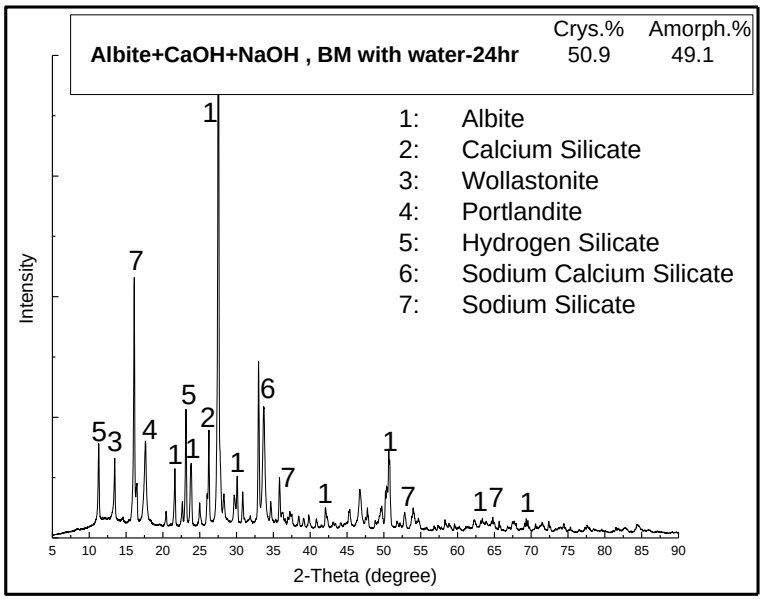

Figure 103. XRD spectra of albite (75 wt%) + NaOH (15 wt%) + CaOH (15 wt%) mixture ball-milled with water

CHAPTER 4

4. Discussion

4.1. Conformity of XRD and TGA results

There are already some studies discussing the application of calcined kaolinite with some calcite impurities as SCMs. Kaolinite is the simplest clay structure that can be reactivated by low-temperature thermal treatment. Based on the reports, it is the best candidate for cement substitution after being de-hydroxylated. This study illustrates the possibility of activation in terms of any class of clayey materials i. e. kaolinitic, smectitic, and illitic when they were calcined properly. The schist type materials could be considered as SCMs when a proper calcination scenario could be designed for each of them. The only criteria for the schist type materials for being used as an SCM is the thresholds for clay content (at least more than 40 wt%). Hence, in order to evaluate the pozzolanic reactivity of any schist type material, initially, the amount of clay content in the schist should be determined. In other words, the actiavtability (potential for activation) and also the value of a schist type materials to be used efficiently as an SCM depends on the portion of activatable aluminosilicate i. e. clayey phases. The amount of each existing phase based on XRD results was calculated and given in the results section. The phase amounts can also be extracted from the TGA weight loss values. According to the literature, clay decomposition occurs in a wide temperature range of 250-700℃. Note that the accurate temperature range directly depends on the type of clay. The kaolinitic type clays with a simple structure usually decompose in lower temperatures. The other two types of clays need more heat to be decomposed and therefore the decomposition occurs in higher temperatures. The phase content based on the clayey materials' weight loss in TG

analysis was calculated according to the chemical formula and molecular weight of the clay before and after calcination. For example, in the case of kaolinitic clays, the calculations are the same as what was mentioned in the introduction section. Briefly, kaolinite loses almost 14% ($\sim\frac{1}{7}$) of its initial weight during calcination (equation 4). For the more complex types of clayey minerals, this fraction is $\sim\frac{1}{8}$. In order to be sure about the portion of the activatable phases inside the schist materials, the XRD and TGA results of every schist sample before and after the calcination process will be compared in this section.

Equation 8. Kaolinite Calcination Reaction

$$Al_4Si_4O_{10}(OH)_8 \rightarrow 2Al_2Si_2O_7 + 4H_2O\ (\uparrow) \qquad \text{(Eq. 3)}$$

Equation 9. Weight Loss Process of Kaolinite during Calcination

$$4(27) + 4(28) + 10(16) + 8(16 + 8(1) \rightarrow 2[2(27) + 2(28) + 7(16)] + 4[2(1) + 16] \qquad \text{(Eq. 4)}$$

$$516 \rightarrow 444 + 72\ (\uparrow) \qquad \Longrightarrow \qquad \left(\frac{72}{516}\right) \times 100 \simeq 14\%$$

As it is visible in the XRD results, the amount of each clayey phase e. g. kaolinite, muscovite were calculated separately according to the XRD peak intensity of each phase. However, it is not possible to calculate the phase amounts separately based on TGA weight losses due to the overlapping of the weight losses related to each clayey phase. Hence, for all types of the clayey phases, the weight loss value in the TGA diagram (in the temperature range of ~300-600°C) was multiplied to 8. For instance, when the weight loss value in the clay decomposition range was 3 wt%, it was concluded that the total clay amount in that sample is approximately 25 wt%. Therefore, some of the discrepancies between TGA and XRD phase amounts come from this original assumption.

4.1.1.1. G Schist

Table 42. Comparison of phase amounts existing in the G schist based on the XRD and TGA results. (G-without $C\bar{C}$ addition, G_{L15}-G schist with 15 wt% $C\bar{C}$ addition, $G_{L22.5}$-G schist with 22.5 wt% $C\bar{C}$ addition, and G_{L30}-G schist with 30 wt% $C\bar{C}$ addition.)

G	Phase Amount	XRD	TGA
Before Calcination	Clay (%)	58.9	~45
	$C\bar{C}$ (%)	0.9	1
After Calcination	Clay (%)	19.8	~16
	$C\bar{C}$ (%)	0.8	1

G_{L15}	Phase Amount	XRD	TGA
Before Calcination	Clay (%)	48.4	~35
	$C\bar{C}$ (%)	14.1	14
After Calcination	Clay (%)	5.3	6.5
	$C\bar{C}$ (%)	3.4	2

$G_{L22.5}$	Phase Amount	XRD	TGA
Before Calcination	Clay (%)	42.9	~35
	$C\bar{C}$ (%)	23.1	20
After Calcination	Clay (%)	8.7	8
	$C\bar{C}$ (%)	11.1	12

G_{L30}	Phase Amount	XRD	TGA
Before Calcination	Clay (%)	38	~28
	$C\bar{C}$ (%)	28.8	28
After Calcination	Clay (%)	6.1	2
	$C\bar{C}$ (%)	17.3	18

4.1.1.2. C Schist

Table 43. Comparison of phase amounts existing in the C schist based on the XRD and TGA results. (C-without $C\bar{C}$ addition, C_{L15}-C schist with 15 wt% $C\bar{C}$ addition, $C_{L22.5}$-C schist with 22.5 wt% $C\bar{C}$ addition, and C_{L30}-C schist with 30 wt% $C\bar{C}$ addition.)

C	Phase Amount	XRD	TGA
Before Calcination	Clay (%)	51.3	~35
	$C\bar{C}$ (%)	3.8	4
After Calcination	Clay (%)	21.8	12
	$C\bar{C}$ (%)	3.2	4

C_{L15}	Phase Amount	XRD	TGA
Before Calcination	Clay (%)	49.7	~40
	$C\bar{C}$ (%)	14.6	14
After Calcination	Clay (%)	11.3	10
	$C\bar{C}$ (%)	2.9	1

$C_{L22.5}$	Phase Amount	XRD	TGA
Before Calcination	Clay (%)	42.5	~35
	$C\bar{C}$ (%)	22.2	22
After Calcination	Clay (%)	11.3	12
	$C\bar{C}$ (%)	10.9	12

C_{L30}	Phase Amount	XRD	TGA
Before Calcination	Clay (%)	37.9	~25
	$C\bar{C}$ (%)	29.6	27
After Calcination	Clay (%)	9.1	8
	$C\bar{C}$ (%)	14.4	16

4.1.1.3. P Schist

Table 44. Comparison of phase amounts existing in the P schist based on the XRD and TGA results. (P-without $C\bar{C}$ addition, P_{L15}-P schist with 15 wt% $C\bar{C}$ addition, $P_{L22.5}$-P schist with 22.5 wt% $C\bar{C}$ addition, and P_{L30}-P schist with 30 wt% $C\bar{C}$ addition)

P	Phase Amount	XRD	TGA
Before Calcination	Clay (%)	52.5	~35
	$C\bar{C}$ (%)	5	6
After Calcination	Clay (%)	19.7	10
	$C\bar{C}$ (%)	4.3	4

P_{L15}	Phase Amount	XRD	TGA
Before Calcination	Clay (%)	47.5	~30
	$C\bar{C}$ (%)	14.7	14
After Calcination	Clay (%)	13.3	8
	$C\bar{C}$ (%)	4.5	5

$P_{L22.5}$	Phase Amount	XRD	TGA
Before Calcination	Clay (%)	45	~30
	$C\bar{C}$ (%)	22	21
After Calcination	Clay (%)	11.1	8
	$C\bar{C}$ (%)	9.8	12

P_{L30}	Phase Amount	XRD	TGA
Before Calcination	Clay (%)	41.9	~30
	$C\bar{C}$ (%)	30.2	28
After Calcination	Clay (%)	9.3	12
	$C\bar{C}$ (%)	15.3	18

4.1.1.4. B Schist

Table 45. Comparison of phase amounts existing in the B schist based on the XRD and TGA results. (B-without $C\bar{C}$ addition, and $B_{L22.5}$-B schist with 22.5 wt% $C\bar{C}$ addition)

B	Phase Amount	XRD	TGA
Before Calcination	Clay (%)	18.5	~16
	$C\bar{C}$ (%)	8.9	16
After Calcination	Clay (%)	6.4	0
	$C\bar{C}$ (%)	3.8	6

$B_{L22.5}$	Phase Amount	XRD	TGA
Before Calcination	Clay (%)	31.3	~32
	$C\bar{C}$ (%)	21.2	24
After Calcination	Clay (%)	3.1	5
	$C\bar{C}$ (%)	4.2	6

4.1.1.5. L Schist

Table 46. Comparison of phase amounts existing in the L schist based on the XRD and TGA results. (L-without $C\bar{C}$ addition, L_{L15}-L schist with 15 wt% $C\bar{C}$ addition, and L_{L30}-L schist with 30 wt% $C\bar{C}$ addition)

L	Phase Amount	XRD	TGA
Before Calcination	Clay (%)	26.8	~35
	$C\bar{C}$ (%)	8.7	8
After Calcination	Clay (%)	3.1	4
	$C\bar{C}$ (%)	4.1	3

L_{L15}	Phase Amount	XRD	TGA
Before Calcination	Clay (%)	21.3	~30
	$C\bar{C}$ (%)	14.4	14
After Calcination	Clay (%)	2.4	4
	$C\bar{C}$ (%)	6.9	8

L_{L30}	Phase Amount	XRD	TGA
Before Calcination	Clay (%)	18.8	30
	$C\bar{C}$ (%)	31.4	32
After Calcination	Clay (%)	2.3	4
	$C\bar{C}$ (%)	8.3	6

As it can be seen in tables 42-46, the clay and carbonate phase amounts before and after the calcination (80%) which were extracted from the XRD and TGA results, largely confirmed each other. However, there are some minor differences in the phase amounts due to some errors arising from experimental or computational mistakes. The amount of sample used for the TGA test was not the same as XRD. In TG analysis, only 50 mg of the samples were used in every run. Whereas, this amount was almost 500 mg for every XRD run. Therefore, one of the error sources could be the sampling error which causes non-homogeneity in the existing phases inside the sample and variation in the XRD and TGA results. Another error source could be the overlapping of the clay and carbonate weight losses in TGA graphs. This problem would cause miscalculations and discrepancies between TGA and XRD phase amounts. One more error source could be the amorphous content of the samples which contains clay and carbonate. The amorphous clay and

carbonates are not considered in XRD phase quantifications. Albeit, they exist in the TGA weight losses and cannot be distinguished from the crystalline clay or carbonate phases.

4.2. Inconsistency of lab-scale vs pilot-scale calcination

The thermal activation of clay-type minerals for cement replacement (i.e. pozzolanic reactivity) has to be done properly. Clay type aluminosilicates become de-stabilized and reactive as they lose their hydroxyl groups in the aluminum hydroxyl layers in their sheets. The conversion of kaolinite to meta-kaolinite is the simplest structural example of this activation process. Additionally, the degree of activation during the calcination process of any clayey material existing in the schist samples showed that it is possible to modify this technology by using any class of clay more than kaolinitic clays. The findings of this study illustrate that the destabilization process through thermal treatment can be optimized for the best reactivity of aluminosilicate hydrates for pozzolanic reactions: (I) Too little de-stabilization wastes the potential in the mineral and falls short of best activation: (II) An overkill of de-stabilization can blunt the active sites by sintering and strongly hamper the pozzolanic potential of these aluminosilicate minerals for hydration reactions. The following discussions treat these fine details of the activation process and how the reactivity of ordinary schist minerals containing various clay types could be prepared for optimized pozzolanic reactions.

According to phase distribution and thermal analysis results of untreated materials, G, C, P, and B schist type materials contain adequate amounts of clayey minerals in their compositions (40-50% of total) to be considered as viable cement substitution candidates. In addition, it was expected that the higher the amounts of activatable clay phases in the samples, the higher is the potential of the sample as an SCM. However, the primary compression strength test results did not confirm this assumption. Based on the results, the best compressive strength among the 80% calcined schist samples corresponded to B schist, i.e. the sample with only 32% clay minerals. Therefore, there must be another parameter affecting the strength of the cement pastes prepared with G, C, and P samples to be lower than that of the composite cement prepared with B powders. By reviewing the weight loss amounts of untreated and calcined schist powders in tables 38-42, it would be possible to justify this apparent contradiction. As it was mentioned before, B schist contains 5 wt% of graphite in its composition. Graphite could be assumed to burn during the calcination of the B schist sample and provide more heat in addition to the given heat and cause further de-

hydroxylation of the clayey phases of this schist. Therefore B and $B_{L22.5}$ schist samples may have better activation and more reactivity than the other schists. For G schist samples, after performing a heat-treatment process up to a temperature that would correspond to 80% of their total weight loss, the residual clay amount in calcined G schist should have been about 20% of the clay amount of untreated sample. However, based on the XRD and TGA results of the calcined G sample, this residual value is almost 35% of the untreated one. It appeared that performing the heat-treatment process inside a box furnace of a bulk amount of schist powders caused uncompleted decomposition. The applied heat to a large amount (600 g) of powders was not distributed uniformly and transferred to all over the powder inside the furnace as well as it usually was in thermal analysis equipment with an extremely small amount of sample (50 mg). A similar result was obtained for the same powder where the amount of carbonate in the schist was topped off to 15 wt%. This was also the case for the virgin or $C\bar{C}$ augmented C and P schist samples. Since the thermal conductivity of clay is very low and in these samples there is not any other internal heat generator during calcination, the calcination process was not completed for the entire bulk samples to the levels of activation (i.e. 80%) as intended. Based on these experiences, it has been decided to perform the calcination process on G and G_{L15} samples in two higher temperatures correspond to 100% and 110% of their total weight loss. According to the thermal analysis results of the 100% and 110% activated G and G_{L15} samples, the degree of activation was acceptable in the 100% calcined samples. These results showed that in the case of calcination to 100% of weight loss, the sample would be more activated. The 100% activated sample reaches the expected degree of calcination. Moreover, after calcination up to the temperature associated with 110% of total weight loss, the calcined G and G_{L15} samples were dead-burnt.

4.3. Calcination Energy

The mentioned interpretations demonstrate that the ideal activation of clay-based aluminosilicates corresponds to the full decomposition of the hydroxyls. However, going beyond the full decomposition will lead to sintering and dead-burning of clays. So far, the calcination and clay decomposition schedules were designed based on the calcination temperatures. Nevertheless, the calcination temperature itself cannot be a general criterion for the calcination of any clay type material. In the case of calcination of limestone augmented schist samples, even at temperatures higher than the clay decomposition range, the clay does not get dead-burnt. The reason for this is

that in the presence of limestone in schist, the excess heat gets consumed by limestone to be decomposed. Briefly, limestone will use the excess heat as latent heat state of matter and will not let clay to be sintered and dead-burnt. Therefore, the amount of heat that is provided to clay/carbonate decomposition should be considered as a critical parameter in designing a calcination process for any schist type material. By controlling the given heat according to the required energy for a certain magnitude of calcination, it is possible to receive the optimum activated clayey materials. Hence, the amount of heat that is necessary to decompose all the hydroxyls in different types of clayey materials e. g. kaolinitic or smectitic types were measured with the help of the DSC test.

Based on the DSC diagrams, the area under the peak corresponding to each step of decomposition was calculated for each sample. These integrated values are equivalent to the energy which is expected to be consumed during the decomposition. By dividing the energy value of one step by the weight loss of the same step, the enthalpy (ΔH/g) value could be calculated. Table 47 represents the ΔH values of the kaolinite (benchmark) sample.

Table 47. Enthalpy (ΔH) values of the kaolinite samples based on DSC results showed in figure 64.

Sample	Decomposition Enthalpy (KJ/g)		Total (KJ/g)
Kaolinite	ΔH_1	_	0.55
	ΔH_2	0.55	
	ΔH_3	0	

Table 48 represents the ΔH values of the L, L_{L15}, and L_{L30} samples.

Table 48. Enthalpy (ΔH) values of the L, L_{L15}, and L_{L30} samples based on DSC results showed in figures 65,66, and 67. (L_{L15}: L schist with 15 wt% $C\bar{C}$ addition, and L_{L30}: L schist with 30 wt% $C\bar{C}$ addition)

Sample	Decomposition Enthalpy (KJ/g)		Total (KJ/g)
L	ΔH_1	2.22	2.87
	ΔH_2	0.13	
	ΔH_3	0.52	
L_{L15}	ΔH_1	2.37	3.33
	ΔH_2	0.18	
	ΔH_3	0.78	
L_{L30}	ΔH_1	2.58	3.51
	ΔH_2	0.1	
	ΔH_3	0.83	

In both kaolinite and L samples tables, ΔH_2 value corresponds to the energy needed for clay decomposition, and ΔH_3 value corresponds to the energy needed for calcium carbonate decomposition. ΔH_1 is the energy value of moisture evaporation for all samples. It is obvious that the decomposition energy of the samples increases by increasing the amount of calcium carbonate. It indicates that with respect to the carbonate content of the sample, the calcination temperature and the total given energy should be changed. However, based on our experiences, there should be a limit for calcination energy. Even for the samples with a high amount of calcium carbonate (e. g. 30 wt%), the amount of calcination energy should not be too much. Owing to the fact that the clay decomposition starts and ends earlier than calcium carbonate decomposition if we induce excessive energy for calcium carbonate decomposition, and if the decomposition of carbonate phase is driven to the end, it will make dead-burnt clay. The dead-burnt clay samples will not contain any reactive clayey materials for playing a role in cement pozzolanic reactions. In order to avoid this problem, the decomposition energies of clay and calcium carbonate should be calculated separately. Furthermore, there should be a balance between clay and carbonate decomposition based on the decomposition energies. For schist-type materials, we should make sure that all the calcium carbonate is NOT decomposed. For the decomposition of calcium carbonate, a moderate decomposition portion is about 80% of the total carbonate amount.

4.4. Activation of Feldspars

This study claims that activatable aluminosilicates are not limited to clay type materials. In addition to clays, it is also possible to reactivate another class of aluminosilicates like feldspars. These materials are more abundant than clay on the earth's crust in terms of volume and they are also the precursor for clays. Before being used as SCMs, the feldspars also need to be activated (de-stabilized) as well as clays such that they can take part in cementitious reactions. One of the schist samples in this study i. e. L sample contained a significant portion of feldspar (albite) in its phase composition. Based on the XRD results corresponding to the calcined L schist sample, it appeared that there was no trace of de-stabilized albite. It indicated that the thermal treatment is not an effective activation method for feldspars. Therefore, it was decided to perform a mechanical activation process on L, and L_{L30} schist samples by using common ball-milling. The XRD results showed that after performing ball-milling for 24 hours, a significant portion of the albite phase in the XRD spectra of thermally and mechanically activated L sample decomposed into the anhydrous mica. It means that under certain conditions it is possible to convert the feldspars existing in the schist materials to the clays and take advantage of them in cement hydration reactions as pozzolans. Moreover, the compressive strength test results confirmed this hypothesis. According to the figure compression test results, there was a considerable improvement in the strength of thermally and mechanically activated L and L_{30} samples compared to the ones which were only thermally activated. Nonetheless, when the same mechanical activation process was performed on a pure albite sample, it did not turn into mica or any other clayey phase. The ball-milling process only affects the crystallinity to the amorphous ratio in pure albite by the disintegration of crystal structure and increasing the amorphous portion. In order to be able to take advantage of any type of feldspars in cement pozzolanic reactions, this inconsistency should be justified and an effective activation method should be designed for pure albite as well as L schist sample. In the meanwhile, one factor that can justify this inconsistency is that in the L schist sample there are some other phases besides albite which may influence the decomposition of albite. Co-existing of the other phases with feldspar in the schist composition which maybe is changing the pH or other parameters and contributing to the decomposition of these phases to clays. Finding a certain and comprehensive activation method for any type of feldspars in order to be used as a pozzolan source is suggested as the future work for the next generation of scientists to continue.

4.5. Effect of Calcined Calcia Amount on Hydration Products

As it is known, the pozzolanic reaction requires a proper amount of calcium hydroxide. The calcium hydroxide (CH-Portlandite) will be provided by hydration reactions. Afterward, the alkaline solution of the hydration process could attack the unstable structures and cause a reaction between reactive aluminosilicates and calcium ions leading to the C-S-H and C-A-S-H formation. This reaction is through the polymerization process of dissolved silicate and aluminate meres with calcium ions (Eq. 6). Hence, the proper amount of free lime (CaO) could compensate for the calcium ion requirement of pozzolanic reactions and provide more strength. Based on this hypothesis, the efficiency of SCMs depends on the amount of de-hydroxylated aluminosilicates and also an adequate source of calcium ions. Calcined calcia (calcium carbonate) could provide an excess source of calcium ions. Therefore, it is possible to calculate the required ratio of CaO in calcined schists and insert the needed amount of calcined carbonate into the hydration system. In this study, the portion of the calcium carbonate inside the schists was topped off to 15 wt%, 22.5 wt%, and 30 wt%. Afterward, the virgin and calcium carbonate augmented schists went through a certain calcination process for being used as SCM in the composite cement mixture. The strength development of blended cement pastes that are prepared with activated as virgin or carbonate added schists were observed. The results were compared to the strength of pure OPC paste. The effectiveness of calcined carbonate addition in strength development confirmed the hypothesis of this study.

According to the theoretical calculations and chemical formula of the C-S-H ($Ca_5Si_6O_{16}(OH)_2 \cdot 4H_2O$) and C-A-S-H ($Ca_5Al_2Si_6O_{16}(OH)_2 \cdot 4H_2O$), it seemed that there was a possibility to increase the amount of carbonate portion into the schist. However, as it was mentioned in the introduction section, the stability and strength of the C-S-H phase mostly depend on its Ca/Si ratio which ranges from 1.3 to 2.1. Therefore, there should be a limit in calcium carbonate amount in the composite cement mixture such that the Ca/Si ratio does not exceed 2. There will be two calcium sources in the calcined clay and calcined Calcia added blended cement; the Ca source existing in OPC phases' composition e. g. alite and belite, and the Ca source inside the virgin or $C\bar{C}$ augmented schists. Based on these assumptions, it was decided to top off the carbonate amount of the schists up to 30 wt% to control the strength performance of the blended cement. The compressive strength test results confirmed that the strength values of the $C\bar{C}$

augmented schist samples are higher than the virgin ones. Moreover, The strength of the the $C\bar{C}$ augmented schist samples are also very close to the pure OPC sample's strength value.

Generally, it is assumed that the pozzolanic reactions in composite cement pastes are slow to take part in cement hydration. They contribute mostly to late strength. Therefore, it is safe to assume that the early strength values for 2 and 7 days of setting time are mostly associated with the cement's contribution to the strength. In addition, there is one more factor affecting the early strength of cement paste. Although the CH phase (Portlandite) affects the durability of the cement samples negatively, it could enhance the early strength of the samples. Hence, there is also an enhancement in the early strength of the composite cement samples made up of the $C\bar{C}$ augmented schist samples due to the excess amount of Portlandite at early ages (as it was indicated in figures 91 and 92). As it can be seen in the compressive strength results, the samples in which the $C\bar{C}$ the amount was topped off to 22.5 wt% showed higher compressive strength compared to the others after 28, 50, and 90 days of hydration. However, the highest strength value corresponded to the $B_{L22.5}$ sample in which there was an excess heat provider i. e. graphite during calcination. It is predicted that the rest of the schist samples containing 22.5 wt% of calcium carbonate would show a compressive strength even better than the B sample if the calcination process would be performed properly.

CHAPTER 5

5. Conclusion

One of the purposes of this study is the evaluation of the effect of carbonate either as calcined or virgin limestone powder on compressive strength. The effect of limestone as a source of virgin carbonate was already discussed in several studies. Filler effect and the promotion of hemi-carboaluminates are the two main applications of carbonate in composite cement pastes. This study could entail the advantages of a proper amount of carbonate additive as an excess source of calcium. Hence it is possible to evaluate the pozzolanic reactivity of any clay and carbonate-containing abundant materials according to the de-hydroxylation of clay and decarbonization of calcite. This will be manifested through the temperature range up to around 800ºC. The amount of carbonate should be adjusted with the calcium requirement to use full activated phases potential. Another privilege of calcite is to reduce the specific surface area of the clay which makes it more reactive. Since, schist-type materials containing a proper amount of clay and carbonate which are thermally or mechanically co-activated, could be a potential SCMs for OPC substitution, it is possible to use most of the abundant or mine overburdens for this aim. Therefore, the existence of carbonate as calcined carbonate in the activated materials for composite cement paste is going to be more beneficial. The expected pozzolanic minerals could help to avoid the production of the excessive amount of Portlandite in cement or concrete which can cause inevitable damages especially in the durability of cement due to the reactions at late age's of the paste.

All the schist types mine powders were calcined, according to the determined and calculated temperatures to activate them. The heat treatment temperatures corresponding to partial activation of possible pozzolanic phases were chosen accurately to avoid dead-burning of the clayey materials. Therefore, at the first stage, the calcination temperature was the temperature associated with 80% of the total weight loss due to de-hydroxylation. These exact temperatures were determined for the virgin and calcite augmented schist powders with the help of thermal analysis equipment. The schist powders were investigated for their potential of activation in as-received composition and as modified composition mixed-powders with their weight percentage of the carbonate topped off to 15%, 22.5%, and 30%. The calcined materials partially substituted the cement powder when preparing composite cement pastes. Also, after getting some results it was determined that the 80% calcination might not be enough for activation of the schist. Therefore, The G sample with and without carbonate addition was calcined up to 100% and 110% of total weight loss, and the 100% calcined sample showed better strength results compared to the 80% calcined one. The 110% calcined sample showed the lowest strength value due to over-heating which causes sintering of clayey phases i. e. dead-burnt clay. Moreover, the strength measurement results revealed that the $B_{L22.5}$ sample (B with 22.5 wt% $C\overline{C}$) was the best potential candidate.

The study also illustrated the importance of proper heat treatment to reach the targeted activation amount in the schist powder mixtures. In the other studies related to this topic, all information about the calcination of the aluminosilicates was summarized as temperature and time. However, the difference in the amount of material between laboratory scale and industrial scale causes some errors in this case. As it was mentioned earlier, it is better to design and perform the calcination process based on a parameter that does not change with the sample's mass. In order to be more precise about the calcination method, we decided to calculate the given energy to each sample during calcination. With the help of DSC test results, it was concluded that the decomposition energy of the samples increases by increasing the calcium carbonate amount. It means that with respect to the carbonate amount of the sample, the calcination temperature, and the total given energy should be changed as well. However, based on our experiences, there should be a limit for calcination energy. Briefly, even for the samples with a high amount of calcium carbonate, the amount of calcination energy should not be too much. Owing to the fact that the clay decomposition starts and ends earlier than calcium carbonate decomposition if we spend excessive energy on calcium carbonate decomposition and if the decomposition of carbonate phase is driven

to the end, it will make dead-burnt clay. Therefore, the dead-burnt samples will not contain any reactive clayey phases for being used in cement pozzolanic reactions. In order to avoid this problem, the decomposition energies of clay and calcium carbonate should be calculated separately. Afterward, there should be a balance between clay and carbonate decomposition based on the decomposition energies. For the schist type of materials, it must be made sure that all the calcium carbonate is NOT decomposed. For the decomposition of calcium carbonate, a good amount is about 80% of the total carbonate amount.

Another novelty of this study was several activating methods which were performed to activate the feldspar phases existing in L schist. The mechanical activation leads to the decomposition of a significant portion of the albite phase in the XRD spectra of thermally activated L sample into the anhydrous mica. Therefore, it is possible to convert the feldspars existing in the schist materials to the clays and take advantage of them in cement hydration reactions. However, introducing an effective and comprehensive activation method for the feldspars needs more extensive research it is suggested as the future work to be continued.

REFERENCES

1. Mekhilef, S., R. Saidur, and A. Safari, *A review on solar energy use in industries.* Renewable and sustainable energy reviews, 2011. **15**(4): p. 1777-1790.
2. Cai, B., et al., *Evaluating CO2 emission performance in China's cement industry: an enterprise perspective.* Applied energy, 2016. **166**: p. 191-200.
3. Benhelal, E., et al., *Global strategies and potentials to curb CO2 emissions in cement industry.* Journal of cleaner production, 2013. **51**: p. 142-161.
4. Worrell, E., et al., *Carbon dioxide emissions from the global cement industry.* Annual review of energy and the environment, 2001. **26**(1): p. 303-329.
5. Taylor, M., C. Tam, and D. Gielen, *Energy efficiency and CO2 emissions from the global cement industry.* Korea, 2006. **50**(2.2): p. 61.7.
6. Moumin, G., et al., *CO2 emission reduction in the cement industry by using a solar calciner.* Renewable energy, 2020. **145**: p. 1578-1596.
7. Ansari, N. and A. Seifi, *A system dynamics model for analyzing energy consumption and CO2 emission in Iranian cement industry under various production and export scenarios.* Energy Policy, 2013. **58**: p. 75-89.
8. Oh, D.-Y., et al., *CO2 emission reduction by reuse of building material waste in the Japanese cement industry.* Renewable and Sustainable Energy Reviews, 2014. **38**: p. 796-810.
9. Anand, S., P. Vrat, and R. Dahiya, *Application of a system dynamics approach for assessment and mitigation of CO2 emissions from the cement industry.* Journal of environmental management, 2006. **79**(4): p. 383-398.
10. Hasanbeigi, A., et al., *Energy efficiency improvement and CO2 emission reduction opportunities in the cement industry in China.* Energy Policy, 2013. **57**: p. 287-297.
11. Ke, J., et al., *Potential energy savings and CO2 emissions reduction of China's cement industry.* Energy Policy, 2012. **45**: p. 739-751.
12. Scrivener, K.L. and A. Nonat, *Hydration of cementitious materials, present and future.* Cement and concrete research, 2011. **41**(7): p. 651-665.
13. Lothenbach, B., K. Scrivener, and R. Hooton, *Supplementary cementitious materials.* Cement and concrete research, 2011. **41**(12): p. 1244-1256.
14. Taylor, H.F., *Cement chemistry*. 1997: Thomas Telford.
15. Papadakis, V., S. Antiohos, and S. Tsimas, *Supplementary cementing materials in concrete: Part II: A fundamental estimation of the efficiency factor.* Cement and Concrete research, 2002. **32**(10): p. 1533-1538.

16. Massazza, F. and U. Costa. *Factors determining the development of mechanical strength in lime–pozzolana pastes*. in *Proceedings of the XII Conference on Silicate Industry and Silicate Science*. 1977.

17. Young, J.F., A. Bentur, and S. Mindess, *The science and technology of civil engineering materials.* 1998.

18. Aqel, M. and D. Panesar, *Hydration kinetics and compressive strength of steam-cured cement pastes and mortars containing limestone filler.* Construction and Building Materials, 2016. **113**: p. 359-368.

19. Arora, A., G. Sant, and N. Neithalath, *Ternary blends containing slag and interground/blended limestone: Hydration, strength, and pore structure.* Construction and Building Materials, 2016. **102**: p. 113-124.

20. De Weerdt, K., et al., *Hydration mechanisms of ternary Portland cements containing limestone powder and fly ash.* Cement and Concrete Research, 2011. **41**(3): p. 279-291.

21. Richardson, I. and G. Groves, *Microstructure and microanalysis of hardened ordinary Portland cement pastes.* Journal of Materials Science, 1993. **28**(1): p. 265-277.

22. Richardson, I., *The nature of the hydration products in hardened cement pastes.* Cement and Concrete Composites, 2000. **22**(2): p. 97-113.

23. Martín-Garrido, M., M. Teresa Molina-Delgado, and S. Martínez-Ramírez, *A comparison between experimental and theoretical Ca/Si ratios in C–S–H and C–S(A)–H gels.* Journal of Sol-Gel Science and Technology, 2020. **94**(1): p. 11-21.

24. Moon, J., S. Yoon, and P.J.M. Monteiro, *Mechanical properties of jennite: A theoretical and experimental study.* Cement and Concrete Research, 2015. **71**: p. 106-114.

25. Kunther, W., S. Ferreiro, and J. Skibsted, *Influence of the Ca/Si ratio on the compressive strength of cementitious calcium–silicate–hydrate binders.* Journal of Materials Chemistry A, 2017. **5**(33): p. 17401-17412.

26. Shi, C., C. Meyer, and A. Behnood, *Utilization of copper slag in cement and concrete.* Resources, Conservation and recycling, 2008. **52**(10): p. 1115-1120.

27. Zhao, F.-Q., et al., *Activated fly ash/slag blended cement.* Resources, Conservation and recycling, 2007. **52**(2): p. 303-313.

28. Cheng-Yi, H. and R.F. Feldman, *Hydration reactions in portland cement-silica fume blends.* Cement and Concrete Research, 1985. **15**(4): p. 585-592.

29. Rajamma, R., et al., *Characterisation and use of biomass fly ash in cement-based materials.* Journal of hazardous materials, 2009. **172**(2-3): p. 1049-1060.

30. Palomo, A., M. Grutzeck, and M. Blanco, *Alkali-activated fly ashes: A cement for the future.* Cement and concrete research, 1999. **29**(8): p. 1323-1329.

31. Wu, X., D. Roy, and C. Langton, *Early stage hydration of slag-cement.* Cement and Concrete Research, 1983. **13**(2): p. 277-286.

32. Fernández-Jiménez, A. and F. Puertas, *Setting of alkali-activated slag cement. Influence of activator nature.* Advances in Cement Research, 2001. **13**(3): p. 115-121.

33. Malhotra, V.M. and P.K. Mehta, *Pozzolanic and cementitious materials*. Vol. 1. 1996: Taylor & Francis.

34. Celik, K., et al., *Effect of volcanic ash pozzolan or limestone replacement on hydration of Portland cement.* Construction and Building Materials, 2019. **197**: p. 803-812.

35. Shi, C. and R.L. Day, *Chemical activation of blended cements made with lime and natural pozzolans.* Cement and Concrete Research, 1993. **23**(6): p. 1389-1396.

36. Celik, K., et al., *High-volume natural volcanic pozzolan and limestone powder as partial replacements for portland cement in self-compacting and sustainable concrete.* Cement and concrete composites, 2014. **45**: p. 136-147.

37. Colak, A., *Characteristics of pastes from a Portland cement containing different amounts of natural pozzolan.* Cement and Concrete Research, 2003. **33**(4): p. 585-593.

38. Association, N.S., *Production and uses of blast furnace slag in Japan.* and ‘‘production and uses of steel slag in Japan.’’Tokyo, Japan: Nippon Slag Association.

39. Carrasco, M., et al., *Strength optimization of “tailor-made cement” with limestone filler and blast furnace slag.* Cement and Concrete Research, 2005. **35**(7): p. 1324-1331.

40. Güneyisi, E. and M. Gesoğlu, *Properties of self-compacting portland pozzolana and limestone blended cement concretes containing different replacement levels of slag.* Materials and structures, 2011. **44**(8): p. 1399-1410.

41. Menéndez, G., V. Bonavetti, and E. Irassar, *Strength development of ternary blended cement with limestone filler and blast-furnace slag.* Cement and Concrete Composites, 2003. **25**(1): p. 61-67.

42. Mounanga, P., et al., *Improvement of the early-age reactivity of fly ash and blast furnace slag cementitious systems using limestone filler.* Materials and structures, 2011. **44**(2): p. 437-453.

43. Crossin, E., *The greenhouse gas implications of using ground granulated blast furnace slag as a cement substitute.* Journal of Cleaner Production, 2015. **95**: p. 101-108.

44. Li, G., *Properties of high-volume fly ash concrete incorporating nano-SiO2.* Cement and Concrete research, 2004. **34**(6): p. 1043-1049.

45. Naik, T.R., B.W. Ramme, and J.H. Tews, *Use of high volumes of class C and class F fly ash in concrete.* Cement, Concrete and Aggregates, 1994. **16**(1): p. 12-20.

46. Hanif, A., Z. Lu, and Z. Li, *Utilization of fly ash cenosphere as lightweight filler in cement-based composites–a review.* Construction and Building Materials, 2017. **144**: p. 373-384.

47. Langan, B., K. Weng, and M. Ward, *Effect of silica fume and fly ash on heat of hydration of Portland cement.* Cement and Concrete research, 2002. **32**(7): p. 1045-1051.

48. P. Mokhtari, K.H., S. Semsari Parapari, Y. Akyol and M. A. Gulgun *Calcined schist as promising ordinary Portland cement substitution: C4.* Cement and Concrete Composites,, 2020.

49. Kingery, W.D., *Introduction to ceramics*. 2nd ed.. ed, ed. H.K. Bowen and D.R.j.a. Uhlmann. 1976, New York: New York : Wiley.

50. Hendricks, S.B., *Lattice structure of clay minerals and some properties of clays.* The Journal of Geology, 1942. **50**(3): p. 276-290.

51. Brigatti, M.F., E. Galan, and B. Theng, *Structure and mineralogy of clay minerals*, in *Developments in clay science*. 2013, Elsevier. p. 21-81.

52. Joussein, E., et al., *Halloysite clay minerals—a review.* Clay minerals, 2005. **40**(4): p. 383-426.

53. Sperinck, S., et al., *Dehydroxylation of kaolinite to metakaolin—a molecular dynamics study.* Journal of Materials Chemistry, 2011. **21**(7): p. 2118-2125.

54. Hollanders, S., et al., *Pozzolanic reactivity of pure calcined clays.* Applied Clay Science, 2016. **132**: p. 552-560.

55. Sabir, B., S. Wild, and J. Bai, *Metakaolin and calcined clays as pozzolans for concrete: a review.* Cement and concrete composites, 2001. **23**(6): p. 441-454.

56. !!! INVALID CITATION !!! {}.

57. Antoni, M., et al., *Cement substitution by a combination of metakaolin and limestone.* Cement and Concrete Research, 2012. **42**(12): p. 1579-1589.

58. San Nicolas, R., *Approche performantielle des bétons avec métakaolins obtenus par calcination flash*. 2011, Université de Toulouse, Université Toulouse III-Paul Sabatier.

59. He, C., E. Makovicky, and B. Osbæck, *Thermal stability and pozzolanic activity of calcined kaolin.* Applied Clay Science, 1994. **9**(3): p. 165-187.

60. Alujas, A., et al., *Pozzolanic reactivity of low grade kaolinitic clays: Influence of calcination temperature and impact of calcination products on OPC hydration.* Applied Clay Science, 2015. **108**: p. 94-101.

61. He, C., B. Osbaeck, and E. Makovicky, *Pozzolanic reactions of six principal clay minerals: activation, reactivity assessments and technological effects.* Cement and concrete research, 1995. **25**(8): p. 1691-1702.

62. Souri, A., et al., *Pozzolanic activity of mechanochemically and thermally activated kaolins in cement.* Cement and Concrete Research, 2015. **77**: p. 47-59.

63. Ramezanianpour, A. and H.B. Jovein, *Influence of metakaolin as supplementary cementing material on strength and durability of concretes.* Construction and Building materials, 2012. **30**: p. 470-479.

64. Grapes, R. and T. Watanabe, *Mineral composition variation in Alpine Schist, Southern Alps, New Zealand: implications for recrystallization and exhumation.* Island Arc, 1994. **3**(3): p. 163-181.

65. Zhang, Y., et al., *Systematic review of feldspar beneficiation and its comprehensive application.* Minerals Engineering, 2018. **128**: p. 141-152.

66. Heyes, G., et al., *Review of flotation of feldspar.* Mineral Processing and Extractive Metallurgy, 2012. **121**(2): p. 72-78.

67. Parsons, I., *Feldspars and their reactions*. Vol. 421. 2012: Springer Science & Business Media.

68. Holdren, G.R. and R.A. Berner, *Mechanism of feldspar weathering—I. Experimental studies.* Geochimica et Cosmochimica Acta, 1979. **43**(8): p. 1161-1171.

69. Gooding, J.L., R.E. Arvidson, and M.I. Zolotov, *Physical and chemical weathering*. 1992. p. 626.

70. Berner, R.A. and G.R. Holdren, Jr., *Mechanism of feldspar weathering: Some observational evidence.* Geology, 1977. **5**(6): p. 369-372.

71. Correns, C.W., *Experiments on the decomposition of silicates and discussion of chemical weathering.* Clays and clay minerals, 1961. **10**(1): p. 443-459.

72. Wollast, R., *Kinetics of the alteration of K-feldspar in buffered solutions at low temperature.* Geochimica et Cosmochimica Acta, 1967. **31**(4): p. 635-648.

73. Engelhardt, J.F., et al., *Feldspar 40Ar/39Ar dating of ICDP PALEOVAN cores.* Geochimica et Cosmochimica Acta, 2017. **217**: p. 144-170.

74. Tazaki, K. and W.S. Fyfe, *Primitive clay precursors formed on feldspar.* Canadian Journal of Earth Sciences, 1987. **24**(3): p. 506-527.

75. Keller, W.D., *Kaolinization of feldspar as displayed in scanning electron micrographs.* Geology, 1978. **6**(3): p. 184-188.

76. Pera, J., S. Husson, and B. Guilhot, *Influence of finely ground limestone on cement hydration.* Cement and Concrete Composites, 1999. **21**(2): p. 99-105.

77. Delatte, N.J., *Lessons from Roman Cement and Concrete.* Journal of Professional Issues in Engineering Education and Practice, 2001. **127**(3): p. 109-115.

78. Krishnan, S., et al., *Hydration kinetics and mechanisms of carbonates from stone wastes in ternary blends with calcined clay.* Construction and building materials, 2018. **164**: p. 265-274.

79. Krishnan, S., A.C. Emmanuel, and S. Bishnoi, *Hydration and phase assemblage of ternary cements with calcined clay and limestone.* Construction and Building Materials, 2019. **222**: p. 64-72.

80. Zunino, F. and K.L. Scrivener, *The Effect of Calcite and Gibbsite Impurities in Calcined Clay on Its Reactivity*, in *Calcined Clays for Sustainable Concrete*. 2020, Springer. p. 357-362.

81. Yılmaz, B. and A. Olgun, *Studies on cement and mortar containing low-calcium fly ash, limestone, and dolomitic limestone.* Cement and Concrete Composites, 2008. **30**(3): p. 194-201.

82. Bentz, D.P., et al., *Limestone and silica powder replacements for cement: Early-age performance.* Cement and Concrete Composites, 2017. **78**: p. 43-56.

83. Ghafoori, N., R. Spitek, and M. Najimi, *Influence of limestone size and content on transport properties of self-consolidating concrete.* Construction and Building Materials, 2016. **127**: p. 588-595.

84. Lollini, F., E. Redaelli, and L. Bertolini, *Effects of portland cement replacement with limestone on the properties of hardened concrete.* Cement and Concrete Composites, 2014. **46**: p. 32-40.

85. Lothenbach, B., et al., *Influence of limestone on the hydration of Portland cements.* Cement and Concrete Research, 2008. **38**(6): p. 848-860.

86. Nocuń-Wczelik, W., B. Trybalska, and E. Żugaj, *Application of calorimetry as a main tool in evaluation of the effect of carbonate additives on cement hydration.* Journal of thermal analysis and calorimetry, 2013. **113**(1): p. 351-356.

87. Matschei, T., B. Lothenbach, and F.P. Glasser, *The role of calcium carbonate in cement hydration.* Cement and concrete research, 2007. **37**(4): p. 551-558.

88. Krishnan, S. and S. Bishnoi, *Understanding the hydration of dolomite in cementitious systems with reactive aluminosilicates such as calcined clay.* Cement and Concrete Research, 2018. **108**: p. 116-128.

89. Dhandapani, Y., et al., *Mechanical properties and durability performance of concretes with limestone calcined clay cement (LC3).* Cement and Concrete Research, 2018. **107**: p. 136-151.

90. Prince, W., M. Espagne, and P.-C. Aïtcin, *Ettringite formation: A crucial step in cement superplasticizer compatibility.* Cement and Concrete Research, 2003. **33**(5): p. 635-641.

91. Bentz, D., *Modeling the influence of limestone filler on cement hydration using CEMHYD3D.* Cement and Concrete Composites, 2006. **28**(2): p. 124-129.

92. Mohamed, A.R., M. Elsalamawy, and M. Ragab, *Modeling the influence of limestone addition on cement hydration.* Alexandria Engineering Journal, 2015. **54**(1): p. 1-5.

93. Scrivener, K., et al., *Calcined clay limestone cements (LC3).* Cement and concrete research, 2018. **114**: p. 49-56.

94. Avet, F. and K. Scrivener, *Investigation of the calcined kaolinite content on the hydration of Limestone Calcined Clay Cement (LC3).* Cement and Concrete Research, 2018. **107**: p. 124-135.

95. Matschei, T. and F.P. Glasser, *Zum Einfluss von Kalkstein auf die Zementhydratation.* Materials Science, 2006. **59**(12-2006).

96. Damidot, D., et al., *Thermodynamics and cement science.* Cement and Concrete Research, 2011. **41**(7): p. 679-695.

97. Avet, F., et al., *Development of a new rapid, relevant and reliable (R3) test method to evaluate the pozzolanic reactivity of calcined kaolinitic clays.* Cement and Concrete Research, 2016. **85**: p. 1-11.

98. Scrivener, K., R. Snellings, and B. Lothenbach, *A practical guide to microstructural analysis of cementitious materials*. 2018: Crc Press.

99. Traore, K., T.S. Kabre, and P. Blanchart, *Gehlenite and anorthite crystallisation from kaolinite and calcite mix.* Ceramics International, 2003. **29**(4): p. 377-383.

100. Allegretta, I., D. Pinto, and G. Eramo, *Effects of grain size on the reactivity of limestone temper in a kaolinitic clay.* Applied Clay Science, 2016. **126**: p. 223-234.